RFID ANTENNA DESIGN FOR DETERMINATION OF A DIELECTRIC PROPERTY OF MATERIAL

RATTAPONG SUWALAK

A THESIS SUBMITTED IN PARTIAL FULLFILLMENT

OF THE REQUIREMENT FOR THE DEGREE OF

DOCTOR OF ENGINEERING IN ELECTRICAL ENGINEERING

FACULTY OF ENGINEERING

KING MONGKUT'S INSTITUTE OF TECHNOLOGY LADKRABANG

2012

KMITL-2012-EN-D-018-193

หัวข้อวิทยานิพนธ์	การออกแบบสายอากาศระบุลักษณะทางคลื่นความถี่วิทยุสำหรับทำนายคุณสมบัติไดอิเล็กตริกของวัสดุ
นักศึกษา	นายรัฐพงษ์ สุวลักษณ์
รหัสประจำตัว	51060028
ปริญญา	วิศวกรรมศาสตรดุษฎีบัณฑิต
สาขาวิชา	วิศวกรรมไฟฟ้า
พ.ศ.	2555
อาจารย์ที่ปรึกษา	รศ. ดร. ชูวงค์ พงศ์เจริญพาณิชย์
อาจารย์ที่ปรึกษาวิทยานิพนธ์ร่วม	ดร. พรอนงค์ พงษ์ไพบูลย์

บทคัดย่อ

วิทยานิพนธ์นี้นำเสนอสายอากาศระนาบวงแหวนที่มีการเจาะช่องโค้งและช่องสี่เหลี่ยมวางบนระนาบกราวนด์แนวตั้ง สายอากาศประกอบด้วยช่องสองรูปแบบดังกล่าวซึ่งเจาะบนตัวแพร่กระจายคลื่นระนาบวงแหวนเพื่อให้สายอากาศสามารถตอบสนองย่านความถี่คู่คือ ความถี่ยูเอชเอฟและความถี่ไมโครเวฟสำหรับประยุกต์ใช้ในระบบระบุลักษณะทางคลื่นความถี่วิทยุ สายอากาศออกแบบให้มีแบบรูปการแพร่กระจายคลื่นเป็นแบบทิศทางเดียวและมีอัตราขยายสูงเพื่อใช้เป็นสายอากาศสำหรับเครื่องอ่านข้อมูลในระบบระบุลักษณะทางคลื่นความถี่วิทยุ ดังนั้นสายอากาศถูกสร้างจากโลหะตัวนำและหลีกเลี่ยงการใช้วัสดุฐานรองไดอิเล็กตริกโดยแทนที่ด้วยอากาศ ข้อดีของสายอากาศนี้มีโครงสร้างที่ไม่ซับซ้อนและสะดวกในการสร้าง จากผลการทดสอบพบว่าผลการทดสอบมีความสอดคล้องกันดีกับผลที่ได้จากการจำลอง ดังนั้นสายอากาศที่นำเสนอสามารถนำมาใช้เป็นสายอากาศสำหรับเครื่องอ่านข้อมูลในระบบระบุลักษณะทางคลื่นความถี่วิทยุได้ หลังจากนั้นนำสายอากาศระนาบวงแหวนที่มีการเจาะช่องโค้งและช่องสี่เหลี่ยมที่วางตัวบนระนาบกราวนด์แนวตั้งมาประยุกต์ใช้เป็นสายอากาศสำหรับเครื่องอ่านข้อมูลของเซ็นเซอร์ระบุลักษณะทางคลื่นความถี่วิทยุแบบใหม่เพื่อใช้สำหรับทำนายคุณสมบัติไดอิเล็กตริกของวัสดุซึ่งอิฐมวลเบาถูกนำมาใช้ในวิทยานิพนธ์นี้ จากการทดสอบพบว่าเซ็นเซอร์ระบุลักษณะทางคลื่นความถี่วิทยุแบบใหม่มีความถูกต้องน่าเชื่อถือ ดังนั้นวิทยานิพนธ์นี้นำเสนอสายอากาศเพื่อนำไปประยุกต์ใช้สำหรับเซ็นเซอร์ระบุลักษณะทางคลื่นความถี่วิทยุแบบใหม่ได้

Thesis Title	RFID Antenna Design for Determination of a Dielectric Property of Material
Student	Mr. Rattapong Suwalak
Student ID.	51060028
Degree	Doctor of Engineering
Program	Electrical Engineering
Year	2012
Thesis Advisor	Assoc. Prof. Dr. Chuwong Phongcharoenpanich
Thesis Co-advisor	Dr. Pornanong Pongpaibool

ABSTRACT

An annular plate antenna with curved and rectangular slots on vertical ground plane is proposed in this thesis. The proposed antenna is composed of two types of slots (i.e. curved and rectangular slots), cut on the annular plate to operate at dual-band frequency of UHF and microwave bands for RFID applications. This antenna is designed to achieve the unidirectional beam and high-gain for RFID reader. In addition, the antenna structure is made of metallic plate with air substrate to avoid dielectric loss. The advantages of this antenna are simple structure and easy for fabrication. From the results, the simulation and measurement are agreed very well. It is implied that the proposed antenna can be used as an RFID reader antenna. Furthermore, the annular plate antenna with curved and rectangular slots on vertical ground plane is utilized as a novel RFID sensor to determine the dielectric property of material of interest, i.e., Light Weight Concrete (LWC). From the experimental results, it is found that the novel RFID sensor provides reasonably accurate results. Therefore, this thesis accomplishes the antenna that is employed in a novel RFID sensor.

ACKNOWLEDGEMENTS

This work has been supported by Thailand Graduate Institute of Science and Technology (TGIST), National Science and Technology Development Agency (NSTDA) under contract TGIST 01-51-067.

This thesis was successful completion and smooth by assistance and support from many people as below.

In auspicious occasion, I would like to express my grateful to my advisor, Assoc. Prof. Dr. Chuwong Phongcharoenpanich, who has given guidance, helpful suggestion and encouragement. I also would like to express my gratitude to my co-advisor, Dr. Pornanong Pongpaibool at the National Electronics and Computer Technology Center (NECTEC) for her suggestion and kind support. I am particularly grateful to Assoc. Prof. Dr. Danai Torrungrueng for his fruitful suggestion and kind assistance. I also would like to express my appreciation to Prof. Dr. Monai Krairiksh, for his valuable suggestion and encouragement.

I would like to express my cordial thanks to all members in my laboratory (T103) for discussion, friendship and familiarity. I would like to particularly thank to Dr. Kittisak Phaebua and Miss Kittima Lertsakwimarn for their helpful discussion and assistance. Moreover, I also would like to cordial thank to Miss Worada Jaturonlak and her parents for her encouragement and assistance in every matter.

Finally, I am greatly indebted to my parents for their unceasing help.

Rattapong Suwalak

TABLE OF CONTENTS

TABLE OF CONTENTS (CONTINUE)

LIST OF FIGURES

LIST OF FIGURES (CONTINUE)

LIST OF FIGURES (CONTINUE)

LIST OF FIGURES (CONTINUE)

Figure Page

LIST OF FIGURES (CONTINUE)

LIST OF TABLES

CHAPTER 1

INTRODUCTION

This chapter introduces the background of the annular plate antenna and the feasibility to identify and inspect qualities of material of interest through nondestructive testing (NDT) techniques. The literature reviews of the annular plate antenna, the NDT techniques, the objective, the scope and organization of the thesis that summarizes information of the succeeding chapters are addressed.

1.1 Background and Motivation

Recently, Radio Frequency Identification (RFID) system is well known for many applications such as identification, logistics, traceability and many others [1]-[2]. The RFID system consists of two parts that the first part is an interrogator, more often known as a reader, and second part is a transponder or tag as shown Fig. 1.1. In the RFID technology, a key device for transmitting and receiving signal between communication sides is antenna. The antenna designs for both readers and tags are hot issues to improve their performances. The operating frequencies are classified by their applications, such as using the ultra-high frequency and microwave bands for long range applications. In Thailand, the UHF and microwave RFID frequency bands are from 920 MHz to 925 MHz and from 2.4 GHz to 2.5 GHz, respectively [3]. The antenna at reader plays a vital role in communication between the reader and the tags. In the literature works, there are many researches involving with flat structure [4]-[6], slot and printed antennas [7]-[13]. However, all of them are designed at relatively high frequency that the printed circuit board (PCB) is used for the microstrip antenna fabrication. Moreover, these antennas have complicated structure to implement and the gain of antennas are deteriorated from the dielectric material.

To improve the performance of the RFID system hence the proposed annular plate antenna with curved and rectangular slots on vertical ground plane is designed to achieve the unidirectional beam to direct at the tag direction. Also, the high gain antenna is required for RFID reader which results in serious improvement of the communication between the tag and the reader. Therefore, the antenna structure is made of metallic plate with air substrate to avoid dielectric loss. The design procedure and simulations are performed by using CST Microwave Studio simulator based on the Finite Integration Technique (FIT).

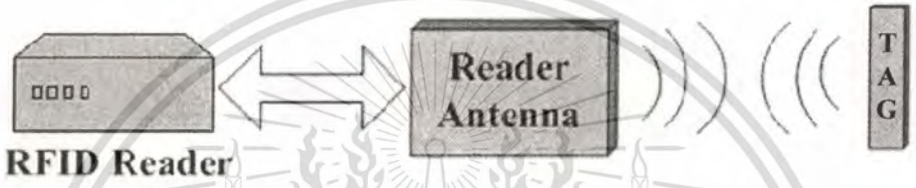

Figure 1.1 The general RFID system.

Furthermore, the demand for traceability to identify and inspect qualities of material products through nondestructive testing (NDT) techniques has been on the rise. Several NDT techniques, such as Radar, Capacimetry, Electrical Resistance and Ultrasonic Waves, have been extensively used [14]-[19]. Each technique however has its advantages and disadvantages, so the selection of an appropriate technique is based on the desired application. For such construction materials (CMs) as Light Weight Concrete (LWC), Mortar specimens and Concrete, a reliable NDT technique is required to evaluate their properties whether they are suitable for construction use. Therefore, the development of a reliable sensor technique to determine material quality in manufacturing and/ or material testing and inspection process is necessary. From the sensor's viewpoint, the dependency of the read range on EM properties of CMs near or in contact with tags can be employed as an approach to determine quality of CMs through their estimated dielectric constants.

RF tag performance is affected by many factors, including EM properties of objects near or in contact with tags [20], [21]. In addition, Siden et al. presented a concept by which pairs of ordinary RFID tags are exploited as remotely read moisture sensors [22]. The moisture sensing label incorporating two RFID tags is embedded in a wall, under which one of the tags is covered with a moisture absorbent material while the other is a naked tag. They are used to detect leaking water pipe connections hidden behind the walls. Additionally, the attenuation and equivalent electric parameters of brick and reinforced concrete walls are estimated [23]. Furthermore, Marrocco et al. have presented the development of very low-cost passive RFID devices capable of monitoring the features of moving objects without the need for specific sensors. Instead, the multiport tag antennas are used as a sensor since they exploit the dependency of the tag's input impedances and the radar cross section on the physical and geometrical features of a real target [24]. However, the purpose of this paper is to describe the possible classification and detection performances of multiport sensor tags in a unitary context.

In this thesis, an NDT technique, called a novel RFID sensor, operating in the UHF band of 922.5 MHz is proposed to determine quality of certain CMs through their estimated dielectric properties. Generally, the traditional RFID sensors require additional specific sensors, such as humidity, temperature, motion, light and sound sensors, to be integrated with RFID tags [25]-[27]. On the other hand, the novel RFID sensor does not require additional specific sensors to determine dielectric properties of the materials under test, thereby more convenient in fabrication and usually of lower cost. In addition, the novel RFID sensor does not require a network analyzer and other expensive accessories. The key component of the novel RFID sensor is the tag specifically designed that will be discussed in greater detail in the remained chapter.

1.2 Objective and Scope of the Thesis

This thesis has proposed a determination of dielectric property of material of interest using a novel RFID sensor that the annular plate antenna with curved and rectangular slots on vertical ground plane and the specifically designed tags (SDTs) are

also proposed to utilize as the RFID reader antenna and a remotely read dielectric-property sensors, respectively. The objective and scope of the thesis are given as follows:

1. To design and analyze of the annular plate antenna with curved and rectangular slots on vertical ground plane to radiate a high-gain unidirectional beam for the RFID reader.

2. To design and analyze of the specifically designed tags (SDTs) to employ as a novel RFID sensor.

3. To apply the novel RFID sensor for determination of dielectric property of construction material products.

1.3 Organization of the Thesis

As referred above that this chapter has mentioned about the overview of this thesis. The annular plate antenna with curved and rectangular slots is designed for RFID reader. Subsequently, the RFID tags are also appropriately designed called the novel RFID sensor to determine qualities of some material of interest. Moreover, the objective, scope of this thesis and organization of the thesis are summarized.

The remaining portion of this thesis consists of five chapters. They are involving theories and applications of the determination of the dielectric constant of material of interest.

Chapter 2 presents the antenna theory and design procedure of the annular plate antenna with curved and rectangular slots on vertical ground plane using the electromagnetic simulator program. In addition, the improvement of the antenna characteristics by using the optimization method in the simulator is performed to determine the optimum antenna parameters and can be applied for the RFID reader.

Chapter 3 discusses the design of RFID tags and the relation between the maximum read range and RFID tag to utilize as a novel RFID sensor for determination of the electrical characteristics of the material of interest.

Chapter 4 verifies the proposed annular plate antenna with curved and rectangular slots on the vertical ground plane that has presented in the preceding chapter by measurement. The prototype of the antenna was fabricated corresponding to the optimum parameters suggested in chapter 2. The experimental results of magnitude of S_{11}, radiation pattern and gain are performed. The measurement results are compared with the results from the simulation to verify the accuracy.

Chapter 5 mentions the experimental results of maximum read range between RFID reader and RFID sensor. In addition, the determination procedure of electrical characteristics of material under test is investigated by using the RFID technology as a sensor viewpoint.

Chapter 6 summarizes the consequence of the material presented in the preceding chapters together with the discussions for the further study.

CHAPTER 2

ANTENNA DESIGN

2.1 Introduction

This chapter presents the antenna theory and antenna design procedure using the electromagnetic simulator to obtain the appropriated antenna parameters that radiates a high-gain unidirectional pattern. The annular plate antenna with curved and rectangular slots on vertical ground plane is proposed to operate at dual-band of UHF and microwave bands of the RFID application.

2.2 Configuration of an Annular Plate Antenna with Curved and Rectangular Slots on Vertical Ground Plane

The antenna at reader plays a vital role in communication between the reader and the tags. The proposed annular plate antenna with curved and rectangular slots on vertical ground plane is investigated to respond the dual-band frequency of RFID systems (UHF and microwave bands) as shown in Fig. 2.1. Note that the proposed antenna is composed of two types of slots (curved and rectangular slots), cut on the annular plate to operate at the upper frequency band (microwave frequency). The antenna is designed to achieve the unidirectional beam to direct at the tag direction. Also, the high-gain antenna is required for RFID reader which results in serious improvement of the communication between the tag and the reader. Therefore, the antenna structure is made of metallic plate with air substrate to avoid dielectric loss. The simulations are performed by using CST Microwave Studio simulator based on the Finite Integration Technique (FIT).

The rest of this chapter, the antenna design procedure and antenna theory are discussed in subsequent sections. Section II presents the characteristics of the annular

plate antenna with curved and rectangular slots on vertical ground plane with the optimum parameters. Finally, brief conclusions are summarized in the last section.

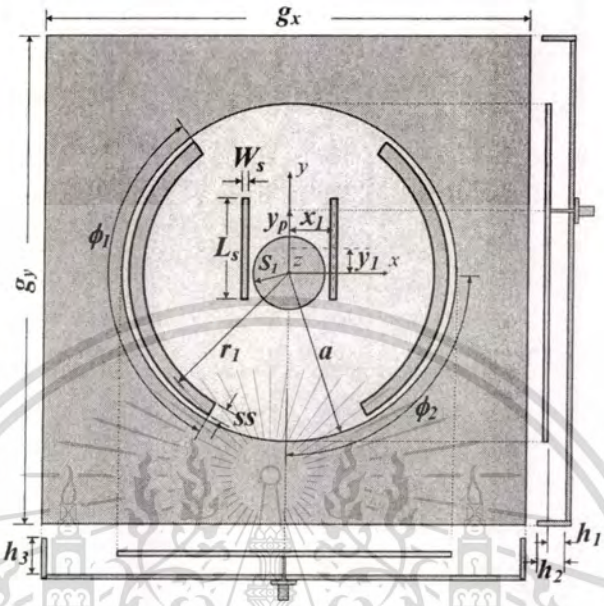

Figure 2.1 The annular plate antenna with curved and rectangular slots on vertical ground plane

2.3 Antenna Design Principle

The determination of the optimal structure and parameters of the antenna for the RFID reader that can be responded a dual-band frequency is separated into 4 steps as follow: the circular plate design, the annular plate design, the design of annular plate with curved and rectangular slots and finally, the design of annular plate antenna with curved and rectangular slots on vertical ground plane.

2.3.1 Circular Plate Antenna

In this section, the antenna design procedures are performed that the designs begin with the lower band (f_L) of operating frequency of 922.5 MHz. The circular plate antenna is the initial structure as shown in Fig. 2.2. Its dimensions were calculated using

the cavity model method [28]. This method is composed of two perfect electric conductors of the radiating plate and the infinite ground plane.

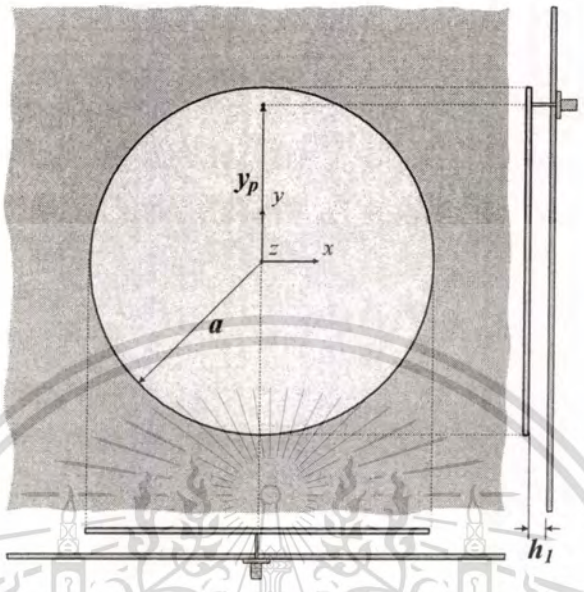

Figure 2.2 A circular plate antenna

According to the cavity model consideration, the radius of the radiating circular plate (a) for the TM^z_{mn0} mode can be expressed as

$$a = \frac{1}{2\pi\sqrt{\mu\varepsilon}}\left(\frac{\chi'_{mn}}{(f_r)_{mn0}}\right), \tag{2.1}$$

where μ is permeability

ε is permittivity

$(f_r)_{mno}$ is resonant frequency at 922.5 MHz

χ'_{mn} is the zeroes of the derivative of the Bessel function $J_m(x)$.

For the dominant mode of the TM^z_{110}, χ'_{11} is 1.8412. Therefore, the radius of the radiating circular plate (a) in (2.1) can be modified and written as

$$a = \frac{1.8412}{2\pi\sqrt{\varepsilon_r}}\left(\frac{v_0}{(f_r)_{110}}\right), \tag{2.2}$$

where v_0 is the speed of light in free-space of 3×10^8 m/s

ε_r is the relative permittivity.

The radius of the radiating circular plate (a) can be calculated by using (2.2). Here, the substrate is the air ($\varepsilon_r = 1$) in order to keep away from the dielectric loss. Thus, the parameter a is equal to 95.3 mm that is used to initial the parameter for simulation. Please keep in mind that based on the cavity model conditions the circular plate antenna has infinite ground plane dimension (the parameters g_x and g_y are determined to infinite layer in CST Microwave Studio program). Moreover, this antenna has the spacing between the radiating plate and the ground plane (h_1) that is significantly smaller than the wavelength ($h_1 << \lambda$) at the desired frequencies of operation. The preliminary spacing between the radiating plate and the ground plane is determined to 1.6 mm. The feeding location (y_p) of the circular plate antenna is important for the radiation pattern. It is well known that in order to obtain the dominant mode (TM^z_{110}), it is closely placed the edge of the radiating circular plate. The initial parameters of the circular plate antenna are tabulated in Table 2.1

Table 2.1 The initial parameters of the circular plate antenna

Parameter	Dimension (mm)
Radius of annular plate (a)	95.3
Spacing between annular plate and ground plane (h_1)	1.6
Dimension of ground plane (g_x, g_y)	∞
Location of feeding in y-axis (y_p)	90

From the initial antenna parameters in Table 2.1, it is evident that the circular plate antenna has impedance mismatch at center of lower band frequency (f_L=922.5 MHz) as shown in Fig. 2.3. Therefore, the parameter analysis is performed to find out the

optimum parameters on magnitude of S_{11}. The parameters of the feeding location along y-axis (y_p), the spacing between the circular plate and the ground plane (h_1) and the radius of the circular plate (a) are studied. As can be seen in Fig. 2.4, it is found that the feeding location along y-axis is expected to significant affect on the impedance matching. However, the magnitude of S_{11} is lower than -10 dB at the 922.5 MHz where the spacing between the radiating circular plate and ground plane (h_1) of 1.6 mm. However, the magnitude of S_{11} better than -10 dB is obtained where h_1 is adjusted as shown in Fig. 2.5. The optimum parameters of circular plate antenna are y_p of 30 mm and h_1 of 3.2 mm.

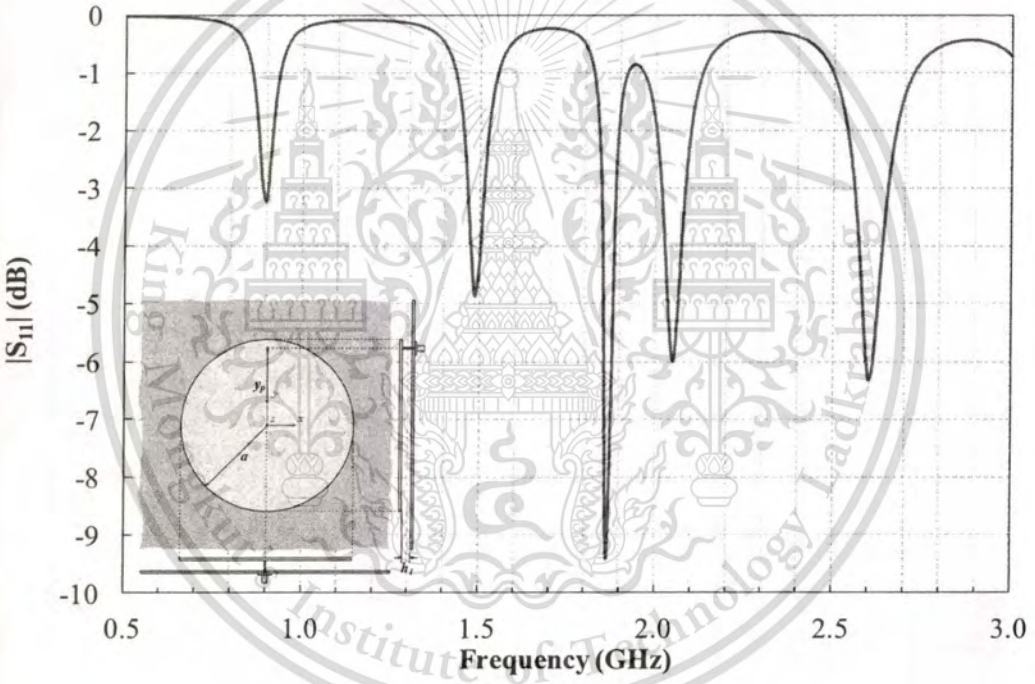

Figure 2.3 Frequency response of the magnitude of S_{11}, when parameters are in Table 2.1

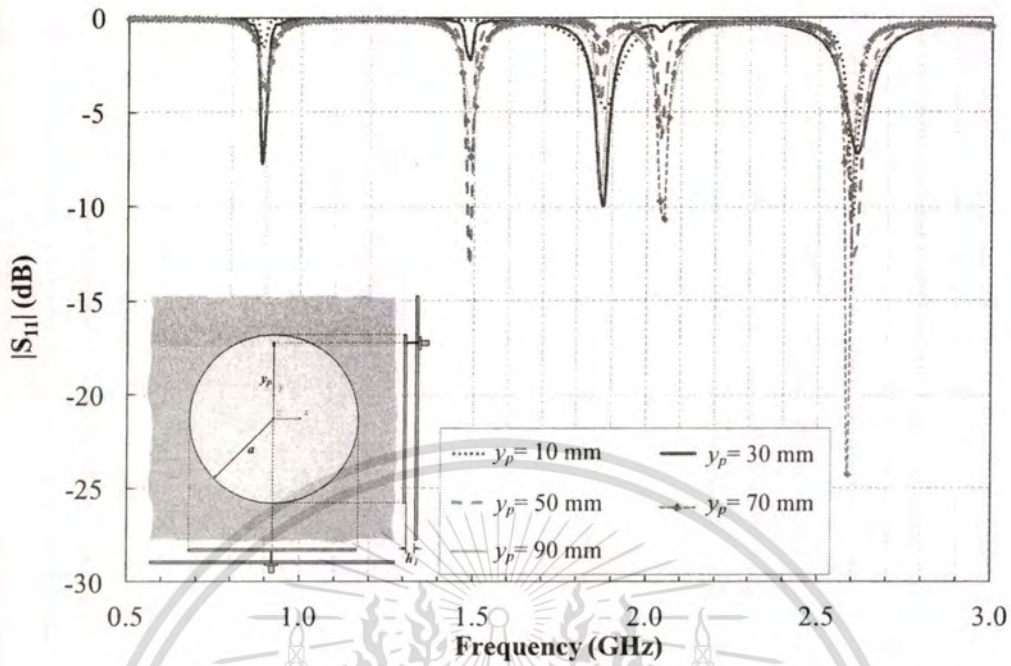

Figure 2.4 Frequency response of the magnitude of S_{11} for various parameter y_p, when remained parameters are in Table 2.1

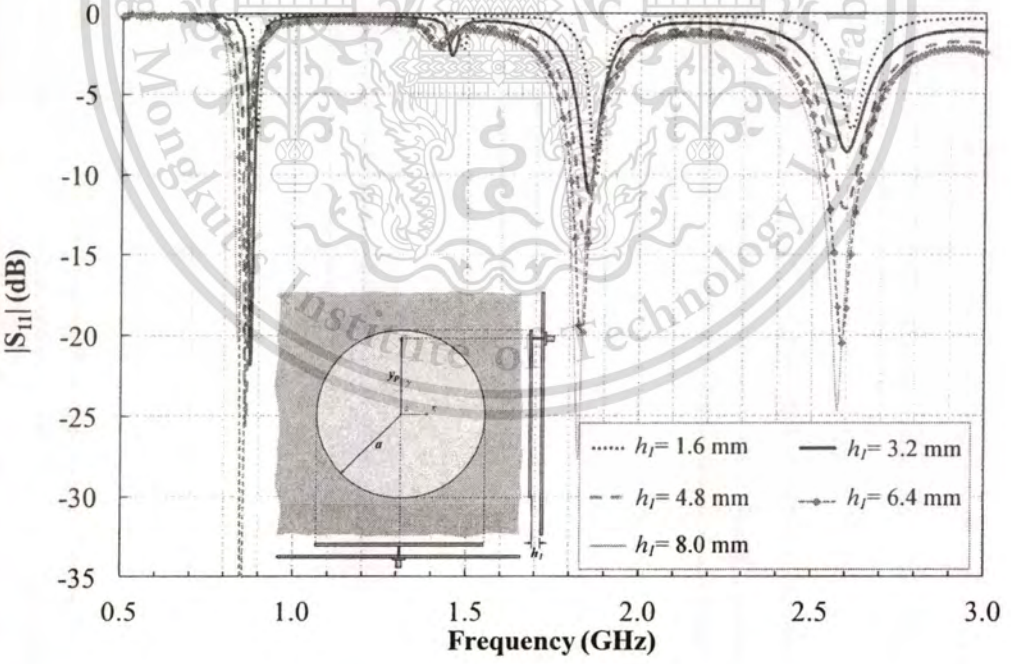

Figure 2.5 Frequency response of the magnitude of S_{11} for various parameter h_1, when y_p=30 mm and remained parameters are in Table 2.1

In addition, the parameter a is adjusted to be 85.3 mm, 90.3 mm and 95.3 mm as shown in Fig. 2.6. It is found that the circular plate antenna can be operated at the frequency of 922.5 MHz when parameter a is 90.3 mm. The optimum parameters of the antenna are tabulated in Table 2.2. Note that the parameters in table 2.2 are used as the initial parameters of the annular plate antenna that will be discussed in detail in the next section.

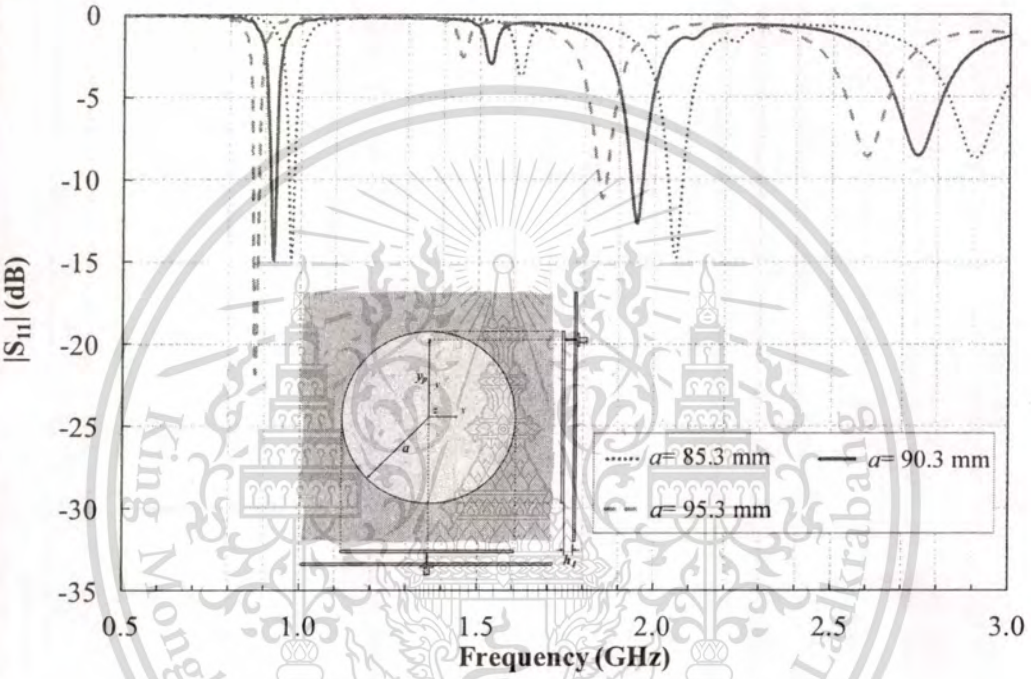

Figure 2.6 Frequency response of the magnitude of S_{11} for various parameter a, when h_1=3.2 mm, y_p=30 mm and remained parameters are in Table 2.1

Table 2.2 The optimum parameters of the circular plate antenna

Parameter	Dimension (mm)
Radius of annular plate (a)	90.3
Spacing between annular plate and ground plane (h_1)	3.2
Dimension of ground plane (g_x, g_y)	∞
Location of feeding in y-axis (y_p)	30

2.3.2 Annular Plate Antenna

From literature review [29]-[31], the annular microstrip antenna has been found that a significant wider bandwidth compared to the other printed circuit resonant antenna. Furthermore, their sizes are substantially smaller than those of corresponding disk antenna with the same operating frequency. A smaller concentric circular slot is proposed to be cut on the original larger circular plate to form an annular-ring antenna as shown in Fig. 2.7. The initial parameters of the annular plate antenna are tabulated in Table 2.3.

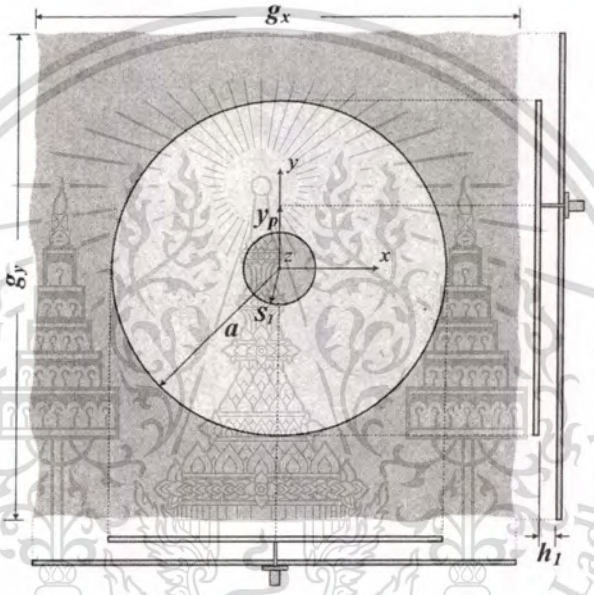

Figure 2.7 An annular plate antenna

Table 2.3 The initial parameters of the annular plate antenna

Parameter	Dimension (mm)
Radius of annular plate (a)	90.3
Spacing between annular plate and ground plane (h_1)	3.2
Dimension of ground plane (g_x, g_y)	∞
Radius of circular slot (S_1)	10
Location of feeding in y-axis (y_p)	30

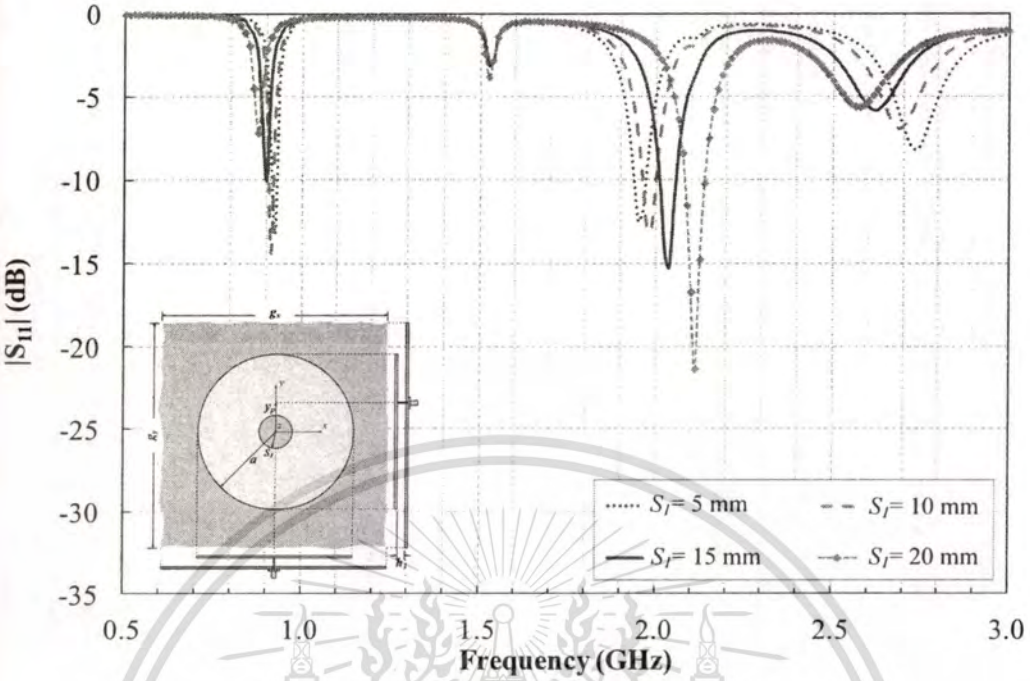

Figure 2.8 Frequency response of the magnitude of S_{11} for various parameter S_1, when remained parameters are in Table 2.3

The radius of a circular slot (S_1) affects to the resonant frequency of the annular plate antenna since the electrical size of the annular plate antenna is longer than the conventional circular plate antenna. It is noticed that the resonant frequency is decreased when the radius is increasing as illustrated in Fig. 2.8. To miniaturize the antenna, the parameter S_1 of 15 mm is selected that the resonant frequency of the annular plate antenna is lower than the center frequency of 922.5 MHz. Therefore, the parameter a must be decreased to reduce the overall size of the annular plate antenna.

In practice, however, the antenna must have a finite size. Consequently, the ground plane dimension is varied in term of the wavelength as depicted in Fig. 2.9. It is obvious that the size of ground plane larger than 243.75 mm (0.75λ) does not affect to the resonant frequency of the annular plate antenna. The parameters g_x and g_y are selected to be 243.75 mm to minimize the antenna size.

Thereafter, the annular plate antenna characteristics are simulated and their parameters are optimized by the CST Microwave Studio. The optimum antenna parameters are obtained as tabulated in Table 2.4. It is found that the annular plate antenna can be operated at the resonant frequency of 922.5 MHz.

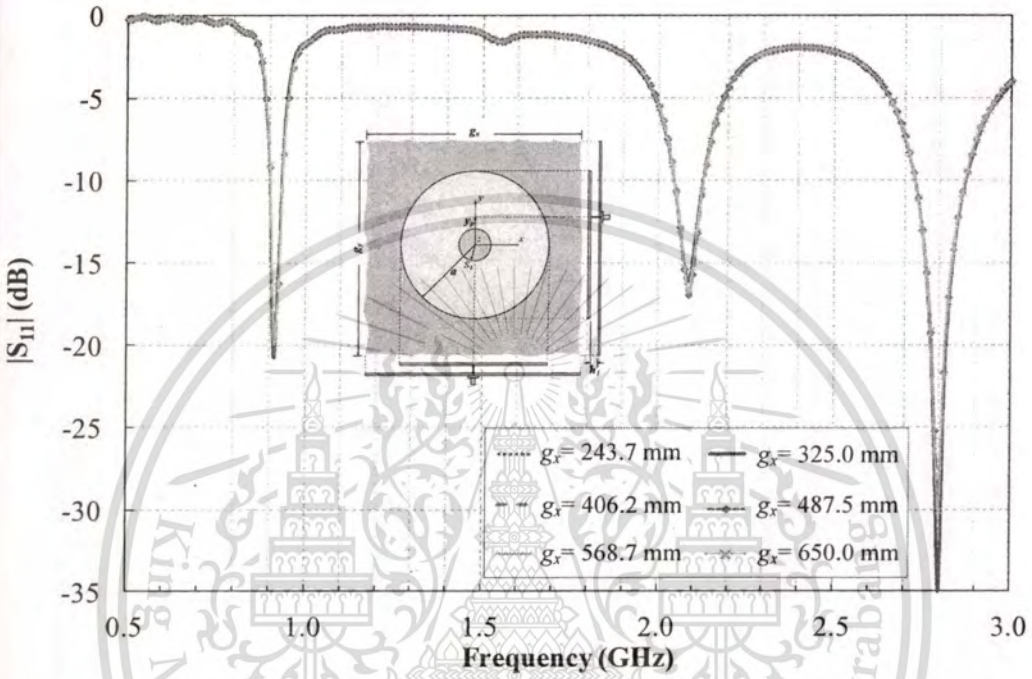

Figure 2.9 Frequency response of the magnitude of S_{11} for various parameter g_x and g_y, when S_1=15 mm and remained parameters are in Table 2.3

Table 2.4 The optimum parameters of the annular plate antenna

Parameter	Dimension (mm)
Radius of annular plate (a)	85.3
Spacing between annular plate and ground plane (h_1)	8
Dimension of ground plane (g_x, g_y)	217
Radius of circular slot (S_1)	15
Location of feeding in y-axis (y_p)	25

Furthermore, in order to achieve the dual-band frequency with unidirectional beam and high-gain antenna, thus the annular plate antenna with curved and rectangular slots is proposed.

2.3.3 Annular plate antenna with curved and rectangular slots

The design of antenna to meet a dual-band for UHF and microwave frequencies is studied. To obtain the dual-band characteristics, the annular plate antenna is modified by cutting on the radiating annular plate with curved and rectangular slots. Figure 2.10 shows the surface current on the radiating plate at the frequency of 922.5 MHz. It is found that the surface current intensity is dense at the outer and inner radius areas. Thereby, the curved and rectangular slots are cut on the radiating annular plate at the areas as depicted in Fig. 2.10. Besides, the radiation pattern is desired to a symmetrical unidirectional beam. For this reason, the curved and rectangular slots are symmetrical etched be along y-axis as illustrated in Fig. 2.11.

This section will be focused on the effect of various parameters on the antenna characteristics in microwave band. Therefore, the parameters under consideration focused on their dimensions and locations of the curved slots (r_1, s_s, ϕ_1 and ϕ_2) and the rectangular slots (L_s, W_s, x_1 and y_1) are varied. The antenna is designed and analyzed to obtain the optimal parameters according to the following procedure.

(1) Varying the radius of curved slot (r_1)

The initial parameters are determined in Table 2.5. Note that the width of curved slot (s_s) is $\lambda_{2.45GHz}/10$. Figure 2.12 exhibits the frequency response of the magnitude of S_{11} for various parameter r_1, when remained parameters are in Table 2.5. It is obvious that the radius of curved slot (r_1) significantly affects only to resonant frequency in microwave band. The optimum parameter r_1 is 77 mm.

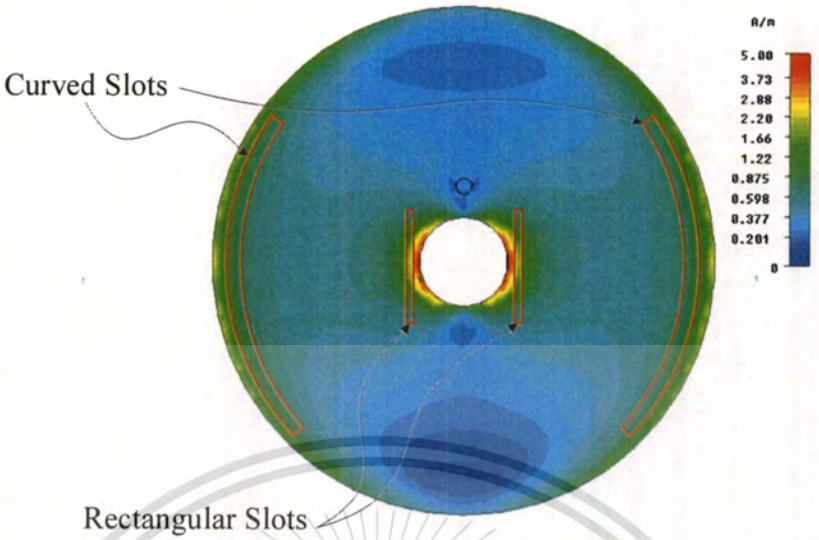

Figure 2.10 Surface current at frequency of 922.5 MHz

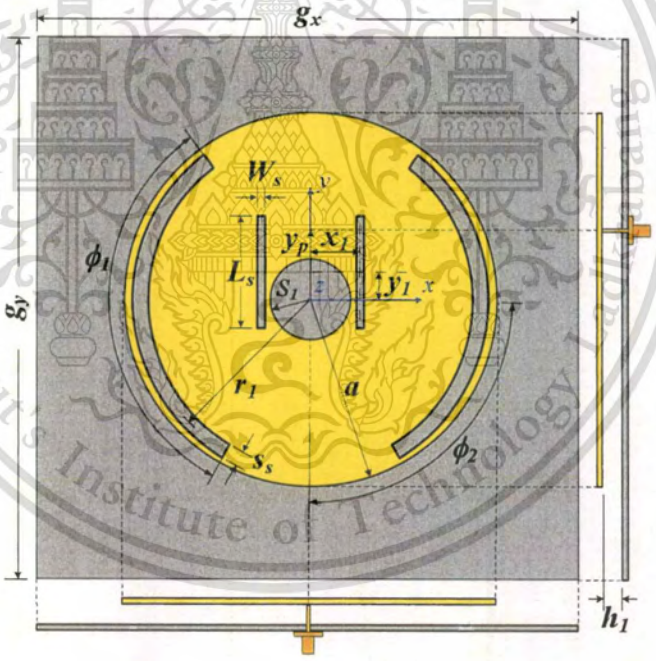

Figure 2.11 An annular plate antenna with curved and rectangular slots

Table 2.5 The initial parameters of the annular plate antenna with curved and rectangular slots.

Parameter	Dimension (mm)
Radius of annular plate (a)	83.5
Spacing between annular plate and ground plane (h_1)	7.5
Width of ground plane (g_x)	217
Length of ground plane (g_y)	217
Length of rectangular slot (L_s)	61
Radius of curved slot (r_1)	75
Radius of circular slot (S_1)	15
Width of curved slot (s_s)	10
Width of rectangular slot (W_s)	2
Spacing between rectangular slot and y-axis (x_1)	17
Spacing between the center of rectangular slot and x-axis (y_1)	0
Location of feeding in y-axis (y_p)	25
Length of curved slot (ϕ_1)	120°
Angle between the center of curved slot and y-axis (ϕ_2)	90°

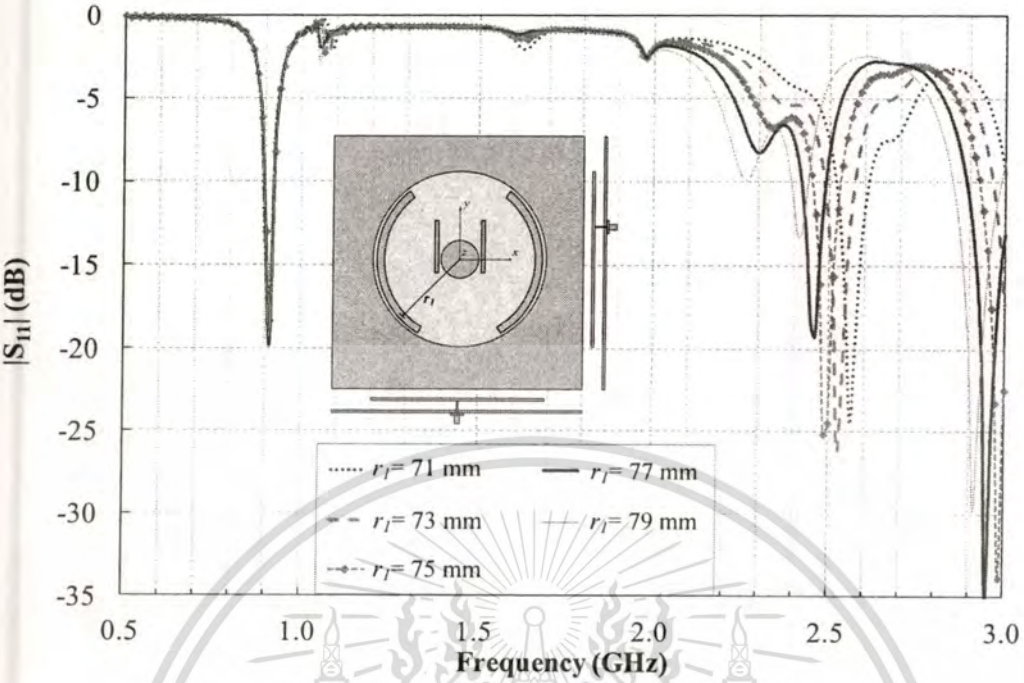

Figure 2.12 Frequency response of the magnitude of S_{11} for various parameter r_1, when remained parameters are in Table 2.5

(2) Varying the length of curved slot (ϕ_1) and the width of curved slot (s_s)

The next considering parameter is the length of the curved slots (ϕ_1). The resonant frequency in microwave band is lower when ϕ_1 is increased as illustrated in Fig. 2.13. Note that ϕ_1 has no important effect to the resonant frequency at the UHF band. The proper length of the curved slots is 90 mm. After that the width of curved slot (s_s) is varied to be 10 mm, 11 mm, 12 mm, 13 mm and 14 mm, which is about $\lambda_{2.45GHz}/10$ as illustrated in Fig. 2.14. It is evident that the parameter s_s does not sinificantly affect to both bands (UHF and microwave bands). The optimum width of curved slot (s_s) is 12 mm. However, the annular plate antenna cannot operate across the microwave band.

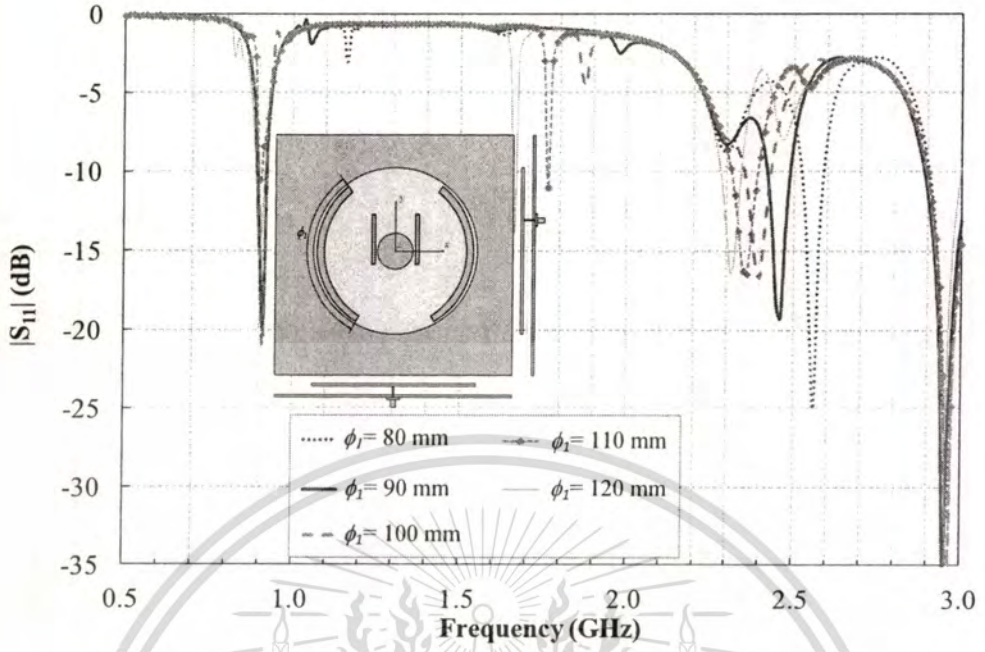

Figure 2.13 Frequency response of the magnitude of S_{11} for various parameter ϕ_1, when r_1=77 mm and remained parameters are in Table 2.5

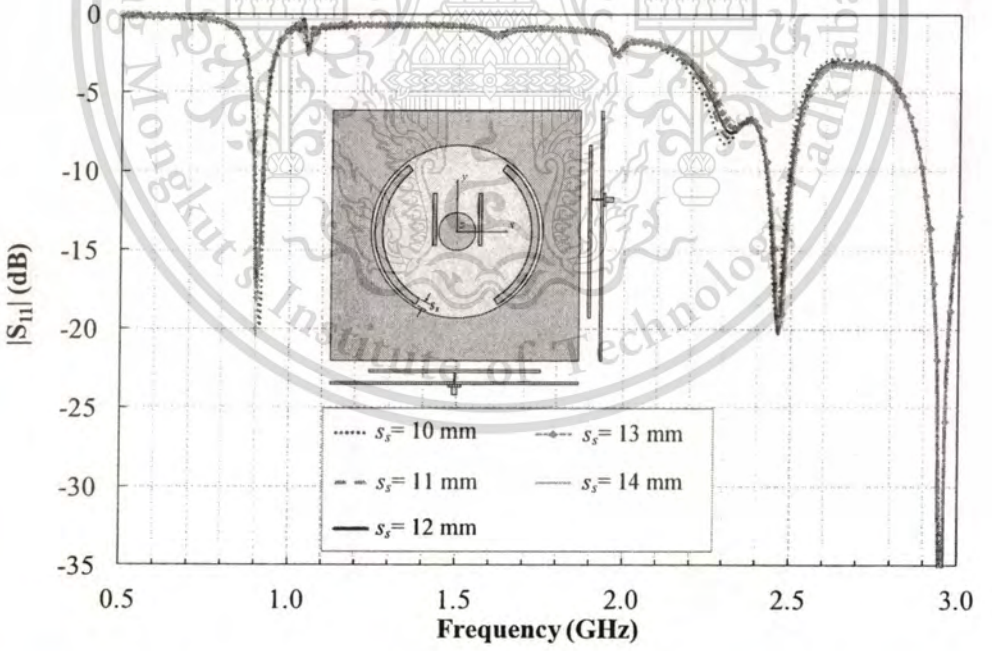

Figure 2.14 Frequency response of the magnitude of S_{11} for various parameter s_s, when r_1=77 mm, ϕ_1=90 mm and remained parameters are in Table 2.5

(3) Varying the length of rectangular slot (L_s) and the width of rectangular slot (W_s) to cover the microwave band

To obtain the magnitude of S_{11} better than -10 dB across the microwave band, the length and width of rectangular slot are adjusted as shown in Fig. 2.15. In the microwave band, the length of the rectangular slots (L_s) has important effect on the antenna bandwidth as illustrated in Fig. 2.15. The length of the rectangular slot (L_s) from 45 mm to 65 mm was varied. When the length is shorter, it tends that the antenna has the broader frequency response. The suitable length of rectangular slot (L_s) is 49 mm.

Besides the width of rectangular slot (W_s) is also adjusted as 1 mm, 2 mm and 3mm. It has slight effects on the level of magnitude of S_{11} as displayed in Fig. 2.16. Thus, the width of rectangular slot (W_s) using the initial parameter is equal to 2 mm.

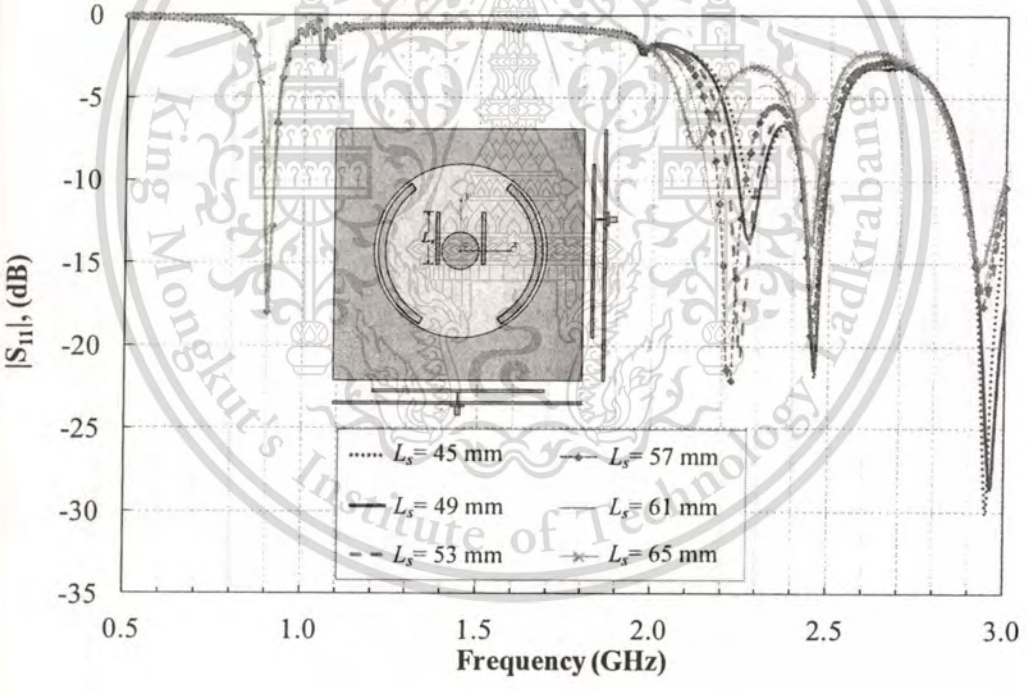

Figure 2.15 Frequency response of the magnitude of S_{11} for various parameter L_s, when r_1=77 mm, ϕ_1=90 mm, s_s=12 mm and remained parameters are in Table 2.5

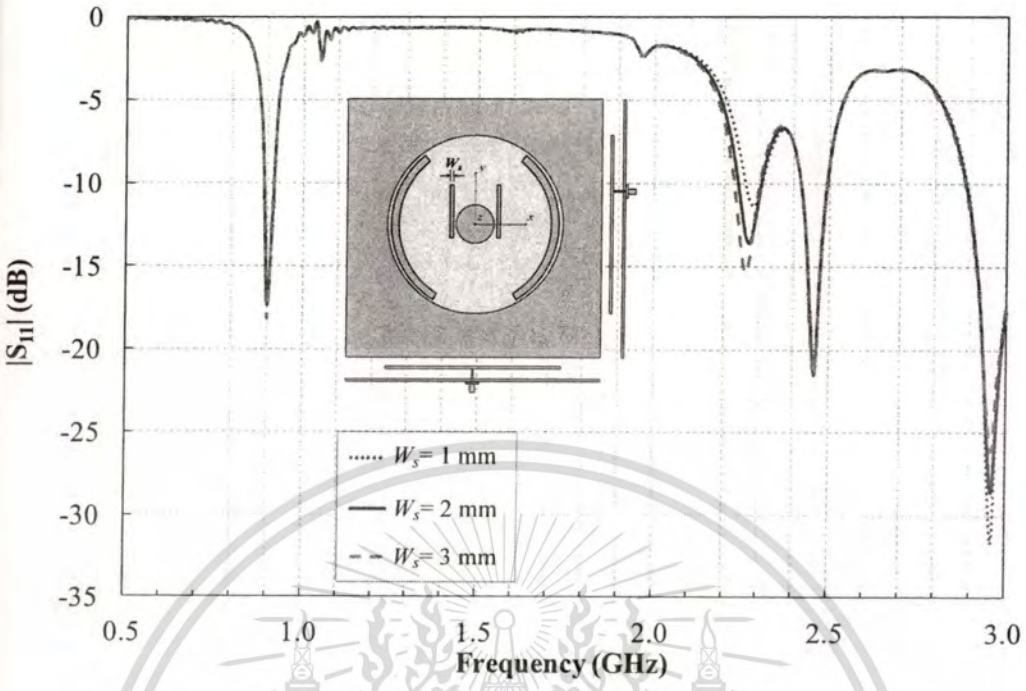

Figure 2.16 Frequency response of the magnitude of S_{11} for various parameter W_s, when r_1=77 mm, ϕ_1=90 mm, s_s=12 mm, L_s=49 mm and remained parameters are in Table 2.5

(4) Varying the spacing between rectangular slot and y-axis (x_1) and spacing between the center of rectangular slot and x-axis (y_1)

Figure 2.17 and Figure 2.18 show the effect of the spacing between rectangular slot and y-axis (x_1) and spacing between the center of rectangular slot and x-axis (y_1) on the magnitude of S_{11}. It is obvious that parameters x_1 and y_1 affect to the antenna bandwidth in microwave band. The appropriate parameters of the spacing between rectangular slot and y-axis (x_1) and spacing between the center of rectangular slot and x-axis (y_1) are 17 mm and 10 mm, respectively. Accordingly, the optimum parameters of the annular plate antenna with curved and rectangular slots are tabulated in Table 2.6.

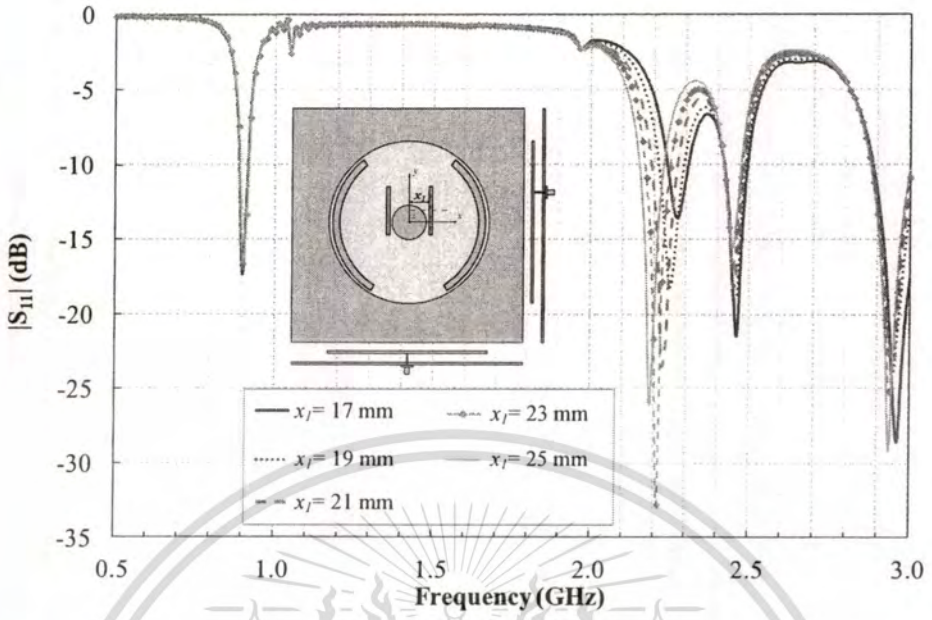

Figure 2.17 Frequency response of the magnitude of S_{11} for various parameter x_1, when r_1=77 mm, ϕ_1=90 mm, s_s=12 mm, L_s=49 mm, W_s=2 mm and remained parameters are in Table 2.5

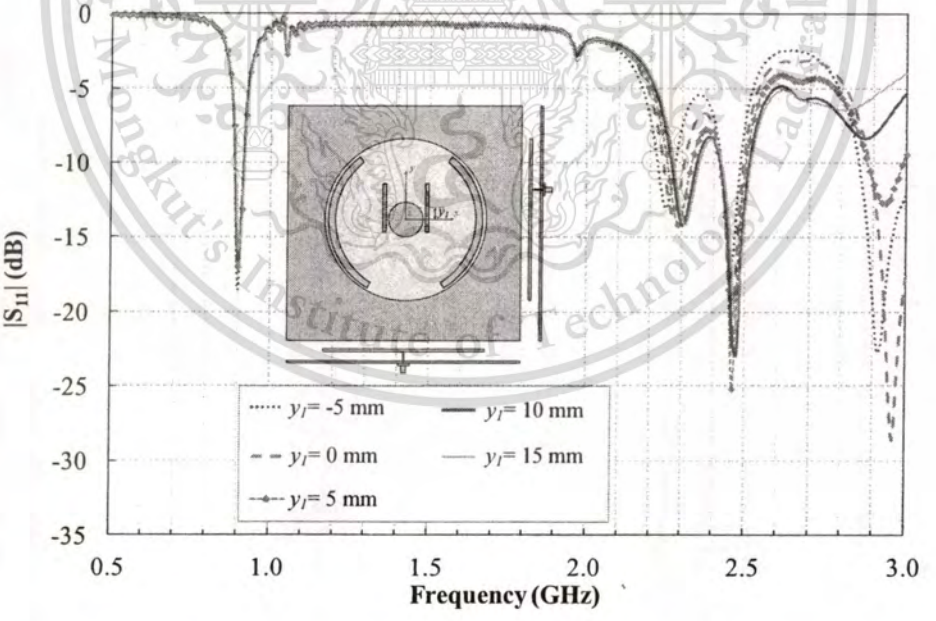

Figure 2.18 Frequency response of the magnitude of S_{11} for various parameter y_1, when r_1=77 mm, ϕ_1=90 mm, s_s=12 mm, L_s=49 mm, W_s=2 mm, x_1=17 mm and remained parameters are in Table 2.5

Table 2.6 The optimum parameters of the annular plate antenna with curved and rectangular slots

Parameter	Dimension (mm)
Radius of annular plate (a)	83.5
Spacing between annular plate and ground plane (h_1)	7.5
Width of ground plane (g_x)	217
Length of ground plane (g_y)	217
Length of rectangular slot (L_s)	49
Radius of curved slot (r_1)	77
Radius of circular slot (S_1)	15
Width of curved slot (s_s)	12
Width of rectangular slot (W_s)	2
Spacing between rectangular slot and y-axis (x_1)	17
Spacing between the center of rectangular slot and x-axis (y_1)	10
Location of feeding in y-axis (y_p)	25
Length of curved slot (ϕ_1)	90°
Angle between the center of curved slot and y-axis (ϕ_2)	90°

From the simulated results of the annular plate antenna with curved and rectangular slots on vertical ground plane with the optimum parameters in Table 2.6, the magnitude of S_{11} is shown in Fig. 2.19. At the center frequency of UHF band of 922.5 MHz, the radiation pattern is a unidirectional beam as illustrated in Fig. 2.20. However, the radiation pattern at frequency of 2.45 GHz is a unidirectional with a tilt angle as shown in Fig. 2.21. Thus, the modified antenna is performed to improve the radiation pattern in microwave band that the vertical ground plane is used, which will be discussed in detail in the next section.

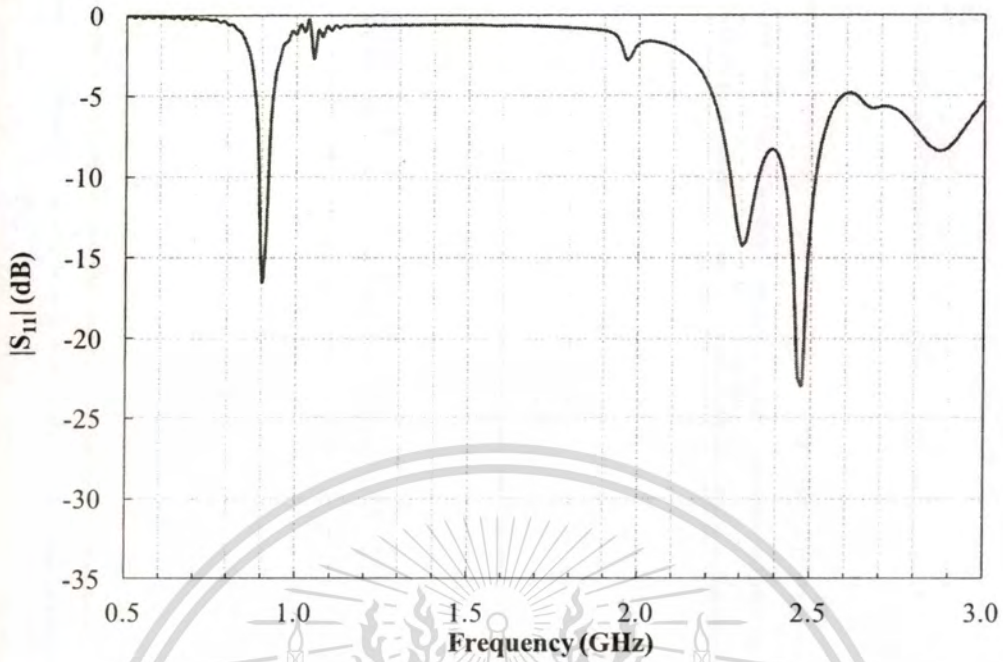

Figure 2.19 Frequency response of the magnitude of S_{11}, when remained parameters are in Table 2.6

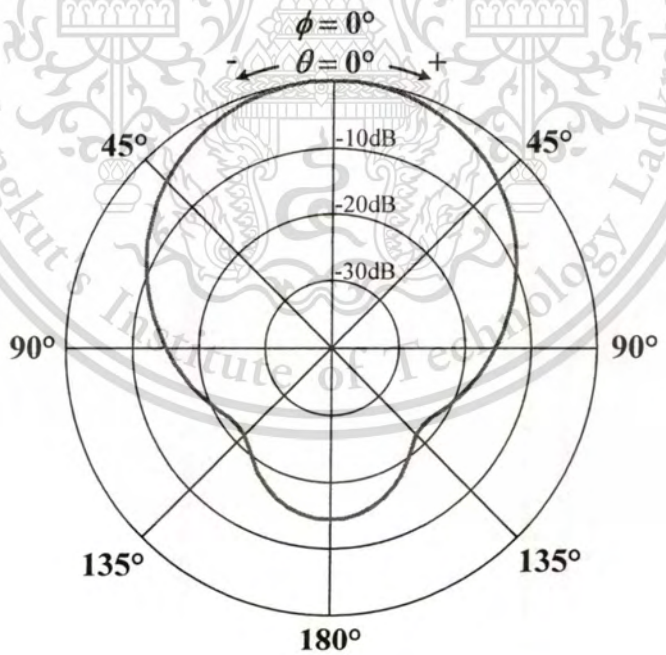

(a)

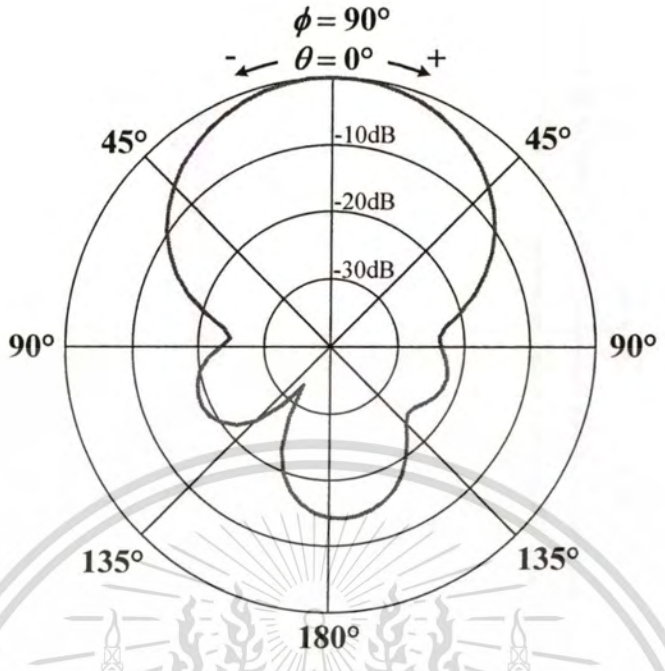

(b)

Figure 2.20 The radiation pattern at the frequency of 922.5 MHz (a) xz-plane (b) yz-plane

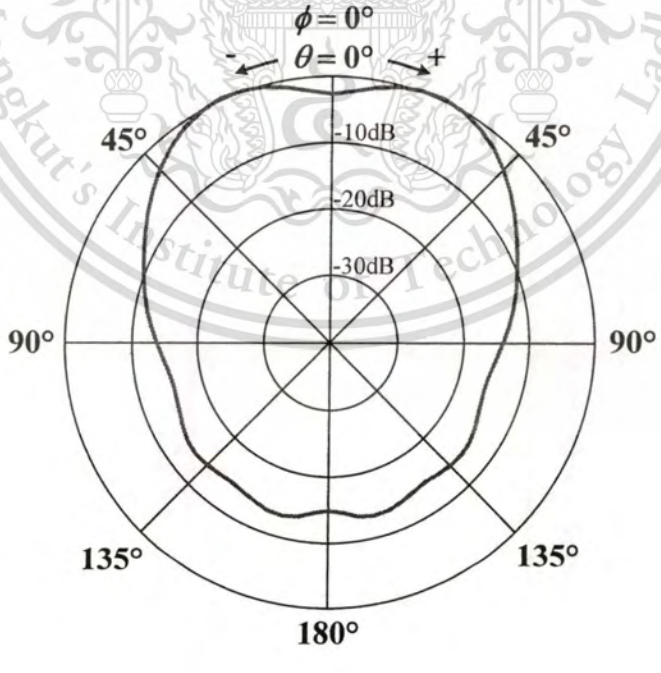

(a)

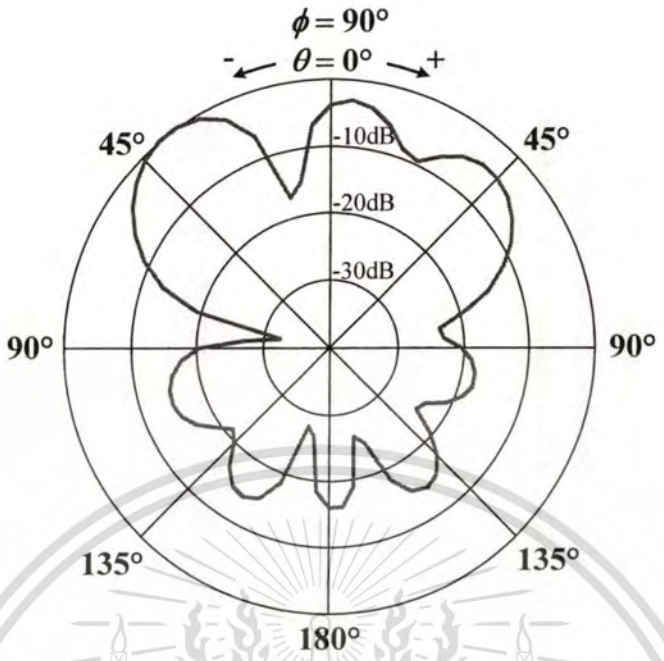

(b)

Figure 2.21 The radiation pattern at the frequency of 2.45 GHz (a) xz-plane (b) yz-plane

2.3.4 An annular plate antenna with curved and rectangular slots on vertical ground plane

From the previous section, in microwave band, the annular plate antenna with curved and rectangular slots has the unidirectional pattern with beam tilt-angle. Several techniques can be used for improvement. In this study, a modified ground plane technique is utilized that can compensate for the beam tilt angles. The vertical ground plane is applied as shown in Fig. 2.22. The initial parameters of the annular plate antenna with curved and rectangular slots on vertical ground plane are illustrated in Table 2.7.

Figure 2.23 and Figure 2.24 present frequency responses of the magnitude of S_{11} and radiation patterns at frequency of 922.5 MHz and 2.45 GHz for various heights of vertical ground plane (h_2 and h_3), when parameters are in Table 2.7. It is obvious that h_2 and h_3 has important effect to the level of magnitude of S_{11}. Furthermore, the height of

vertical ground plane can improve the radiation pattern in microwave band. The selected h_2 and h_3 are 40 mm and 45 mm, respectively.

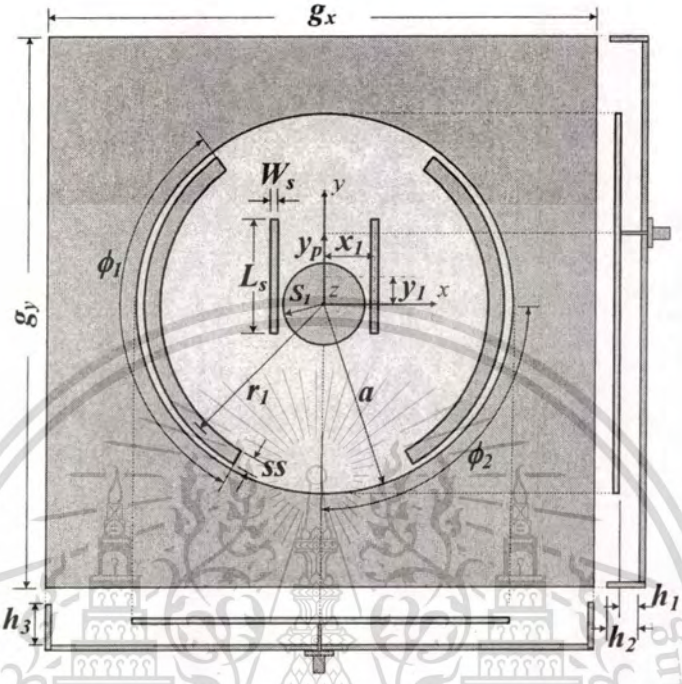

Figure 2.22 An annular plate antenna with curved and rectangular slots on vertical ground plane

Table 2.7 The initial parameters of annular plate antenna with curved and rectangular slots on vertical ground plane

Parameter	Dimension (mm)
Radius of annular plate (a)	83.5
Spacing between annular plate and ground plane (h_1)	7.5
Width of ground plane (g_x)	217
Length of ground plane (g_y)	217
Height of vertical ground plane in x-axis (h_2)	50
Height of vertical ground plane in y-axis (h_3)	50
Length of rectangular slot (L_s)	49
Radius of curved slot (r_1)	77
Radius of circular slot (S_1)	15

Parameter	Dimension (mm)
Width of curved slot (s_s)	12
Width of rectangular slot (W_s)	2
Spacing between rectangular slot and y-axis (x_1)	17
Spacing between the center of rectangular slot and x-axis (y_1)	10
Location of feeding in y-axis (y_p)	25
Length of curved slot (ϕ_1)	90°
Angle between the center of curved slot and y-axis (ϕ_2)	90°

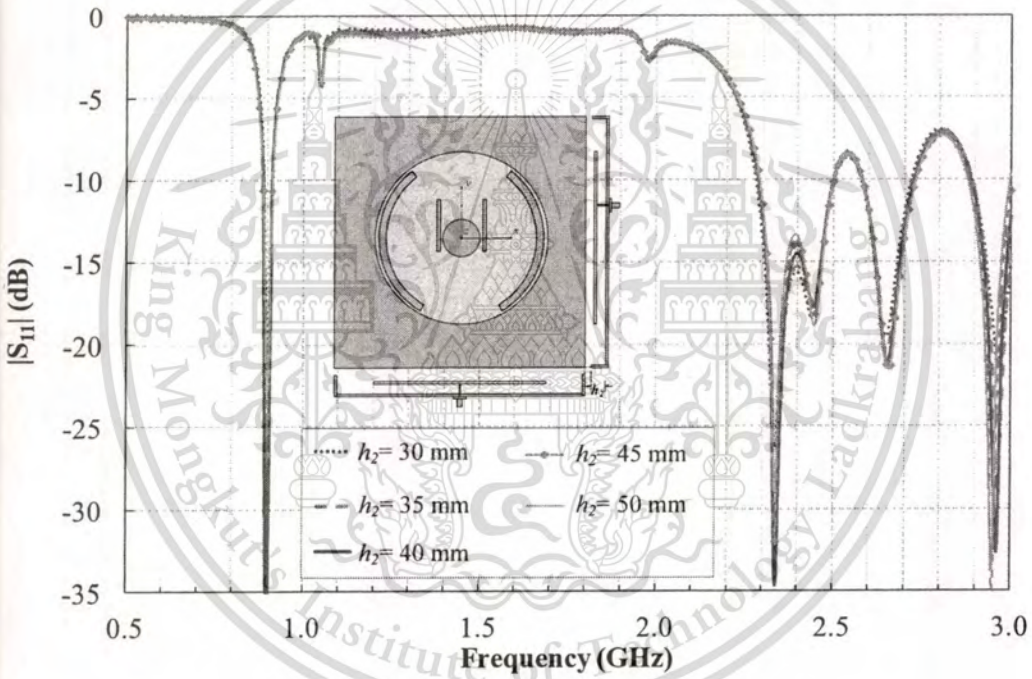

(a) Frequency response of the magnitude of S_{11} for various parameter h_2, when remained parameters are in Table 2.7

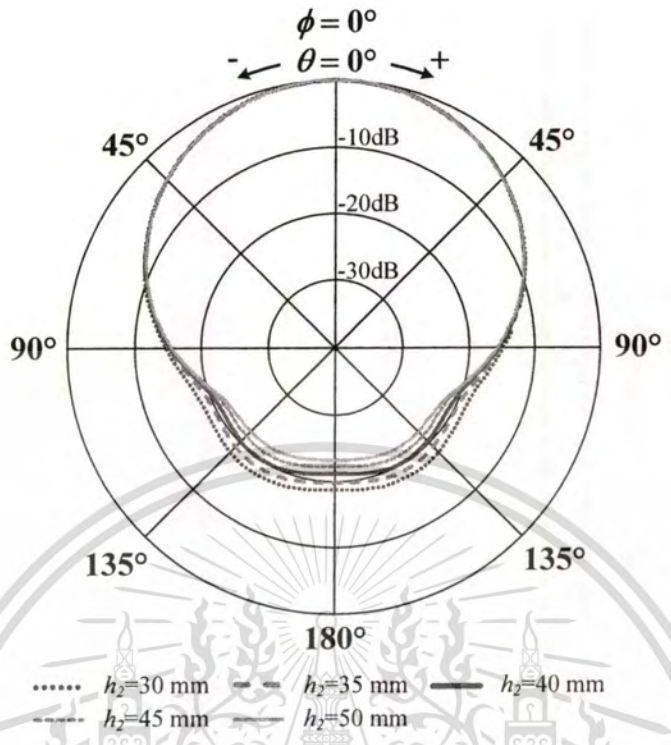

(b) Radiation pattern in xz-plane at the frequency of 922.5 MHz

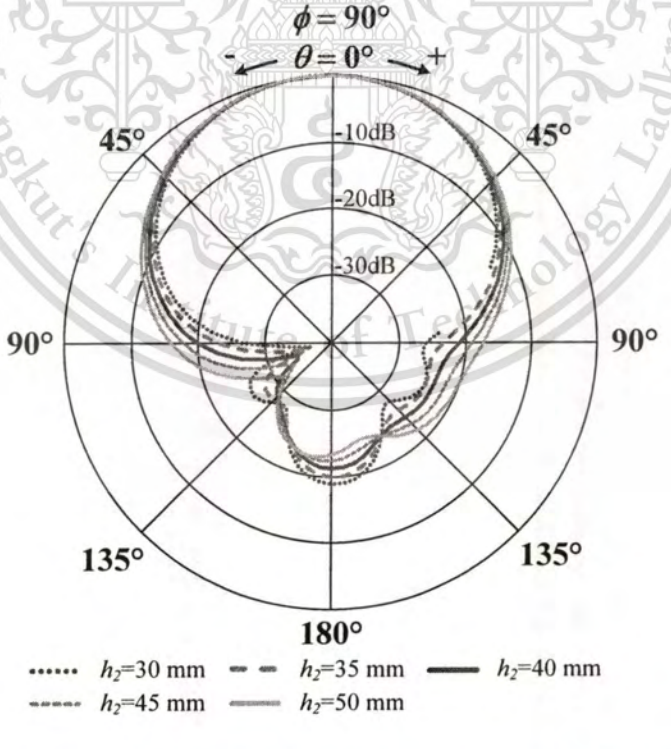

(c) Radiation pattern in yz-plane at the frequency of 922.5 MHz

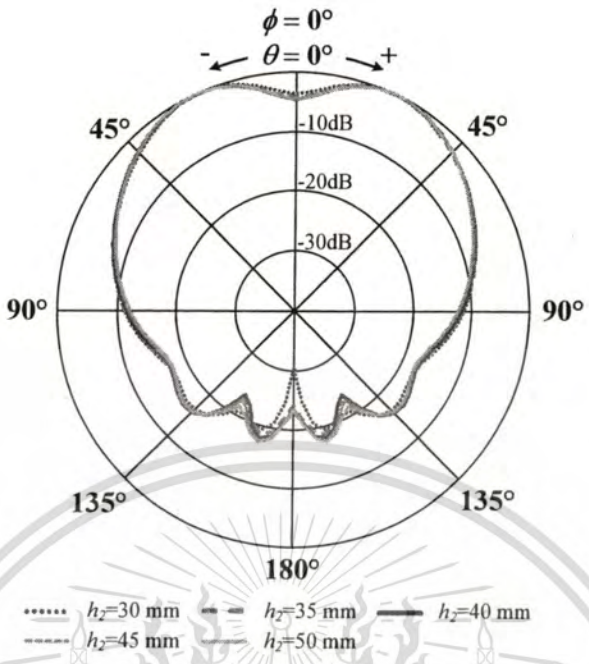

(d) Radiation pattern in xz-plane at the frequency of 2.45 GHz

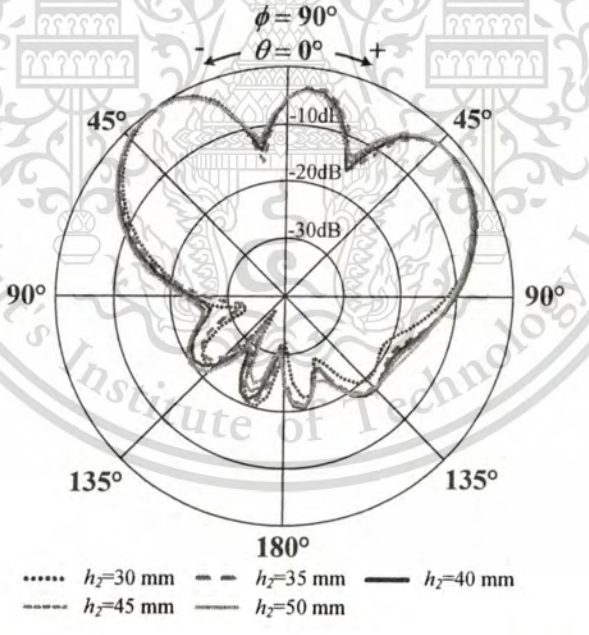

(e) Radiation pattern in yz-plane at the frequency of 2.45 GHz

Figure 2.23 Frequency response of the magnitude of S_{11} for various parameter h_2 and radiation pattern at the frequency of 922.5 MHz and 2.45 GHz, when parameters are in Table 2.7

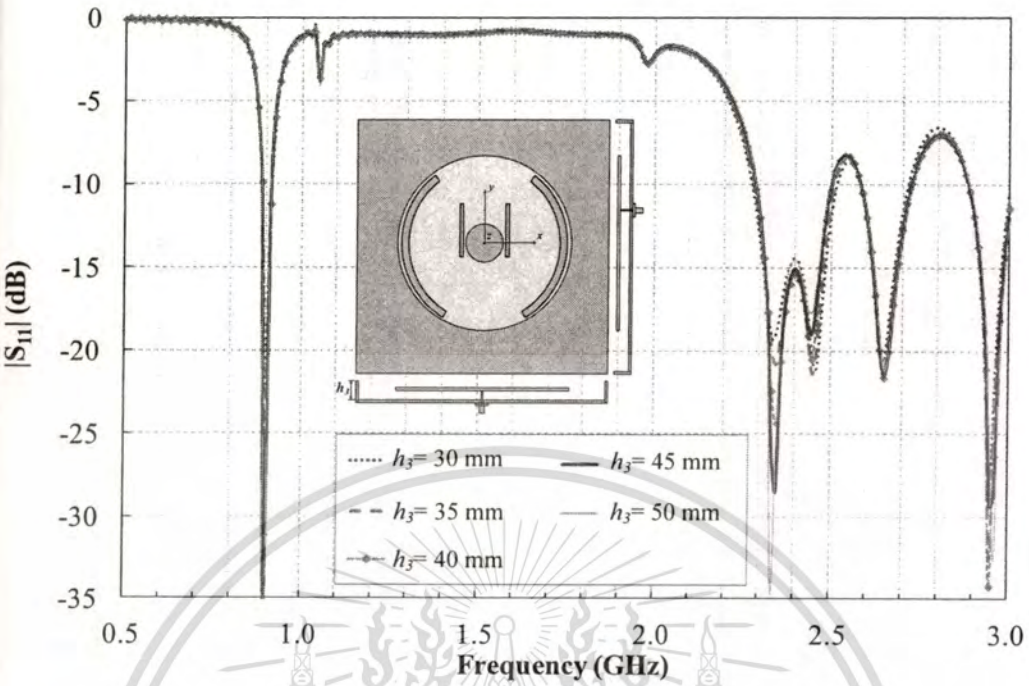

(a) Frequency response of the magnitude of S_{11} for various parameter h_3, when remained parameters are in Table 2.7

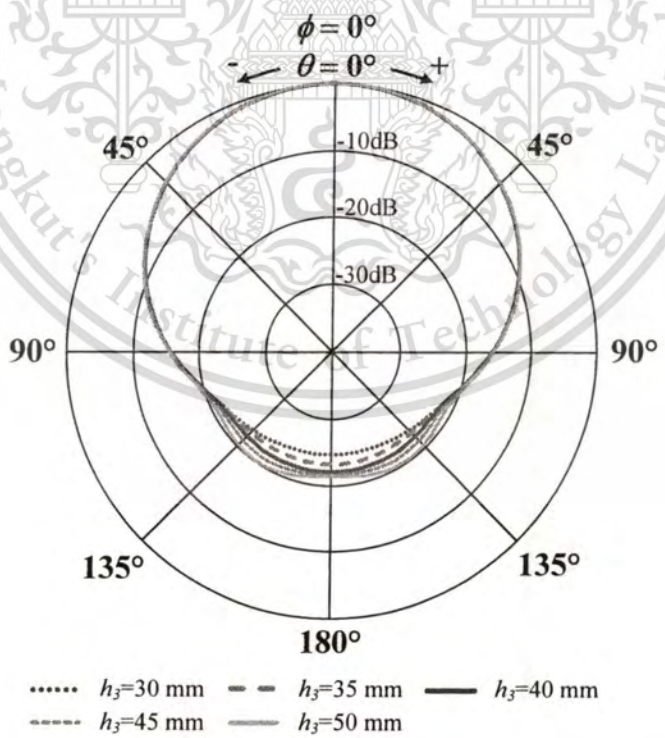

(b) Radiation pattern in xz-plane at the frequency of 922.5 MHz

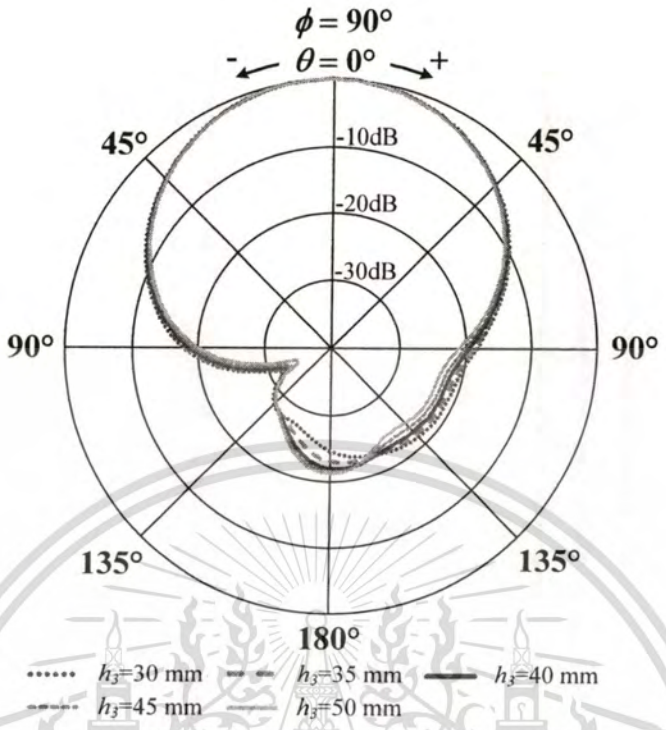

(c) Radiation pattern in yz-plane at the frequency of 922.5 MHz

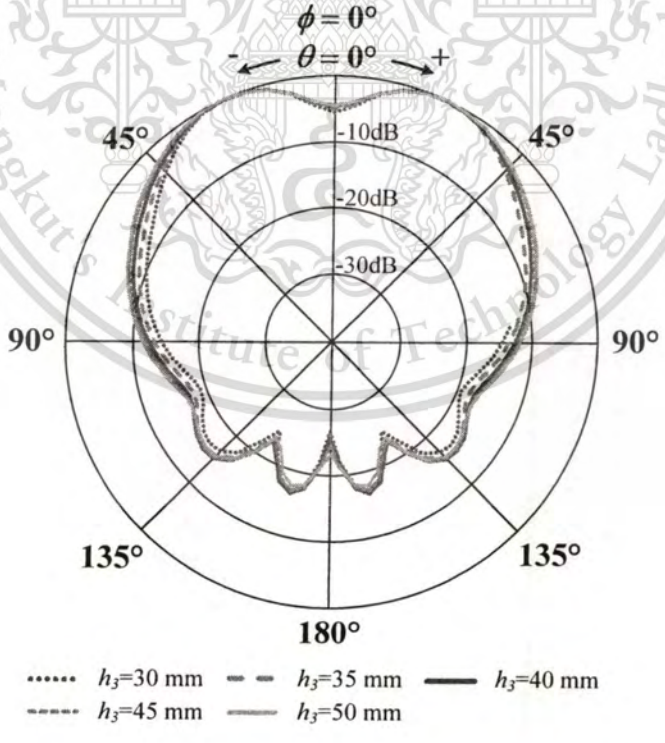

(d) Radiation pattern in xz-plane at the frequency of 2.45 GHz

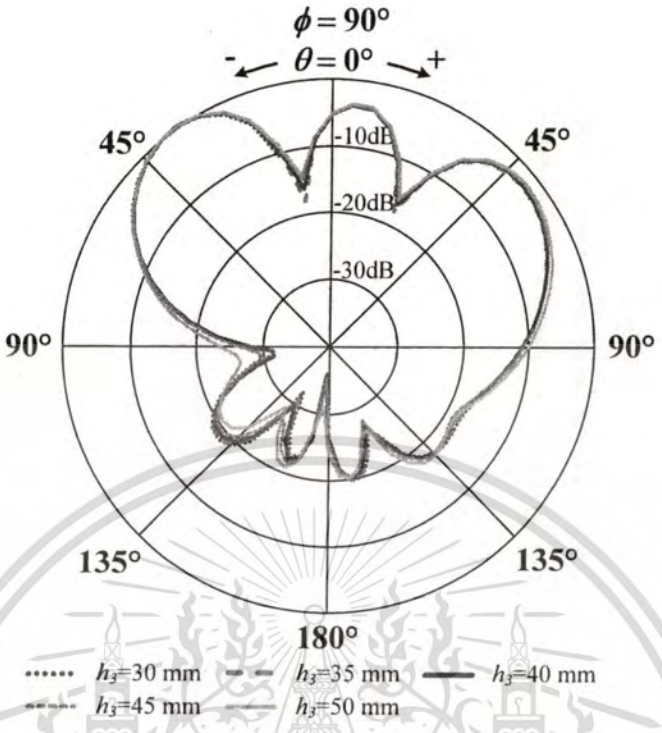

(e) Radiation pattern in yz-plane at the frequency of 2.45 GHz

Figure 2.24 Frequency response of the magnitude of S_{11} for various parameter h_3 and radiation pattern at the frequency of 922.5 MHz and 2.45 GHz, when parameters are in Table 2.7

This section presents the annular plate antenna with curved and rectangular slots on vertical ground plane to operate the dual-band frequency of UHF and microwave band. The optimum parameters are summarized in Table 2.8. Note that the radiation pattern in microwave band trends to be a unidirectional beam in broadside direction that it will be optimized using the optimization function in CST Microwave Studio to achieve a unidirectional pattern.

Table 2.8 The optimum parameters of annular plate antenna with curved and rectangular slots on vertical ground plane.

Parameter	Dimension (mm)
Radius of annular plate (a)	83.5
Spacing between annular plate and ground plane (h_1)	7.5
Width of ground plane (g_x)	217
Length of ground plane (g_y)	217
Height of vertical ground plane in x-axis (h_2)	40
Height of vertical ground plane in y-axis (h_3)	45
Length of rectangular slot (L_s)	49
Radius of curved slot (r_1)	77
Radius of circular slot (S_1)	15
Width of curved slot (s_s)	12
Width of rectangular slot (W_s)	2
Spacing between rectangular slot and y-axis (x_1)	17
Spacing between the center of rectangular slot and x-axis (y_1)	10
Location of feeding in y-axis (y_p)	25
Length of curved slot (ϕ_1)	90°
Angle between the center of curved slot and y-axis (ϕ_2)	90°

2.4 Antenna Optimization

This section presents the characteristics of the annular plate antenna with curved and rectangular slots on vertical ground plane using the optimization function in the CST Microwave Studio. The initial parameters for the optimization function are tabulated in Table 2.8. Subsequently, the optimum parameters are shown in Table 2.9 with the simulated results.

Table 2.9 The parameters of the annular plate antenna with curved and rectangular slots on vertical ground plane using the optimization function in the CST Microwave Studio.

Parameter	Dimension (mm)
Radius of annular plate (a)	83.5
Spacing between annular plate and ground plane (h_1)	7.5
Height of vertical ground plane in x-axis (h_2)	40
Height of vertical ground plane in y-axis (h_3)	50
Width of ground plane (g_x)	187.5
Length of ground plane (g_y)	225.5
Length of rectangular slot (L_s)	49.5
Radius of curved slot (r_1)	72.5
Radius of circular slot (S_1)	18
Width of curved slot (s_s)	11.5
Width of rectangular slot (W_s)	2
Spacing between rectangular slot and y-axis (x_1)	25
Spacing between the center of rectangular slot and x-axis (y_1)	14.5
Location of feeding in y-axis (y_p)	26
Length of curved slot (ϕ_1)	100°
Angle between the center of curved slot and y-axis (ϕ_2)	90°

The annular plate antenna with curved and rectangular slots on vertical ground plane can be operated a dual-band from 912 MHz to 925 MHz (13 MHz) and from 2.32 GHz to 2.69 GHz (360 MHz) as shown in Fig. 2.25.

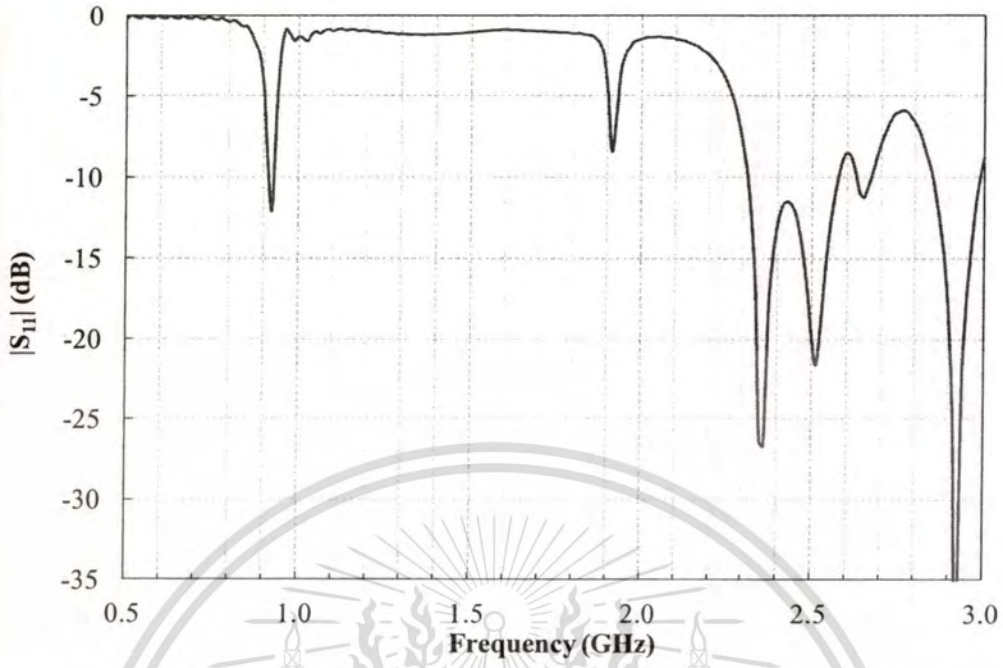

Figure 2.25 Frequency response of the magnitude of S_{11} when remained parameters are in Table 2.9

The radiation patterns are unidirectional beam for both frequencies of UHF and microwave bands. Figures 2.26, 2.27 and 2.28 show the radiation patterns at frequencies of 920 MHz, 922.5 MHz and 925 MHz, respectively. Let us consider at the center frequency the UHF band (922.5 MHz), the half-power beamwidths in xz-plane and yz-plane are 50° and 80°, respectively. The radiation patterns at frequencies of 2.40 GHz, 2.45 GHz and 2.50 GHz are illustrated in Fig. 2.29, 2.30 and 2.31, respectively. At the center frequency of microwave band (2.45 GHz), the half-power beamwidths in xz- and yz-planes are 35° and 10°, respectively.

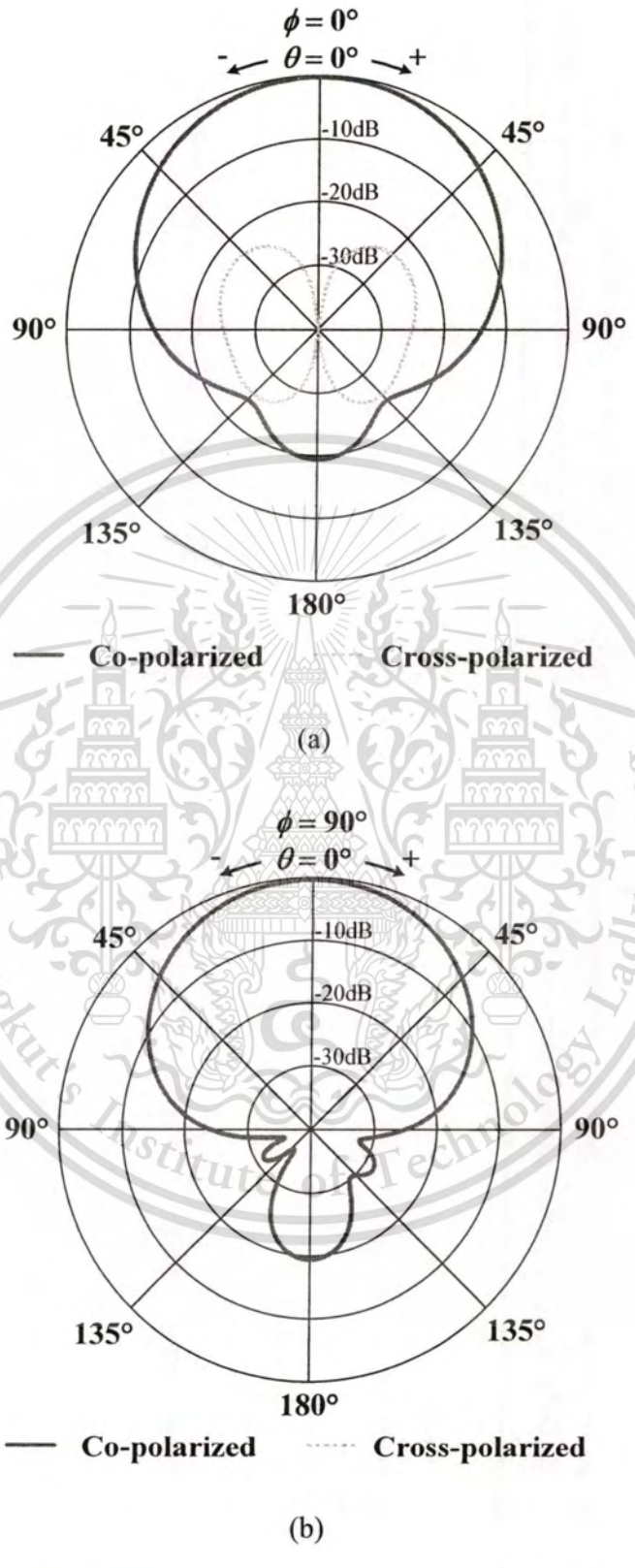

Figure 2.26 Radiation pattern at the frequency of 920 MHz (a) xz-plane (b) yz-plane

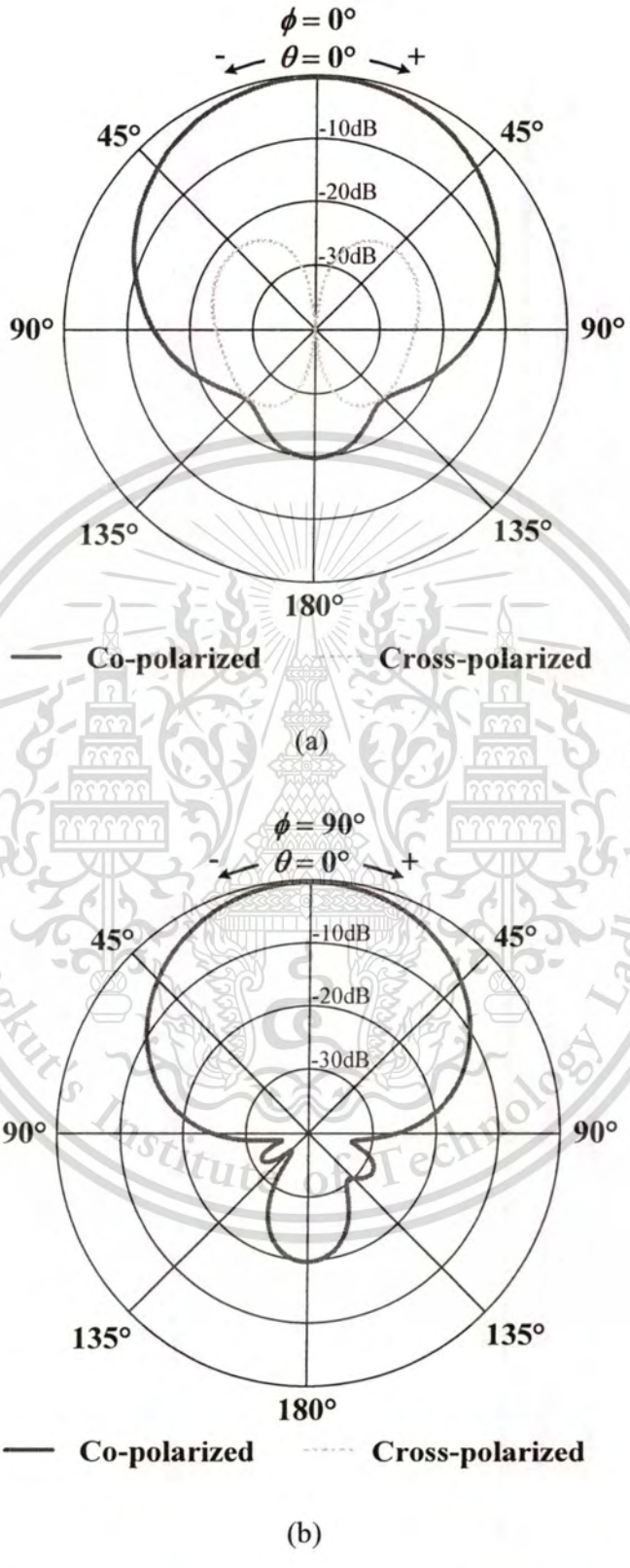

Figure 2.27 Radiation pattern at the frequency of 922.5 MHz (a) xz-plane (b) yz-plane

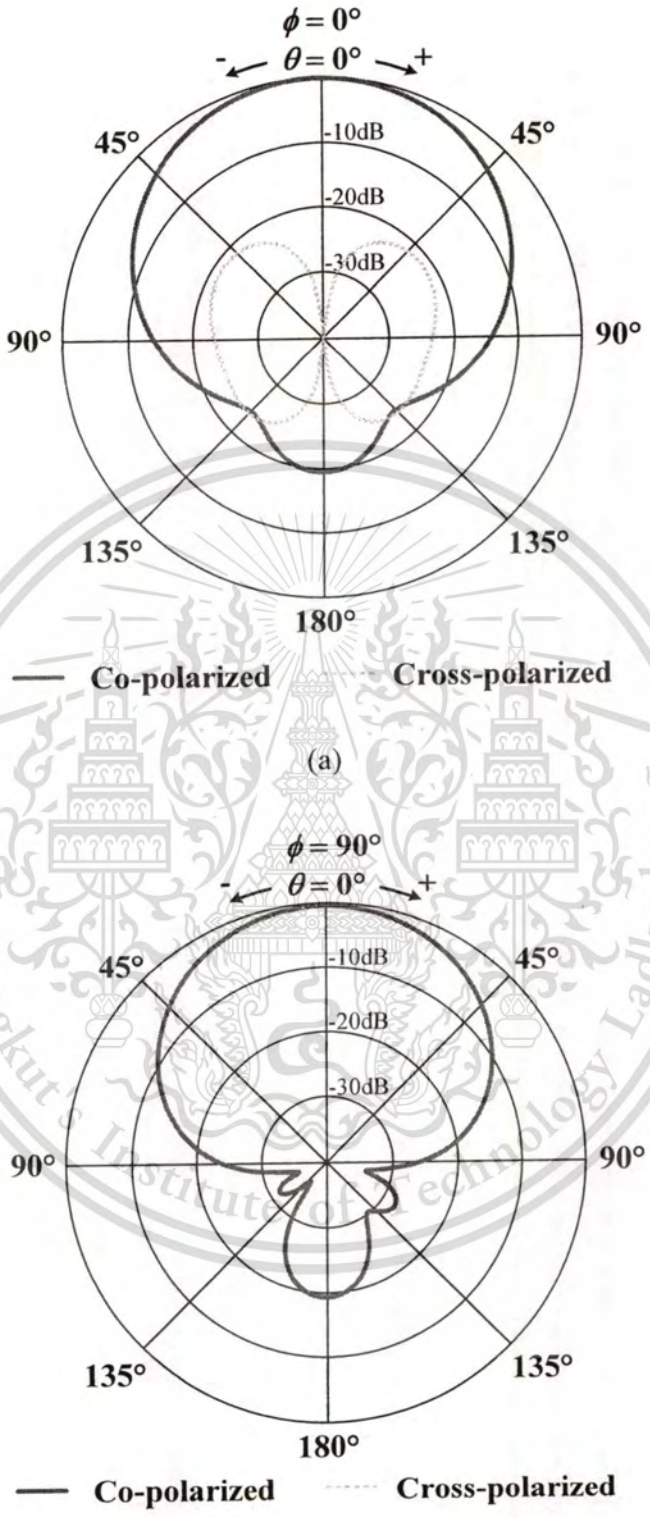

Figure 2.28 Radiation pattern at the frequency of 925 MHz (a) xz-plane (b) yz-plane

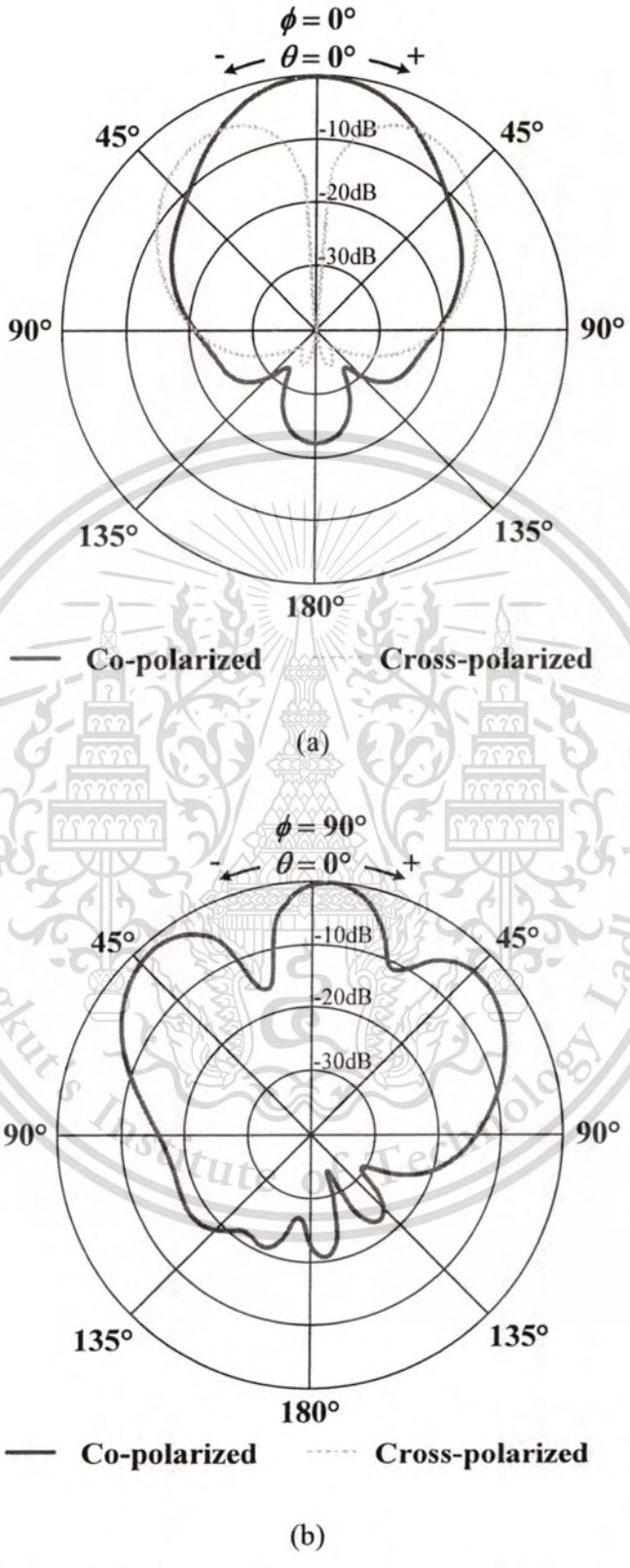

Figure 2.29 Radiation pattern at the frequency of 2.40 GHz (a) xz-plane (b) yz-plane

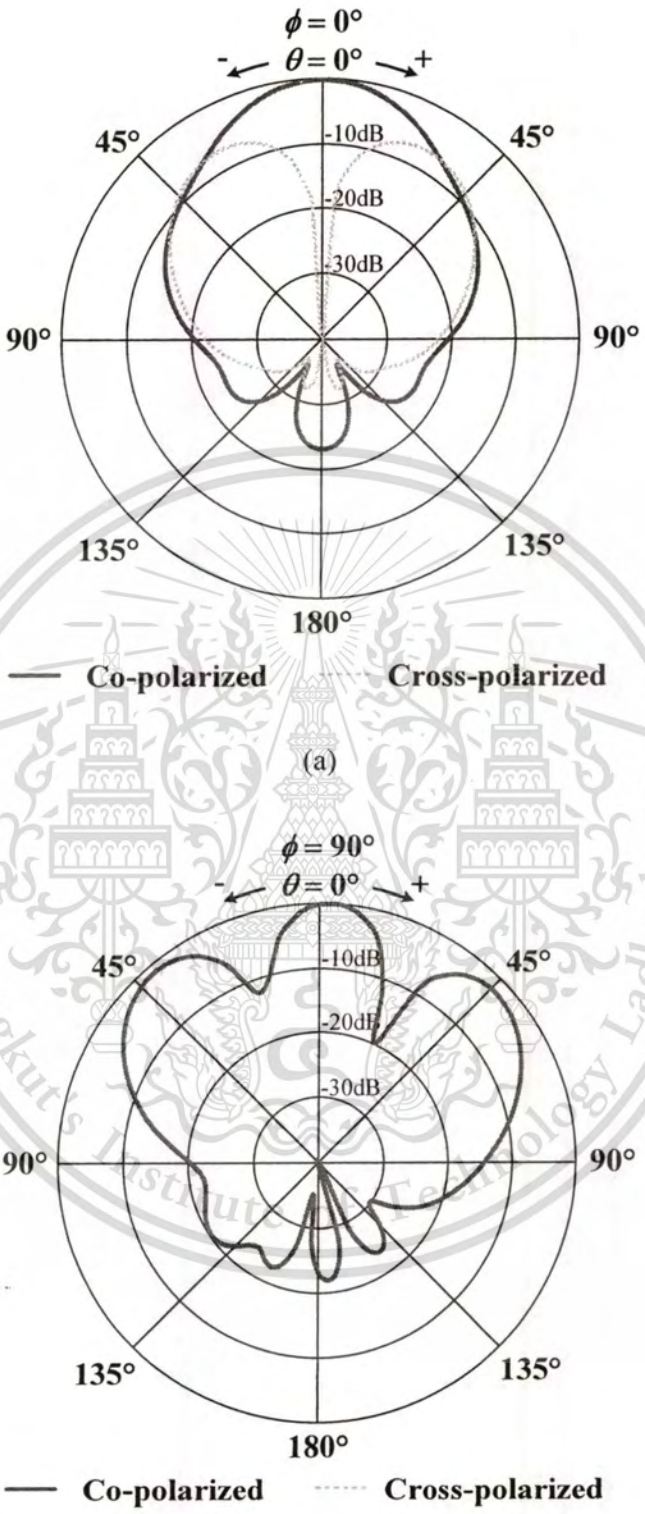

Figure 2.30 Radiation pattern at the frequency of 2.45 GHz (a) xz-plane (b) yz-plane

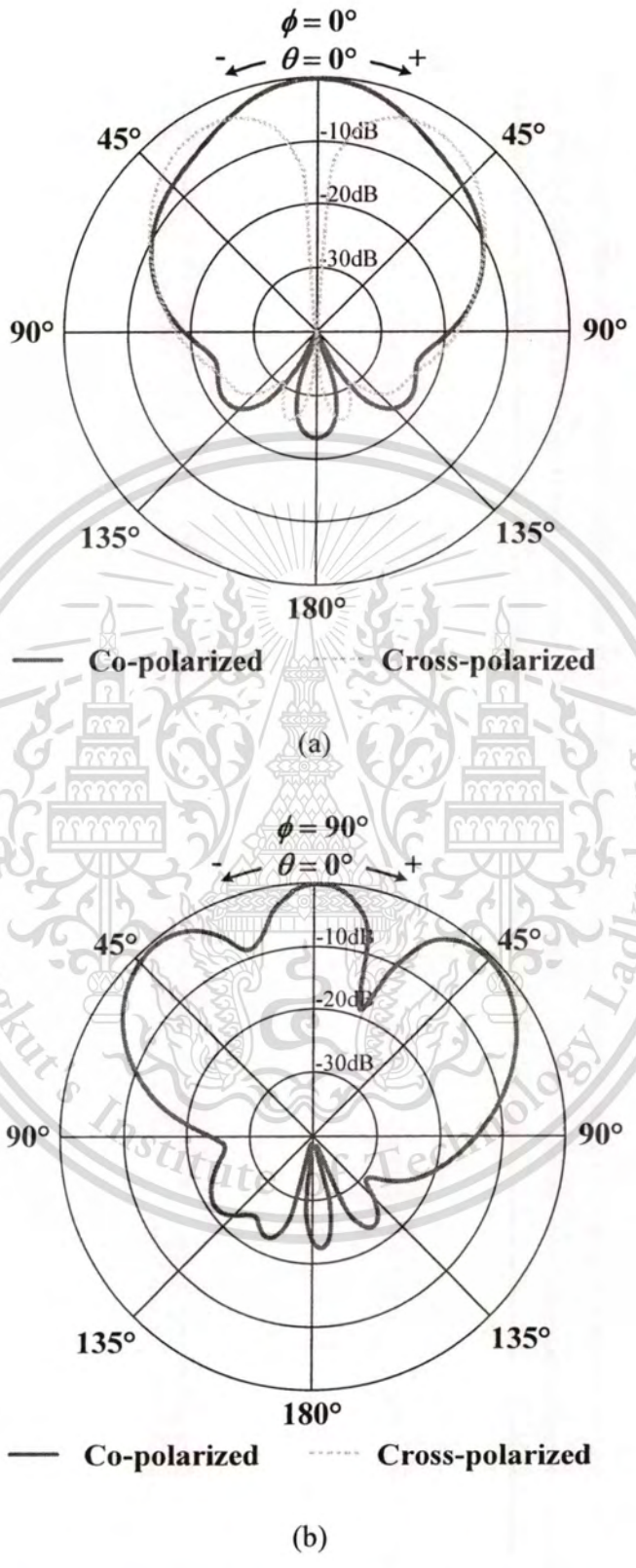

Figure 2.31 Radiation pattern at the frequency of 2.50 GHz (a) xz-plane (b) yz-plane

Considering the frequency ranges from 920 MHz to 925 MHz and from 2.4 GHz to 2.5 GHz, the antenna gain is depicted in Fig. 2.32. It is found that the antenna gains at frequencies of 922.5 MHz and 2.45 GHz are 8.3 dBi and 10.4 dBi, respectively. Besides the radiation efficiencies in UHF band are about 97 % and more than 99 % in microwave band as exhibited in Fig. 2.33.

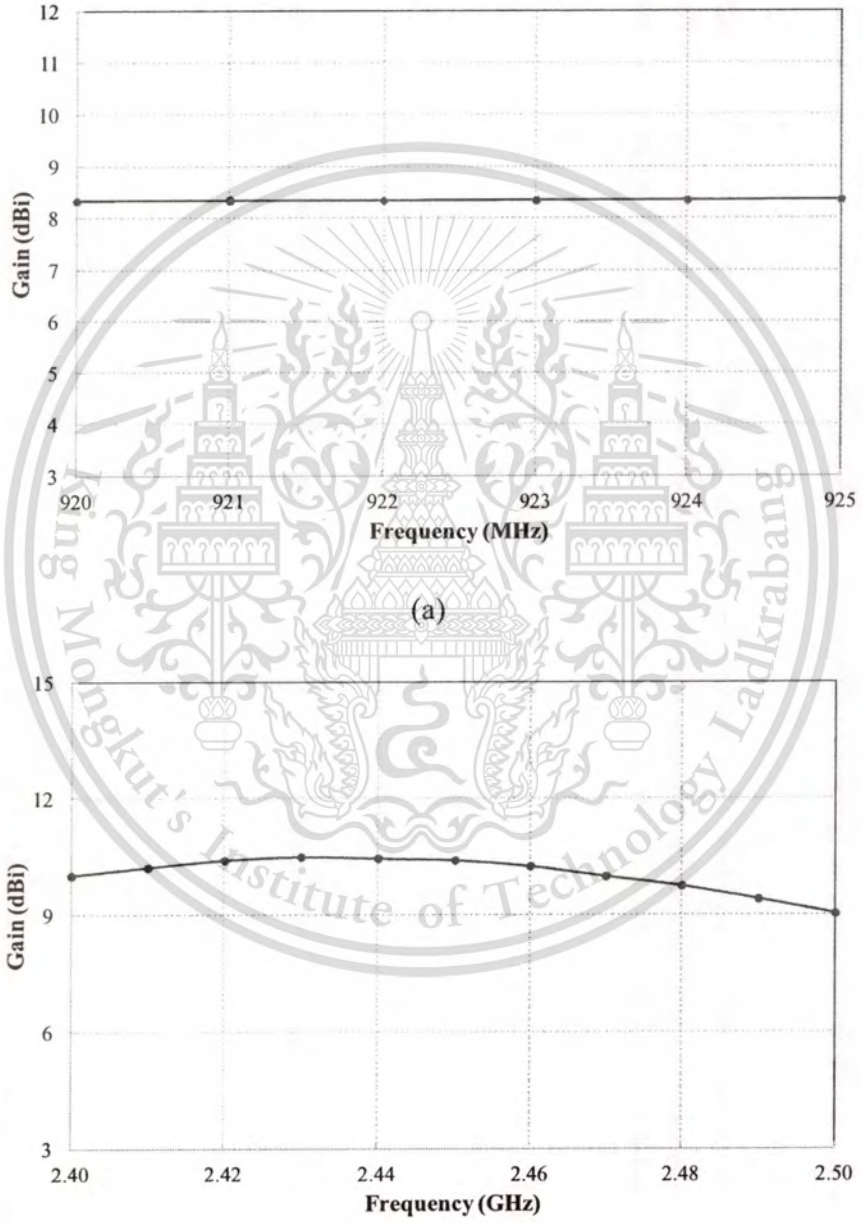

Figure 2.32 Antenna gain (a) UHF band (b) microwave band

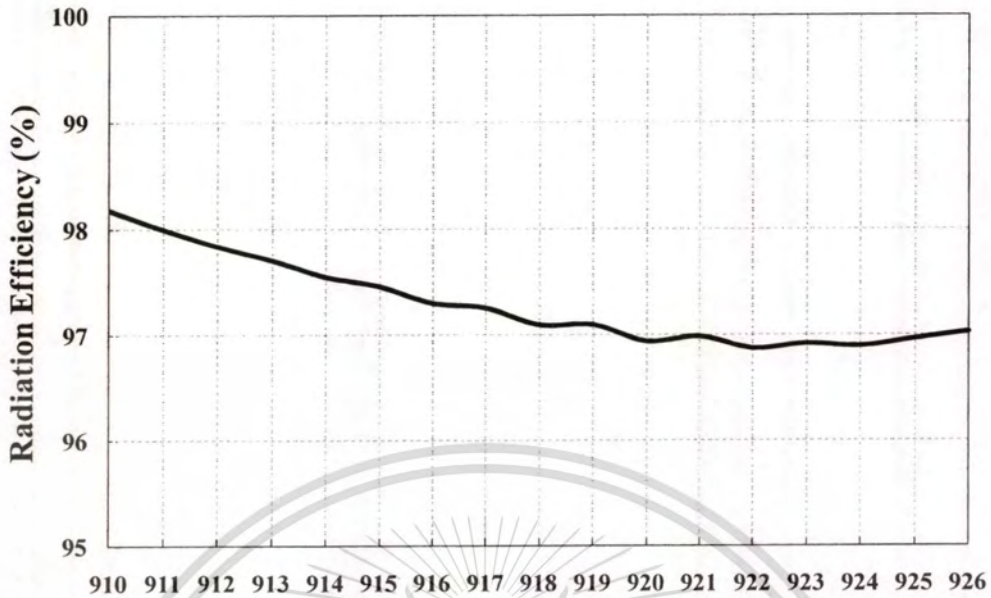

(a)

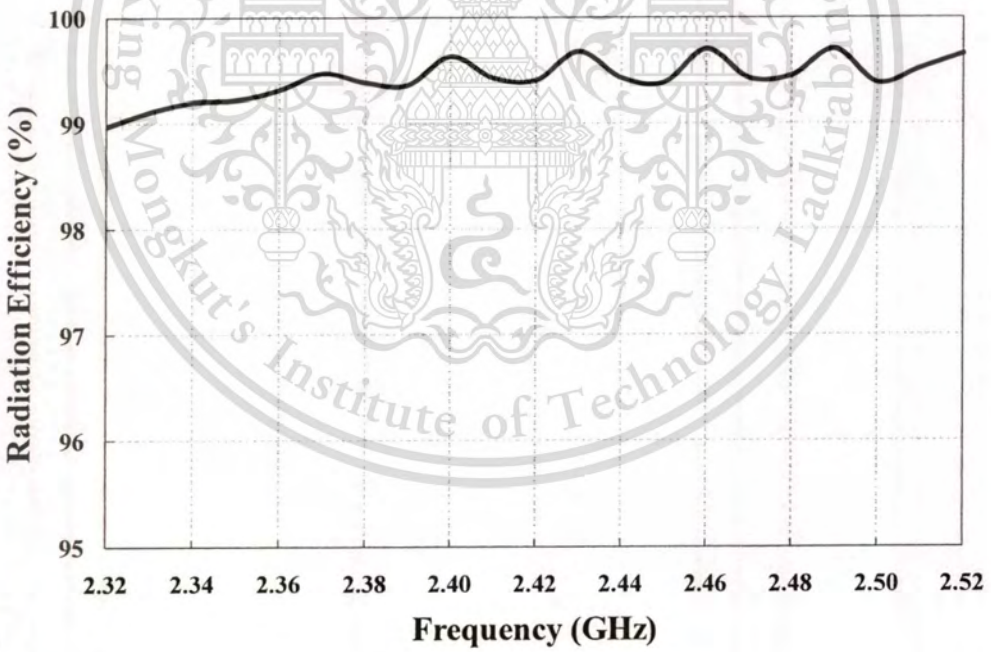

(b)

Figure 2.33 The radiation efficiency (a) UHF band (b) microwave band

Considering the surface current on the radiating annular plate with the curved and rectangular slots, it is evident that the surface current in UHF band is dense at the outer and inner radii of annular plate as shown in Fig. 2.34. For microwave band, the surface current is intense at the curved and rectangular slots as shown in Fig. 2.35. From the results, it is implied that the annular plate is considerable component to respond in UHF band and the curved and rectangular slots are considerable components to respond in microwave band.

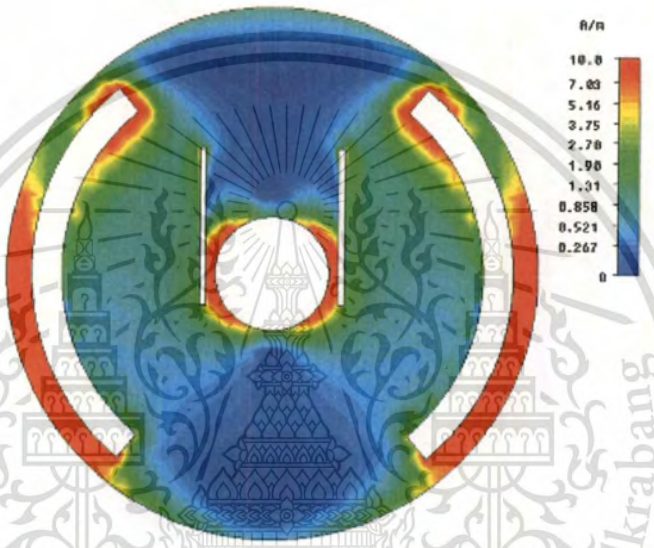

(a) Frequency of 920 MHz

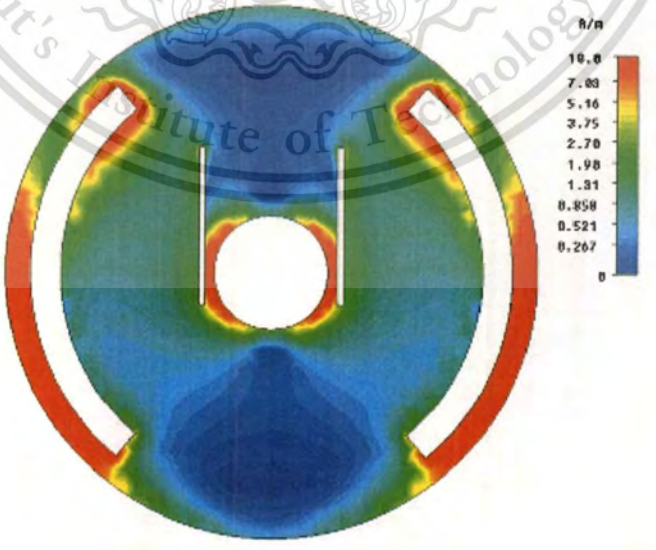

(b) Frequency of 922.5 MHz

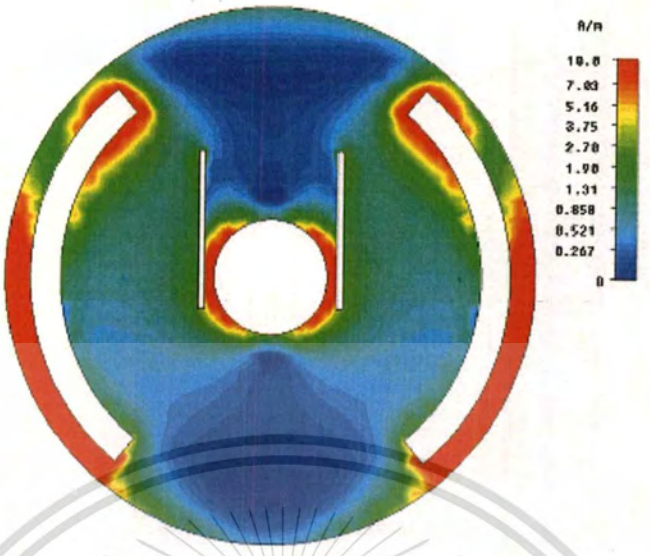

(c) Frequency of 925 MHz

Figure 2.34 Surface current on the radiating annular plate at UHF band

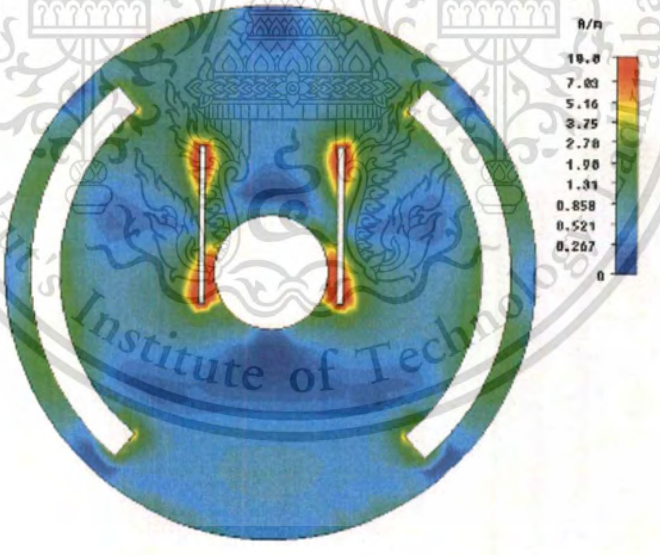

(a) Frequency of 2.40 GHz

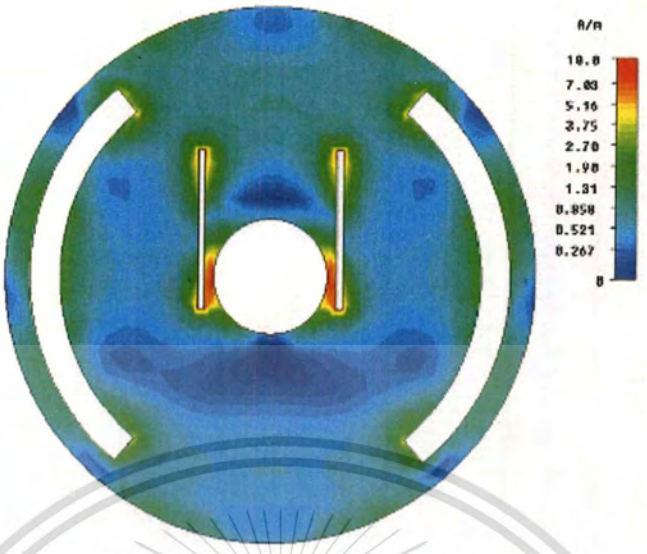

(b) Frequency of 2.45 GHz

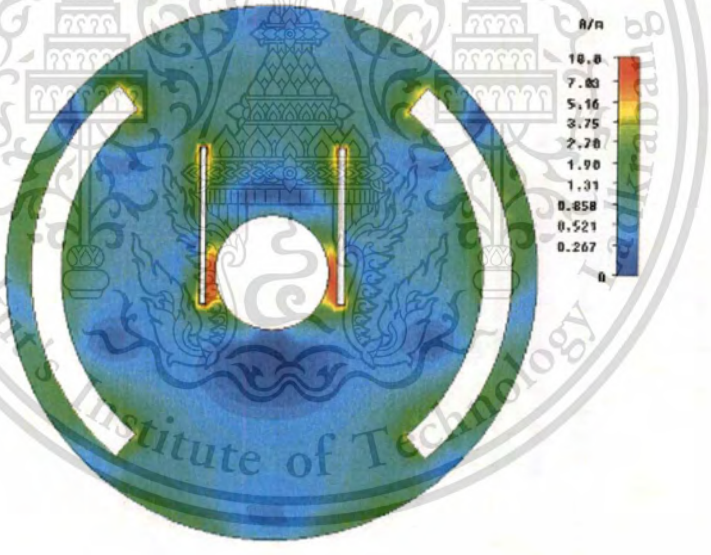

(c) Frequency of 2.5 GHz

Figure 2.35 Surface current on the radiating annular plate at microwave band

2.5 Summary

This chapter discussed the design and simulation to determine the optimum parameters of the annular plate antenna with curved and rectangular slots on vertical ground plane. The proposed antenna is employed to the RFID reader antenna that it can be operated in a dual-band of UHF and microwave band. Using the slot techniques, the antenna can be responded at the dual frequency band. To obtain the high-gain and avoid the dielectric loss in lossy material substrate that air is used as antenna substrate. From the simulated results, the magnitude of S_{11} of the annular plate antenna with curved and rectangular slots on vertical ground plane better than -10 dB from 912 MHz to 925 MHz (13 MHz) and from 2.32 GHz to 2.69 GHz (360 MHz) that can cover the UHF and microwave bands in RFID application. The radiation patterns are unidirectional beam at both of frequencies. The half-power beamwidths in xz-plane and yz-plane are 80° and 50° at frequency of 922.5 MHz and the half-power beamwidths in xz-plane and yz-plane are 35° and 10° at frequency of 2.45 GHz. In addition, the antenna gains are 8.3 dBi in UHF band and in the range of 9 dBi to 10.4 dBi in microwave band. The radiation efficiencies are about 97 % for UHF band and more than 99 % for microwave band.

CHAPTER 3

THE RFID SENSOR DESIGN

3.1 Introduction

In this chapter, the RFID background and theory is discussed, and the RFID tag design is presented by using the electromagnetic simulator to obtain the maximum tag performance. These RFID tags are applied as remotely read dielectric-property sensors, called a novel RFID sensor, to determine qualities of some material of interest. In addition, the relation between the dielectric constant and maximum read range of the RFID reader and RFID tag are illustrated. Finally, the sensitivity analysis of the RFID tag is also mentioned in this chapter.

3.2 Background and Theory

The demand for traceability to identify and inspect qualities of material products through nondestructive testing (NDT) techniques has been on the rise. Several NDT techniques, such as Radar, Capacimetry, Electrical Resistance and Ultrasonic waves, have been extensively used. Each technique however has its advantages and disadvantages, so the selection of an appropriate technique is based on the desired application. For such construction materials (CMs) as Light Weight Concrete (LWC), Mortar specimens and Concrete, a reliable NDT technique is required to evaluate their properties whether they are suitable for construction use. Therefore, the development of a reliable sensor technique to determine material quality in manufacturing and/ or material testing and inspection process is necessary.

For the ultra high frequency (UHF) and microwave frequency identification systems [32], passive modulated backscatter RF tags communicate with a reader, using far-field electromagnetic (EM) waves, and these tags typically modulate the EM waves

scattered from tag antennas using the load modulation [32]. To maximize the tag performance, tag antennas must be appropriately designed to conjugately match the chip impedance [33].

One important factor of tag performance is the read range of the passive RFID system, defined as the maximum distance from which a tag can be detected. One limitation on the read range is the maximum distance from which the tag receives merely sufficient power to turn on and scatter back. Another limitation is the maximum distance from which the reader can detect this scattered signal. The read range is the smaller of the two maximum distances. Typically, the former determines the read range since the RFID reader sensitivity is usually high [34]. From the sensor's viewpoint, the dependency of the read range on EM properties of CMs near or in contact with tags can be employed as an approach to determining quality of CMs through their estimated dielectric constants. Note that the RF tag performance is affected by many factors, including EM properties of objects near or in contact with tags.

In this chapter, an NDT technique, called a novel RFID sensor, operating in the UHF band of 922.5 MHz is proposed to determine quality of certain CMs through their estimated dielectric properties. Generally, the traditional RFID sensors require additional specific sensors, such as humidity, temperature, motion, light and sound sensors, to be integrated with RFID tags. On the other hand, the novel RFID sensor does not require additional specific sensors to determine dielectric properties of the materials under test, thereby more convenient in fabrication and usually of lower cost. In addition, the novel RFID sensor does not require a network analyzer and other expensive accessories. The key component of the novel RFID sensor is the tag specifically designed to achieve the conjugate impedance matching condition between the tag antenna and a chip in the presence of a selected member of the family of materials of interest, which is near or in contact with the tag. Typically, two specifically designed tags (SDTs), to subsequently discuss in greater detail, for selected members of the family are required to uniquely determine the dielectric properties of a lossy CM of interest.

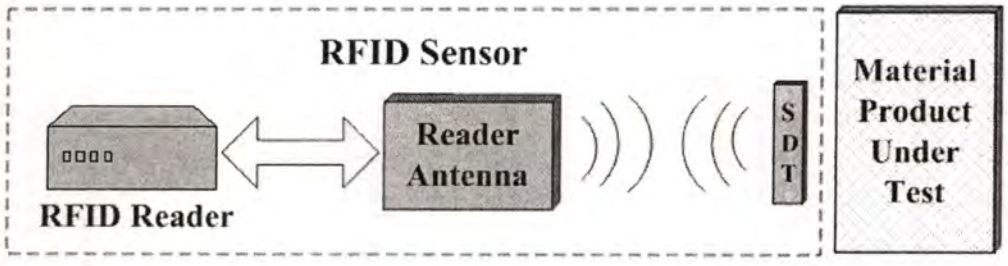

Figure 3.1 A novel RFID sensor system

Figure 3.1 illustrates a novel RFID sensor system consisting of the RFID reader, the reader antenna and SDTs, where each SDT is placed near or in contact with a material under test. Note that the read range is normally governed by the maximum distance from which a tag receives just sufficient power to turn on and scatter back due to the fact that the RFID reader sensitivity is usually high. Generally, the maximum distance can be calculated by using Friis transmission equation [35] that it can be written as

$$R_{\max,mat} = \frac{\lambda}{4\pi}\sqrt{\frac{P_{reader-tx}\cdot G_{reader-tx}\cdot \tau_{reader-tx}\cdot \tau_{tag}\cdot G_{tag,fs}}{L_{sys}\cdot P_{tag,th}}}, \tag{3.1}$$

where $P_{reader-tx}$ is the input power to the reader antenna, L_{sys} is the system loss in both tag and reader, $G_{reader-tx}$ is the gain of the reader antenna, $P_{tag,th}$ is the minimum threshold power necessary to power up the chip, $G_{tag,fs}$ is the tag antenna gain in free space, λ is the free space wavelength, $\tau_{reader-tx}$ and τ_{tag} are the power transmission coefficients of the reader antenna and tag, respectively. Refer to [36], [37] using the modified Friis transmission equation, the maximum distance ($R_{\max,mat}$) of tags in the presence of material products near or in contact with tags can be calculated, under the assumption that the reader antenna has perfect impedance matching and perfect polarization matching to the tag antenna. In addition, Griffin et al. proposed new forms of the power and backscatter communication radio link budgets in terms of the gain penalty based on the modified Friis transmission equation, which is the decrease in tag antenna gain from its free space value when attached to a material, and these forms allow RF tag designers to quantify the effects of tag material attachment [38], [39], as follows:

$$R_{\max,mat} = \frac{\lambda}{4\pi}\sqrt{\frac{P_{reader-tx}\cdot G_{reader-tx}\cdot \tau_{mat}}{L_{sys}\cdot P_{tag,th}}\cdot\left(\frac{G_{tag,fs}}{GP}\right)}, \tag{3.2}$$

Note that the gain penalty GP due to the presence of a material product is mathematically defined as

$$GP \equiv \frac{G_{tag,fs}}{G_{tag,mat}} \tag{3.3}$$

where τ_{mat} is the power transmission coefficient in the presence of a material product. In general, the power transmission coefficient τ can be expressed in terms of the power-wave reflection coefficient Γ_p at the tag antenna terminal as [33], [40]

$$\tau = 1 - \left|\Gamma_p\right|^2, \tag{3.4}$$

where

$$\Gamma_p \equiv \frac{Z_{chip} - Z^*_{ant,tag}}{Z_{chip} + Z_{ant,tag}}. \tag{3.5}$$

In (3.5), the superscript "*" denotes the complex conjugate symbol, and Z_{chip} and $Z_{ant,tag}$ are the chip impedance and the tag antenna impedance, respectively. Note that when the chip impedance and the tag antenna impedance are conjugately matched ($Z_{chip} = Z^*_{ant,tag}$), Γ_p is equal to zero and τ is equal to one as expected.

Similarly, the maximum distance ($R_{\max,fs}$) of tags in free space can be calculated under the same assumption as $R_{\max,mat}$ as follows:

$$R_{\max,fs} = \frac{\lambda}{4\pi}\sqrt{\frac{P_{reader-tx}\cdot G_{reader-tx}\cdot \tau_{fs}\cdot G_{tag,fs}}{L_{sys}\cdot P_{tag,th}}} \tag{3.6}$$

where τ_{fs} is the power transmission coefficient associated with the tag antenna in free space. It should be pointed out that the term GP in (3.6) is equal to 1 since tags are in the free space. From (3.2) and (3.6), the ratio of $R_{\max,mat}$ to $R_{\max,fs}$ can be expressed compactly as

$$\frac{R_{\max,mat}}{R_{\max,fs}} = \sqrt{\frac{\tau_{mat}}{\tau_{fs}}\left(\frac{1}{GP}\right)} \tag{3.7}$$

where all common terms in (3.2) and (3.6) are cancelled out and only terms associated with the power transmission coefficients and the tag antenna gains remain. In (3.7), only terms τ_{mat} and GP are dependent on properties of material products near or in contact with tags; e.g., their dielectric constants, sizes and shapes, in a complicated fashion. Thus, the ratio $R_{\max,mat}/R_{\max,fs}$ can usually be obtained via measurements or numerical simulations of associated problems. Note that all parameters on the right-hand side of (3.7) are related to two parameters of tag antennas; i.e., the tag antenna impedance and the tag antenna gain, in free space and in the presence of a material product. Once the ratio $R_{\max,mat}/R_{\max,fs}$ is known, the dielectric constant of the material product of interest can be estimated to determine their qualities using appropriate data processing. The procedure of dielectric constant determination will be illustrated via specific examples in the chapter 5.

3.3 RFID Tag Design and Simulation

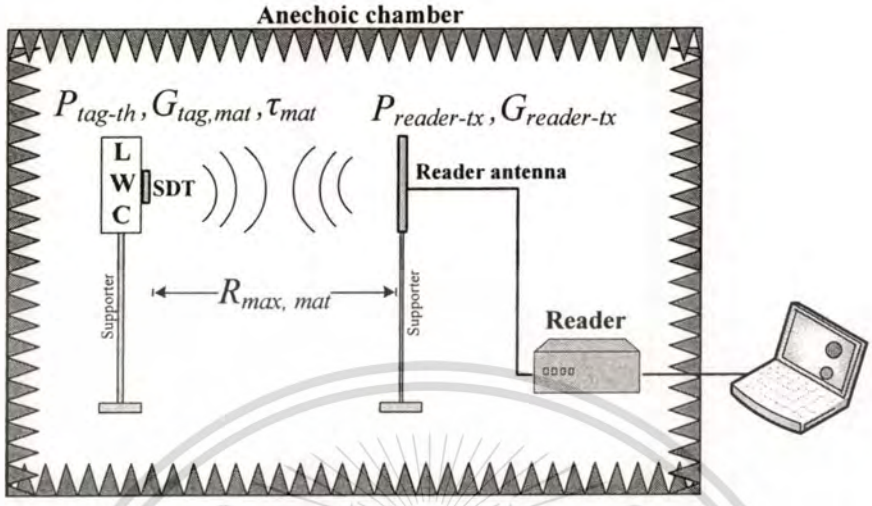

Figure 3.2 The novel RFID sensor setup

Figure 3.2 shows the novel RFID sensor setup in an anechoic chamber, where the operating frequency of interest is 922.5 MHz. The proposed RFID sensor employs the UHF RFID reader of Symbol XR450 and the reader antenna using the Anritsu antenna with the model of MP651A as a half-wavelength standard tuned dipole antenna [41]. Owing to the fact that the standard dipole has the linear polarization and tag antennas are designed to achieve the same polarization as the standard dipole, there is no polarization mismatch. In addition, due to the fact that the RFID reader sensitivity is high, the read range is equal to the maximum distance from tag calculated by using the modified Friis transmission equation as shown in (3.2). In this study, all tags are designed via the CST Microwave Studio simulator [42] and using the IC chip NXP UCODE G2XL, where its input impedance is equal to 16.5 - j148.7 Ω at 922.5 MHz [43]. In Fig. 3.2, the LWC is employed as an example of CMPs to illustrate the concept of the novel RFID sensor. Note that the LWC is assumed to be homogeneous and it can usually be used to construct buildings due to its light weight, easily sawn and sculpted, and nailed or screwed without pre-drilling [44].

Typically, the actual dimension for commercial application of LWC is 20 cm × 60 cm × 7.5 cm [45]. Its sample with the dimension of 20 cm × 15 cm × 7.5 cm is

considered in this chapter. The following parameters are employed: $P_{reader-tx}$ =20 dBm, L_{sys} =1.01 dB, $G_{reader-tx}$ =2.15 dBi and $P_{tag,th}$ =-15 dBm. All SDTs are fabricated on the 0.8 mm-FR4 substrate with the dielectric constant of 4.3. Two cases are considered; i.e., lossless and lossy LWCs. The former will be considered first since it is simpler to understand the methodology of the proposed RFID sensor, while the latter is more complicated, but more realistic.

For the lossy case, two LWC states are considered; i.e., the dry state and the saturated state with water. In literature, the constitutive parameters of building materials were measured [46]-[50]. Note that the dielectric constant of the lossy case can be measured using the dielectric probe [51]. Table 3.1 illustrates the dielectric constants, ε_r, of each lossy LWC state, where ε_r is defined as $\varepsilon_r = \varepsilon_r' - j\varepsilon_r''$. As expected, ε_r' and ε_r'' of the saturated state are larger than ε_r' and ε_r'' of the dry state respectively, due to the water existing in the saturated state.

Table 3.1 Dielectric constant of lossy LWCs.

LWC state	ε_r'	ε_r''
Dry	2.5	0.2
Saturated	8	1.08

To obtain the optimum SDTs, the design process are discussed as follows

3.3.1 Lossless Case

For the lossless LWC case, it is assumed that its dielectric constant is equal to the dielectric constant of LWC in the dry state with no loss; i.e., $\varepsilon_r = \varepsilon_r'$ =2.5 and ε_r'' =0. Using the CST Microwave Studio simulator, the tag antenna of the SDT, called the SDT_{LL}, is appropriately designed to conjugately match with the chip impedance by including effects of the lossless LWC in the simulation, where the SDT_{LL} is attached to

the surface of the lossless LWC at its center as shown in Fig. 3.3 to reduce edge effects. Symmetrical meander line antennas are employed in this chapter with an inductively coupled structure with 1-mm line thickness [52] to flexibly meet the high Q-factor of the IC chip NXP UCODE G2XL. In addition, the tag antenna size must be compact to mount on small LWCs as well. The tag antenna structure is optimized as shown in Fig. 3.4, where its antenna parameters are illustrated in Table 3.2.

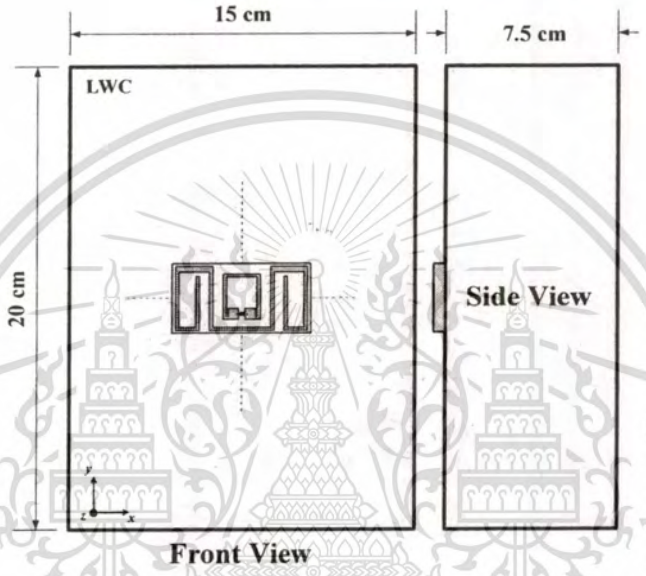

Figure 3.3 The SDT location on the LWC

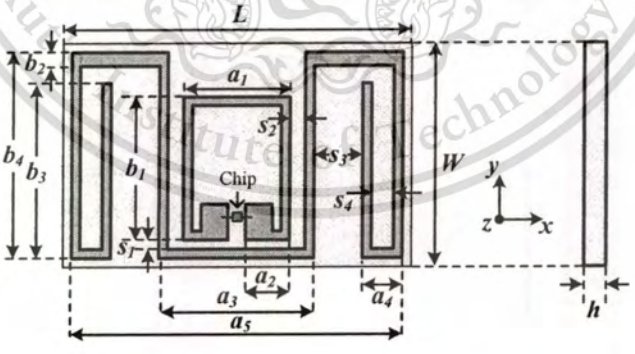

Figure 3.4 The SDT for the lossless LWC

Table 3.2 Parameters of the SDT_{LL} for the lossless LWC with ε_r =2.5.

Parameter	Dimension (mm)	Parameter	Dimension (mm)
a_1	12	b_4	23
a_2	5	L	39.5
a_3	17.5	s_1	1
a_4	5	s_2	1.75
a_5	38.5	s_3	5
b_1	16.5	s_4	3
b_2	1.5	W	25
b_3	18.5		

Note that the dimensions of the SDT_{LL} are equal to 39.5 mm × 25 mm × 0.8 mm after optimization, where its input impedance is equal to 17.75 + j147.8 Ω, and its polarization in the bore-sight direction looking out from the LWC is horizontal. In addition, its gain and power transmission coefficient ($G_{tag,mat}$ and τ_{mat}) are found to be -0.49 dBi and 99.8 %, respectively. Note that τ_{mat} of the SDT_{LL} is almost equal to 100 % illustrating that the input impedances of the SDT_{LL} and the IC chip are almost conjugately matched as desired.

To show the dependency of $G_{tag,mat}$ and τ_{mat} on ε_r, Fig. 3.5 illustrates the plots of $G_{tag,mat}$ in dBi and τ_{mat} in percentage for the SDT_{LL} as a function of ε_r ranging from 2.5 to 8.0. It is found that its $G_{tag,mat}$ and τ_{mat} monotonically decrease as ε_r increases, where both $G_{tag,mat}$ and τ_{mat} are maximum at ε_r =2.5. Due to the fact that the SDT_{LL} is specifically designed to conjugately match with the chip impedance in the presence of the

lossless LWC with ε_r =2.5, more impedance mismatch occurs as increasing ε_r, resulting in decreasing τ_{mat} as expected.

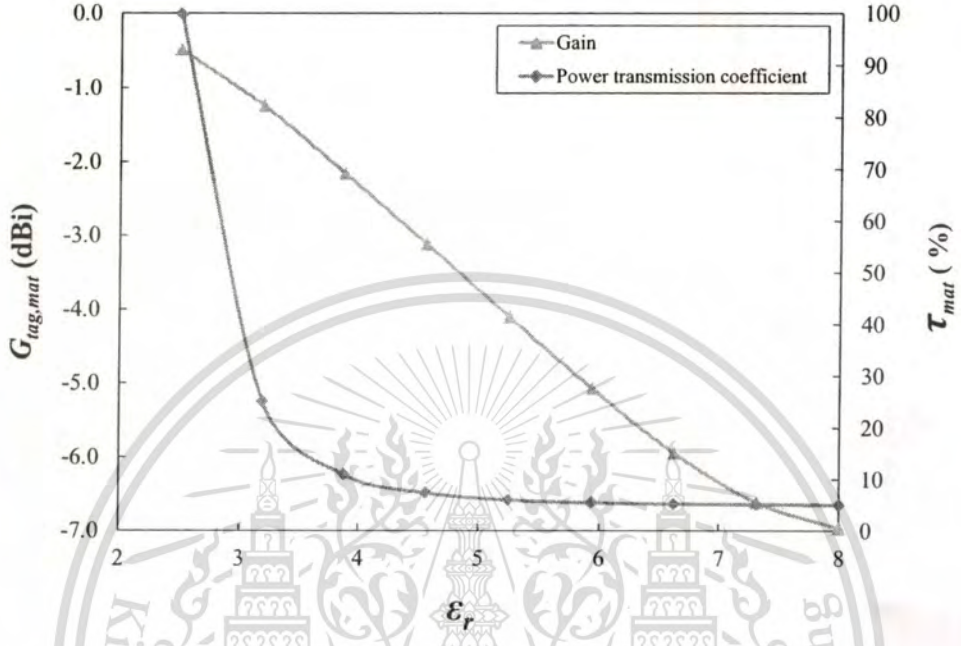

Figure 3.5 $G_{tag,mat}$ and τ_{mat} as a function of ε_r for the SDT_{LL}

3.3.2 Lossy Case

For the lossy LWC case, the tags are specifically designed for optimum performance for each state of lossy LWCs as shown in Table 3.1. The RFID tag structures optimized for the dry LWC state, called the SDT_1, and for the saturated LWC state, called the SDT_2. They are illustrated in Fig. 3.6(a) and Fig. 3.6(b) respectively, where their parameters are shown in Table 3.3. The dimensions of the SDT_1 and the SDT_2 are equal to 39.5 mm × 25 mm × 0.8 mm and 39 mm × 20.5 mm × 0.8 mm respectively, where their characteristics are tabulated in Table 3.4. It should be pointed out that τ_{mat} of both SDT_1 and SDT_2 are nearly equal to 100 % as desired.

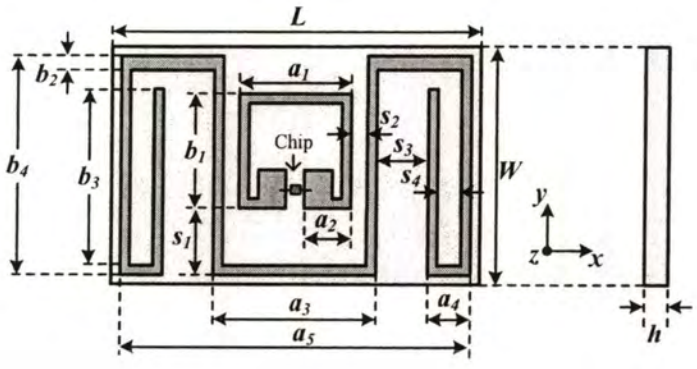

(a) Dry LWC SDT (SDT_1)

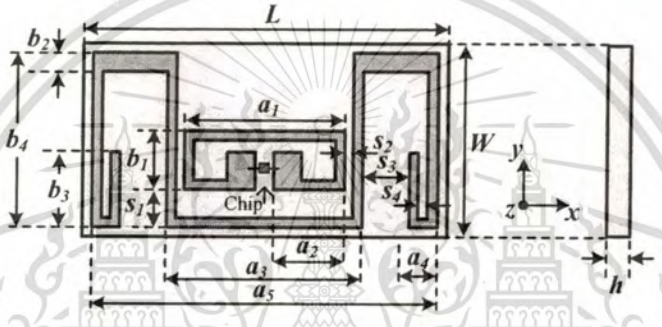

(b) Saturated LWC SDT (SDT_2)

Figure 3.6 The SDTs for the lossy LWCs

To illustrate the dependency of $G_{tag,mat}$ and τ_{mat} on ε_r' for two specific values of ε_r'', let first consider ε_r''=0.2 as shown in Fig. 3.7, where the SDT_1, specifically designed for ε_r=2.5-j0.2, is employed in this study. Like the lossless case, it is found that τ_{mat} tends to decrease as ε_r' increases as expected due to more impedance mismatch. In addition, $G_{tag,mat}$ varies noticeably as ε_r' increases. Next, let consider another case of ε_r''=1.08 as shown in Fig. 3.8, where the SDT_2, specifically designed for ε_r =8.0-j1.08, is employed.

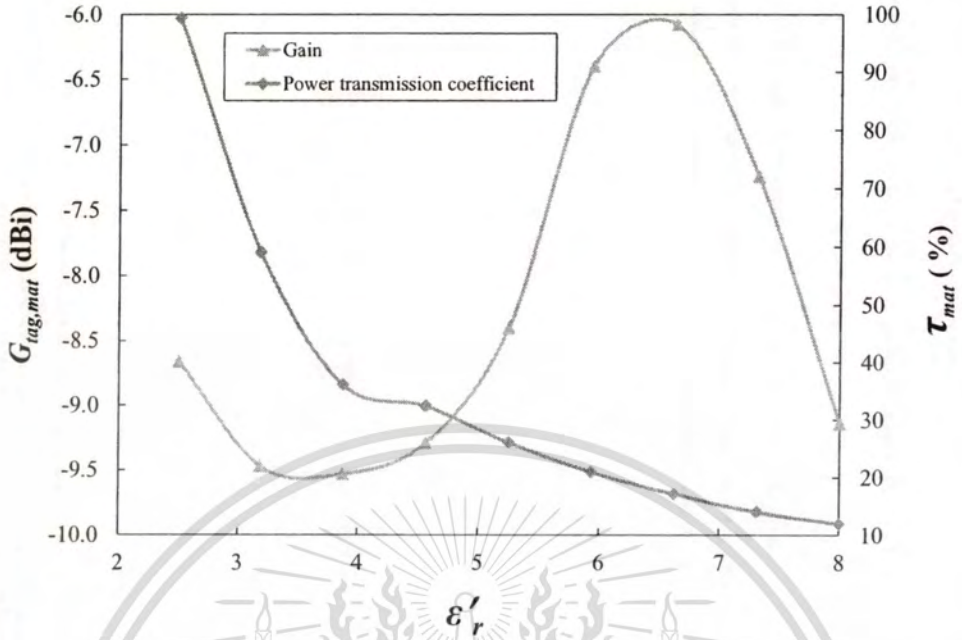

Figure 3.7 $G_{tag,mat}$ and τ_{mat} as a function of ε'_r for the SDT_1 with ε''_r =0.2

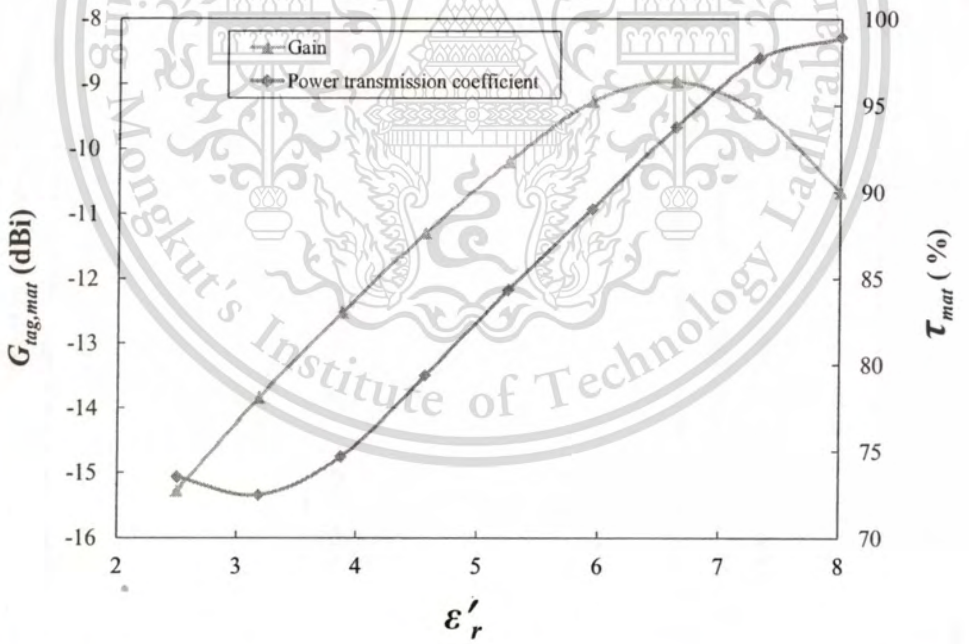

Figure 3.8 $G_{tag,mat}$ and τ_{mat} as a function of ε'_r for the SDT_2 with ε''_r =1.08

Table 3.3 Tag parameters for the lossy LWCs.

Parameter	Dimension (mm)		Parameter	Dimension (mm)	
	SDT_1	SDT_2		SDT_1	SDT_2
a_1	12	17	b_4	23	18.5
a_2	5	7.5	L	39.5	39
a_3	17.5	21	s_1	6	3
a_4	4.5	3	s_2	1.75	1
a_5	37.5	37	s_3	5.5	5
b_1	12	6	s_4	2.5	1
b_2	1.5	2	W	25	20.5
b_3	19.5	8			

Table 3.4 SDT characteristics for the lossy LWCs.

SDT Characteristic	SDT_1	SDT_2
Input impedance (Ω)	14.09 + j149.41	16.09 + j147.64
$G_{tag,mat}$ (dBi)	-8.66	-10.67
τ_{mat} (%)	99.33	98.88
Polarization	Linear	Linear

3.4 The Relation between Dielectric Constant and Maximum Read Range ($R_{\max}$)

This section presents the relation between dielectric constant and maximum read range ($R_{\max}$), which it is used to determine material quality in manufacturing and/ or material testing and inspection process.

3.4.1 Lossless Case

For this case, only ε_r' of the lossless LWC under test is required (ε_r''=0). It will be shown that only one SDT is sufficient to uniquely determine ε_r' from the measurements of associated read ranges. Fig. 3.9 illustrates the plot of $\varepsilon_r = \varepsilon_r'$ versus $R_{\max,mat}/R_{\max,fs}$ for the SDT_{LL}, obtained from the simulation by using (3.6), where $R_{\max,fs}$ is a normalization constant. As expected from Fig. 3.5 and Fig. 3.9, $R_{\max,mat}/R_{\max,fs}$ monotonically decreases as ε_r increases. It is clear from Fig. 3.9 that once $R_{\max,mat}/R_{\max,fs}$ of the SDT_{LL} attached to the lossless LWC under test is known from the measurements, its ε_r can be uniquely estimated using Fig. 3.9.

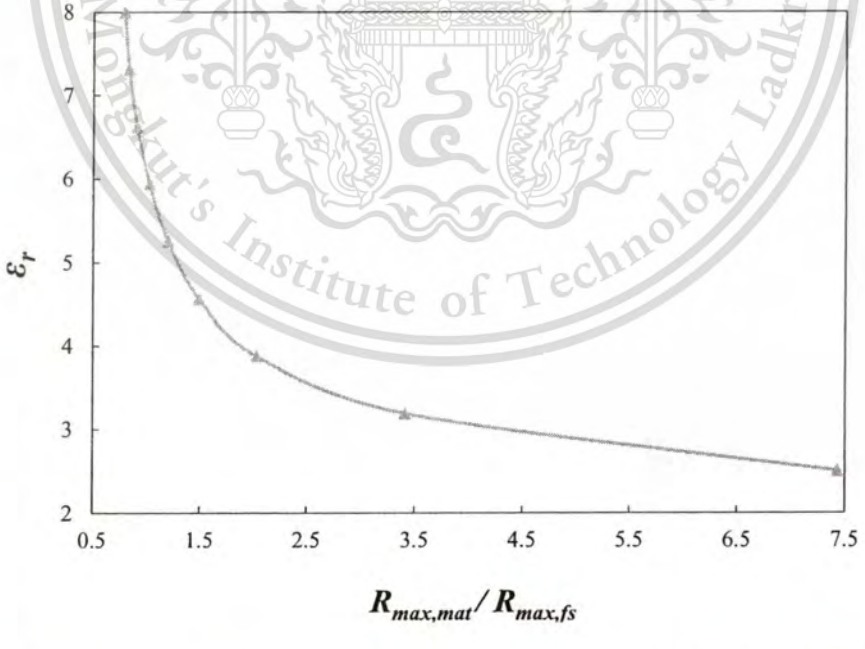

Figure 3.9 The relation between ε_r and $R_{\max,mat}/R_{\max,fs}$ for the SDT_{LL} obtained from the simulations

3.4.2 Lossy Case

Figure 3.10 shows the plot of $\varepsilon_r = \varepsilon_r'$ versus $R_{\max,mat}/R_{\max,fs}$ for the SDT_1 and SDT_2 with ε_r'' =0.20, 0.64 and 1.08 obtained from the simulation. It is found that τ_{mat} tends to increase as ε_r' increases as expected due to less impedance mismatch, and $G_{tag,mat}$ tends to increase and then decrease as ε_r' increases. It can be concluded from these two cases (lossless and lossy cases) that an SDT, specifically designed for an LWC with $\varepsilon_r' = \widetilde{\varepsilon}_r' - j\widetilde{\varepsilon}_r''$, usually possesses the maximum τ_{mat} when $\varepsilon_r' = \widetilde{\varepsilon}_r'$ and $\varepsilon_r'' = \widetilde{\varepsilon}_r''$. However, the associated $G_{tag,mat}$ is not always the maximum. In addition, this case is a realistic situation that it can be used to determine the dielectric constant of material under test in chapter 5.

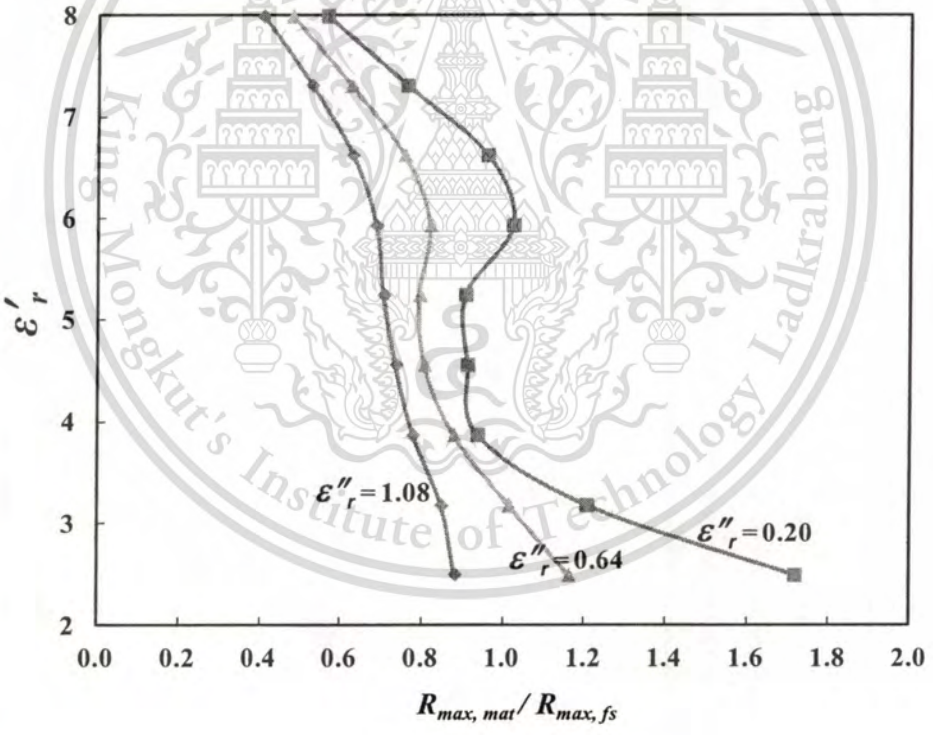

(a)

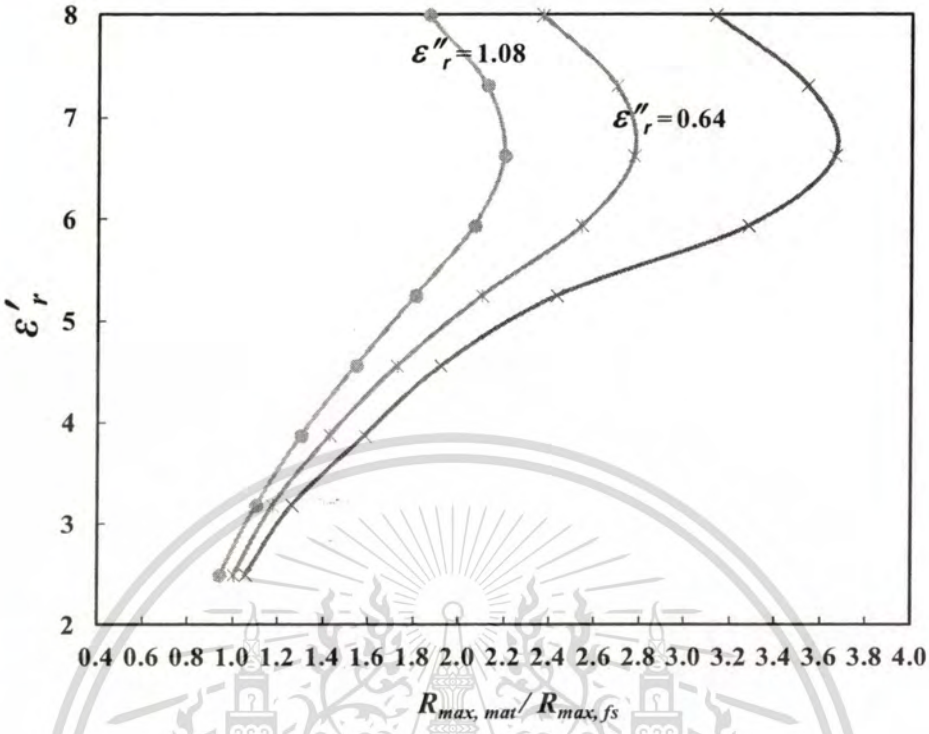

(b)

Figure 3.10 The relation between ε'_r and $R_{\max,mat}/R_{\max,\,fs}$ for the SDT_1 and the SDT_2 with ε''_r =0.20, 0.64 and 1.08 obtained from the simulations

(a) The relation between ε_r and $R_{\max,mat}/R_{\max,\,fs}$ for the SDT_1.

(b) The relation between ε_r and $R_{\max,mat}/R_{\max,\,fs}$ for the SDT_2.

3.5 Sensitivity Analysis

To convenient, in practice, the error of tag location mount on LWC is important. Therefore, the effects of SDT location mounted on LWC are studied in terms of the SDT antenna performances. Furthermore, the tolerance of the SDT is also discussed to analyze the sensitivity of the novel RFID sensor.

The sensitivity of a novel RFID sensor technique can be separated into 2 parts as follow:

3.5.1 Location Error

The folded dipole with an inductive loop tag antenna is used as an SDT to study effects of location on the lossy LWC. In this study, the LWC has dimension of 200 mm × 150 mm × 75 mm with the dielectric property of 2.5-*j*0.2 Ω at 922.5 MHz is employed. Note that the SDT is obtained by optimizing its dimension to almost conjugately match with the chip impedance of 16.5-*j*148.7 Ω in the presence of the lossy LWC, where the SDT is mounted of the location L_8 as shown in Fig. 3.11. The LWC surface area is divided into 15 parts for mounting the SDT. Due to the problem symmetry, only the location L_1, L_2, L_4, L_5, L_7, L_8, L_{10}, L_{11}, L_{13} and L_{14} are considered.

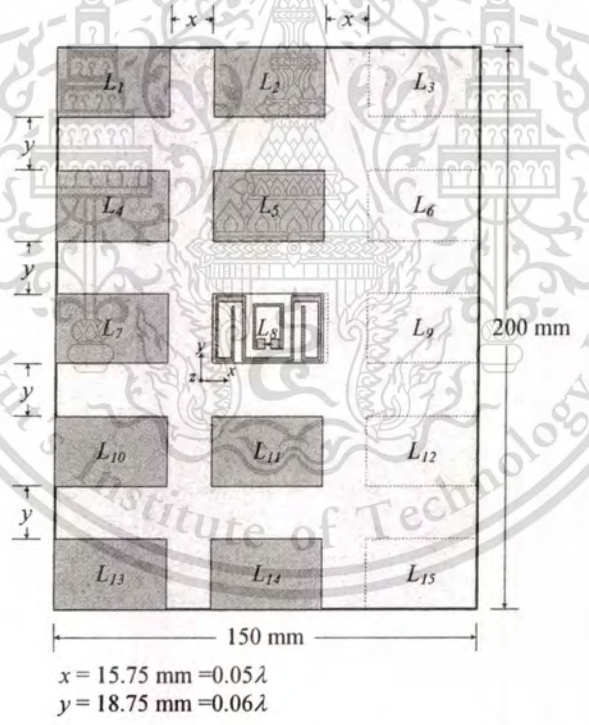

Figure 3.11 The location of the SDT on the lossy LWC

Figure 3.12 shows the SDT input impedance as a function of the SDT location L_n. It is found that the SDT input impedances are similar for location pair as follows: (L_1, L_{13}), (L_2, L_{14}), (L_4, L_{10}) and (L_5, L_{11}). This is due to the fact that back listed pair

possesses almost the same electromagnetic environment for the SDT. In addition, it is observed that the SDT locations L_5, L_8 and L_{11} yield similar SDT input impedance.

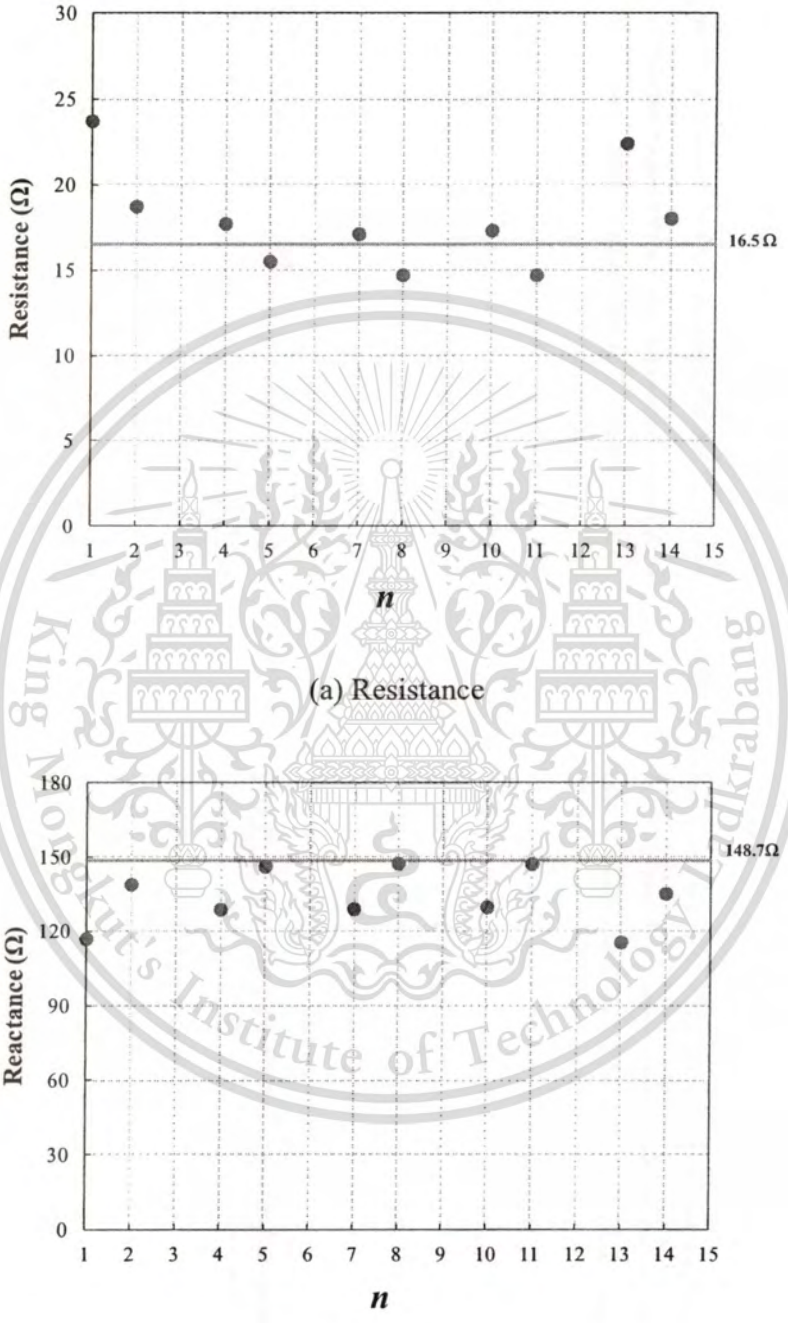

Figure 3.12 The input impedance of the SDT mounting on the LWC surface as a function of the SDT Location (L_n)

The SDT antenna gain as a function of the SDT location L_n is illustrated in Fig. 3.13. Note that the gain varies strongly with L_n. It is found that the gains are similar for each location pair as follows: (L_1, L_{13}) and (L_2, L_{14}). Figure 3.14 illustrates the radiation pattern of the SDT antenna located at L_1 and L_{13}. It is found that the radiation patterns in the xz-plane are similar for both locations. However, the radiation patterns in the yz-plane are noticeably different. In addition, Figure 3.15 shows similar plot as in Fig. 3.14 for the locations L_5, L_8 and L_{11}. Note that the radiation patterns in the xz-plane are similar for all locations. However, the radiation patterns in the yz-plane are noticeably different.

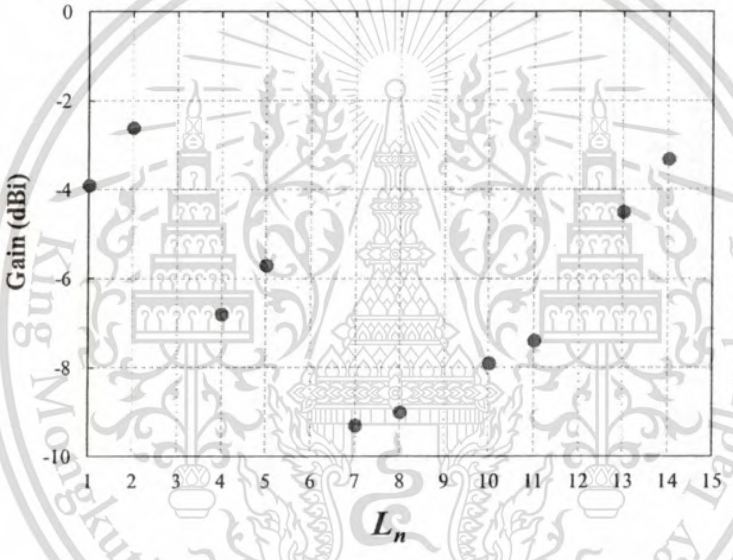

Figure 3.13 The SDT antenna gain as a function of the SDT location (L_n)

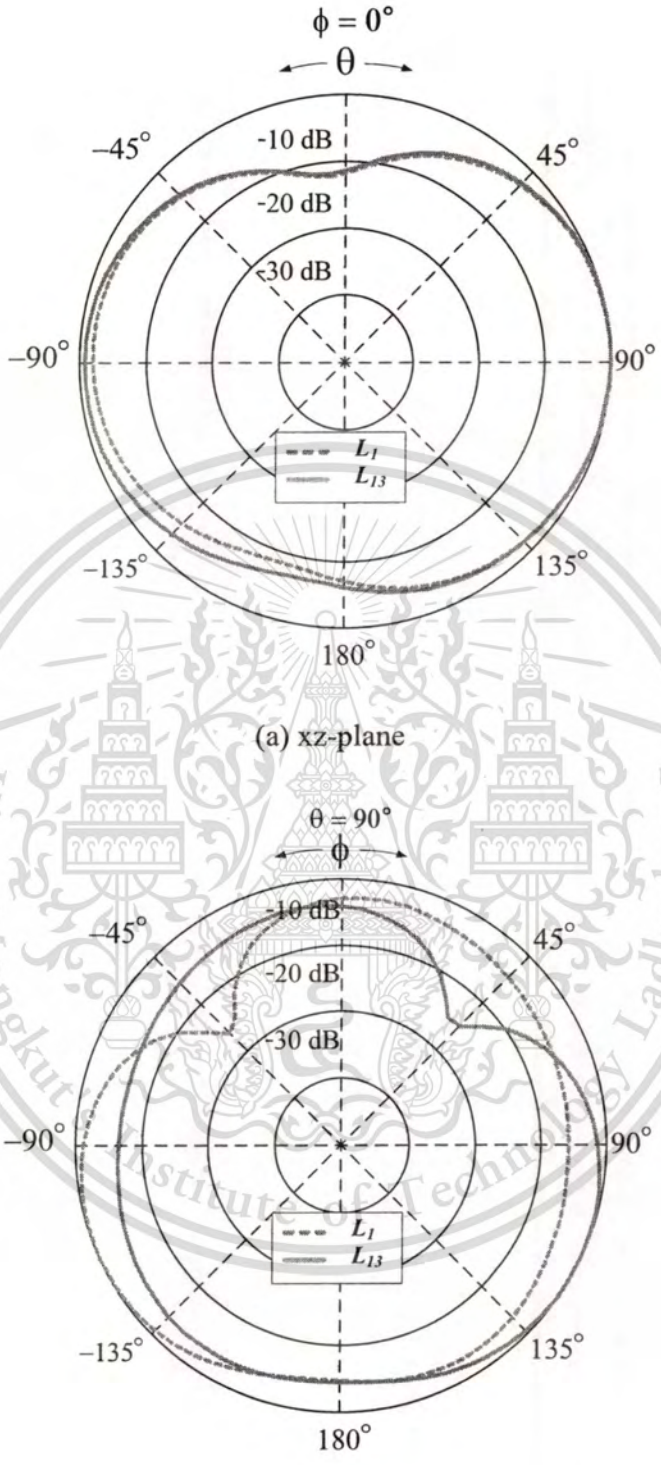

(a) xz-plane

(b) yz-plane

Figure 3.14 Comparison of radiation patterns of the SDT antenna for L_1 and L_{13}

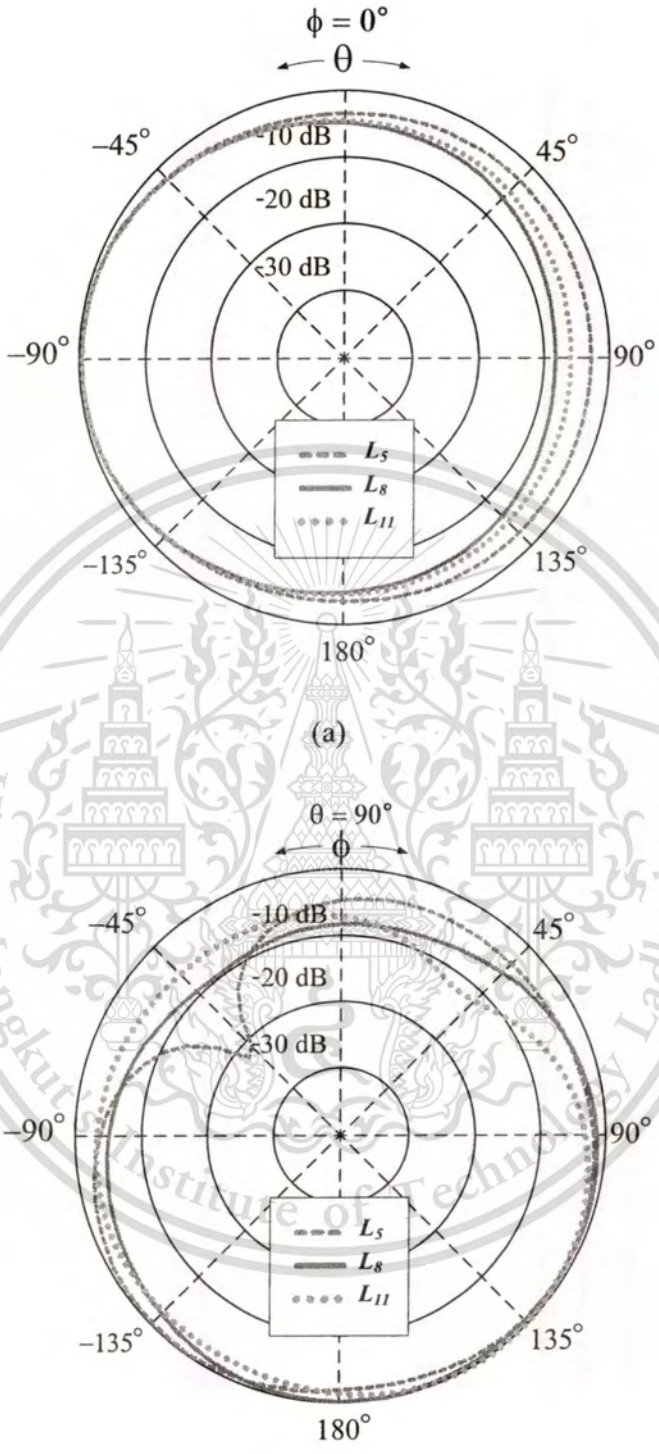

Figure 3.15 Comparison of radiation patterns of the SDT antenna for L_5, L_8 and L_{11}

From the results incorporated with equation (3.2) implied that the read range $R_{max,mat}$ depends on the SDT location on the LWC under test. Recommended SDT location, in practices, is flexible for mounted on the LWC under test.

3.5.2 Tolerance

This section presents the effect of SDT tolerance on the tag performances such as the input impedance, the power transmission coefficient, the tag gain and maximum read range. The SDT structure is shown in Fig. 3.16. And the SDT parameters and characteristics are tabulated in Table 3.5 and Table 3.6, respectively.

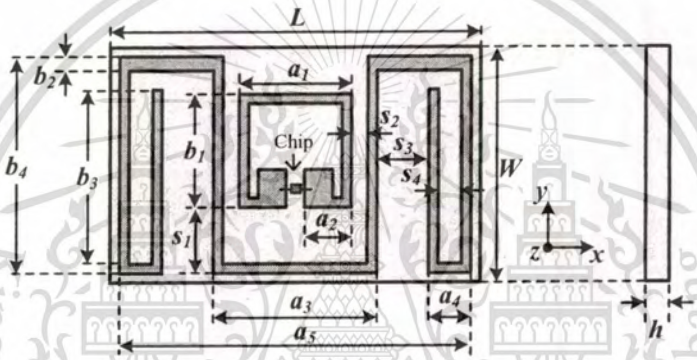

Figure 3.16 The SDT Structure

Table 3.5 Tag parameters.

Parameter	Dimension (mm)	Parameter	Dimension (mm)
a_1	12	b_4	23
a_2	5	L	39.5
a_3	17.5	s_1	6
a_4	4.5	s_2	1.75
a_5	37.5	s_3	5.5
b_1	12	s_4	2.5
b_2	1.5	W	25
b_3	19.5		

Table 3.6 SDT Characteristics

SDT Characteristic	Value
Input impedance (Ω)	14.09 + j149.41
$G_{tag,mat}$ (dBi)	-8.66
τ_{mat} (%)	99.33
Polarization	Linear

Figure 3.17 to Figure 3.32 shows the input impedance, the power transmission coefficient, SDT gain and maximum read range as a function of SDT parameters. From the results, it is found that the power transmission coefficient decrease when the impedance mismatch. Note that the SDT is optimized its dimension to almost conjugately match with the chip impedance of 16.5-*j*148.7 Ω. Moreover, the comparison of the maximum read range is exhibited in Fig. 3.33 that it is obvious that parameter s_3 is important effect to the maximum read range of an SDT sensor.

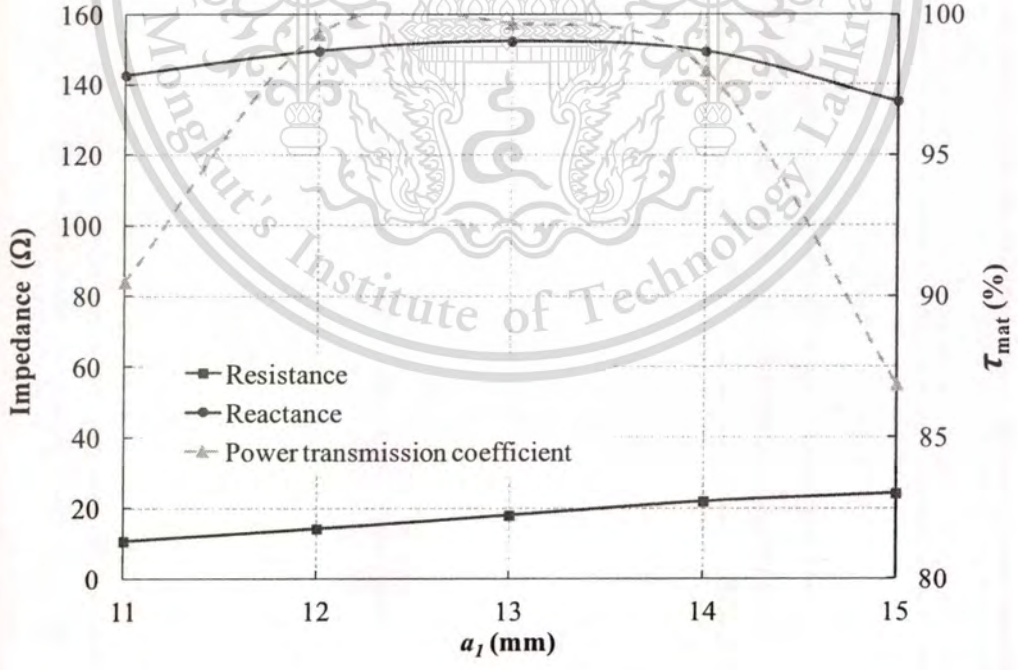

Figure 3.17 The input impedance and the power transmission coefficient as a function of parameter a_1

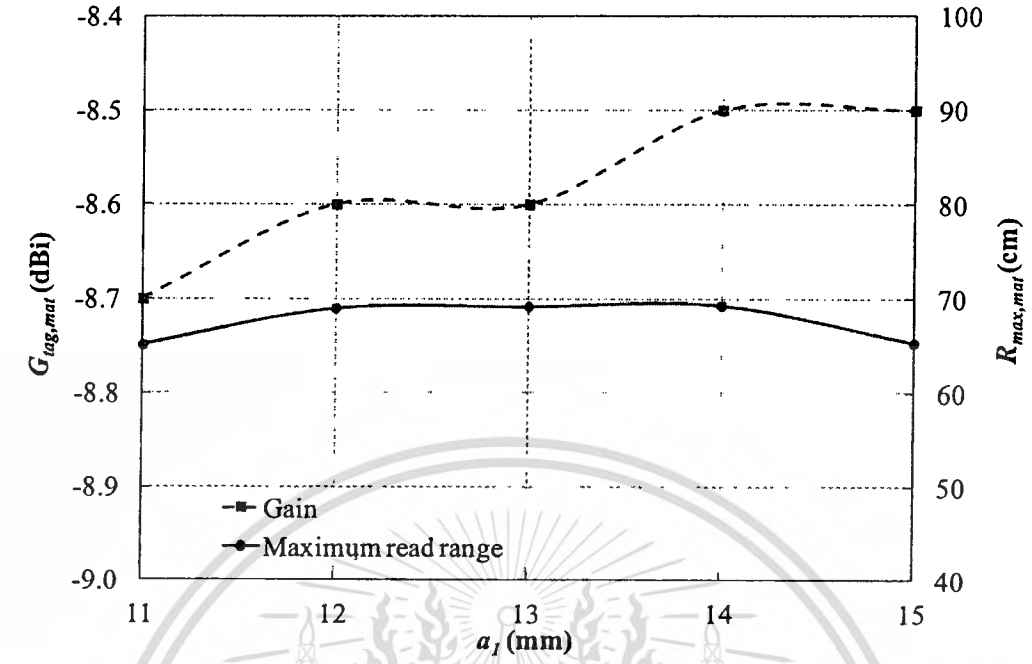

Figure 3.18 The antenna gain and maximum read range as a function of parameter a_1

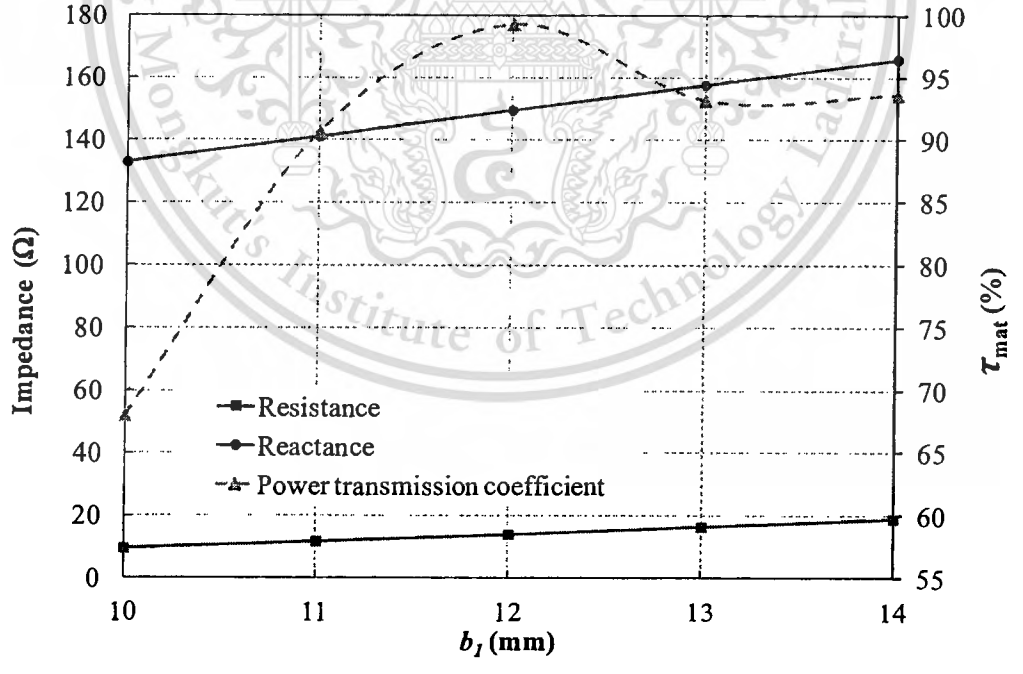

Figure 3.19 The input impedance and the power transmission coefficient as a function of parameter b_1

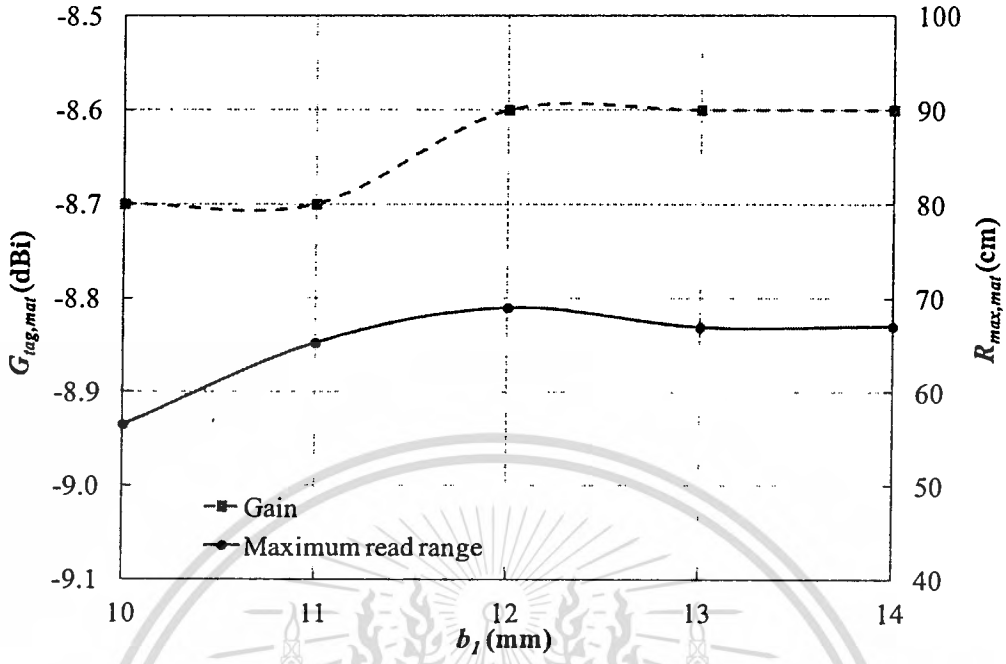

Figure 3.20 The antenna gain and maximum read range as a function of parameter b_1

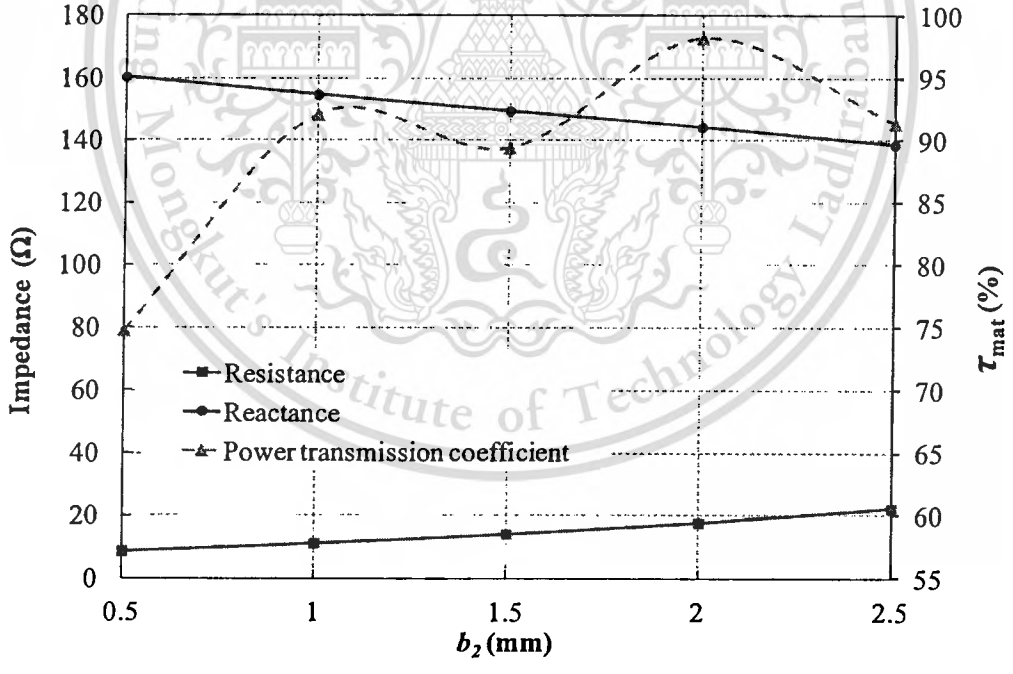

Figure 3.21 The input impedance and the power transmission coefficient as a function of parameter b_2

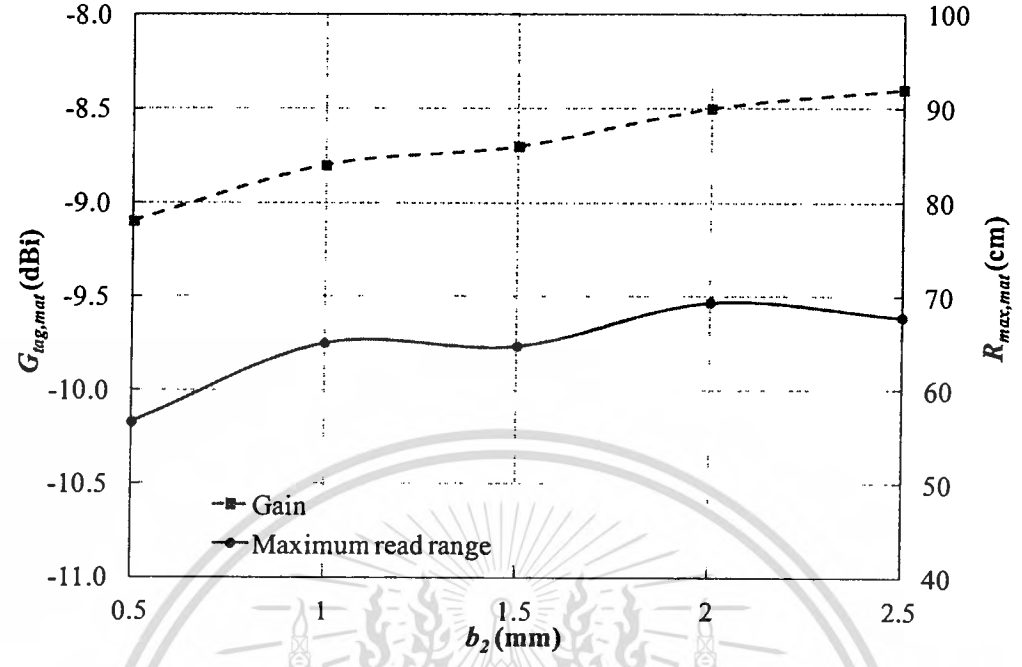

Figure 3.22 The antenna gain and maximum read range as a function of parameter b_2

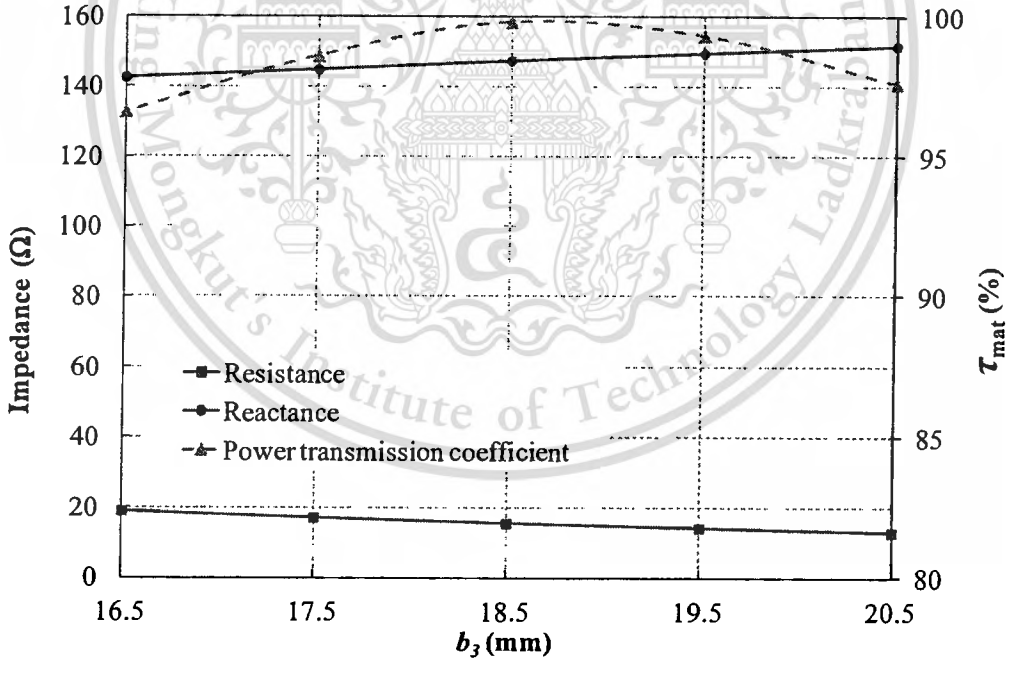

Figure 3.23 The input impedance and the power transmission coefficient as a function of parameter b_3

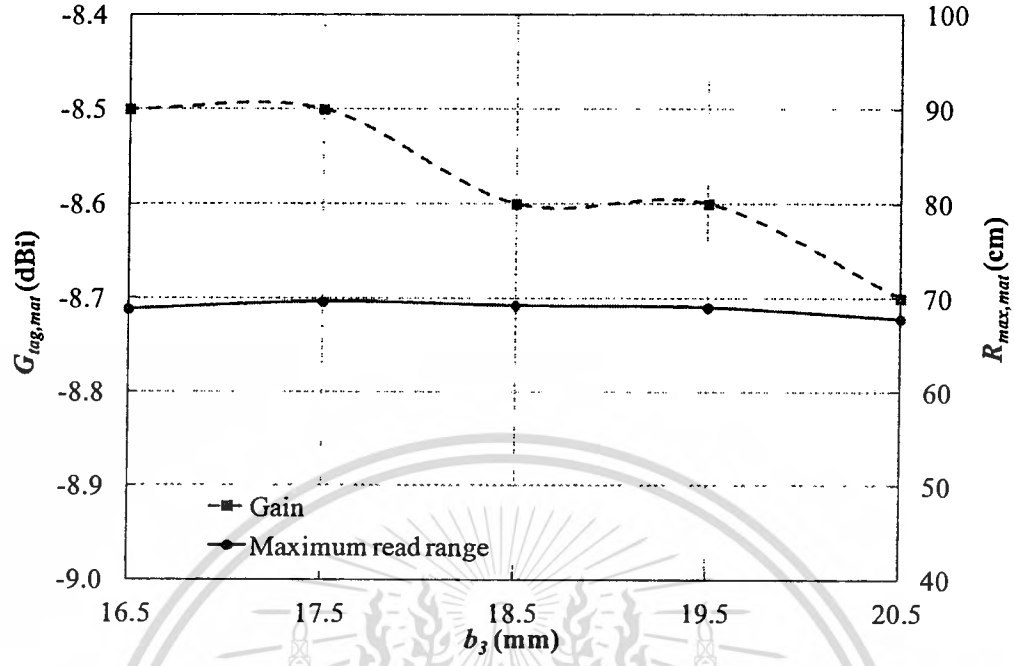

Figure 3.24 The antenna gain and maximum read range as a function of parameter b_3

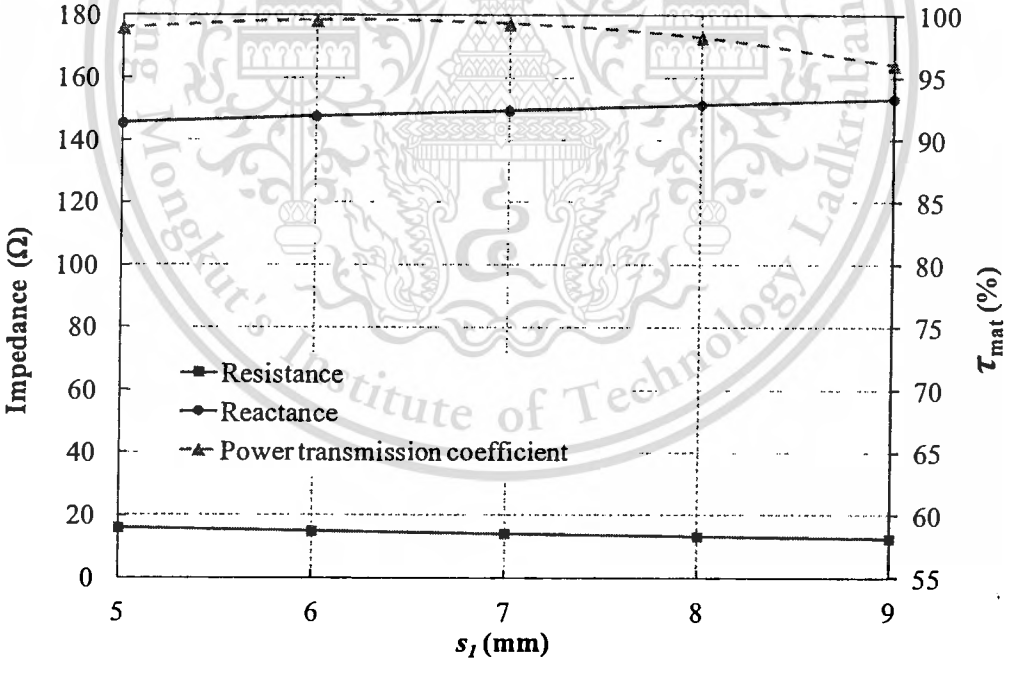

Figure 3.25 The input impedance and the power transmission coefficient as a function of parameter s_1

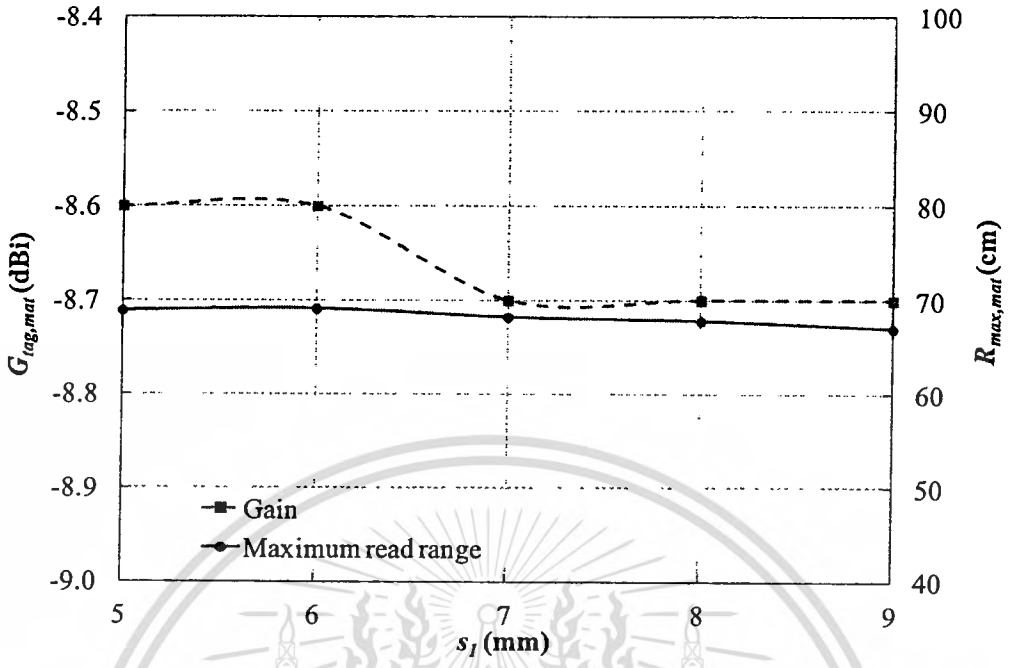

Figure 3.26 The antenna gain and maximum read range as a function of parameter s_1

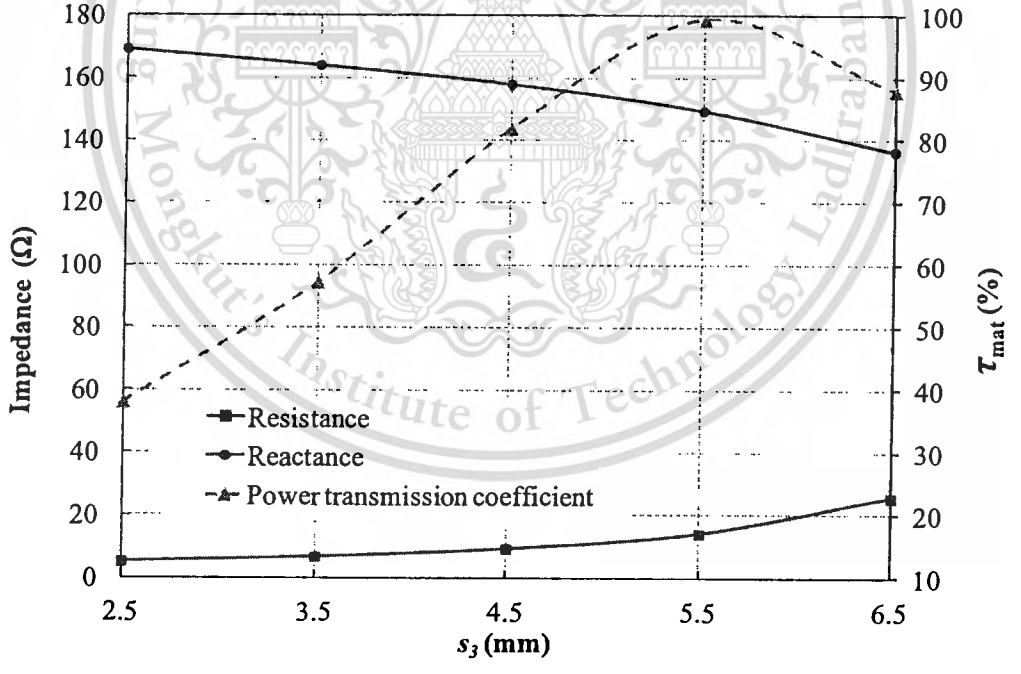

Figure 3.27 The input impedance and the power transmission coefficient as a function of parameter s_3

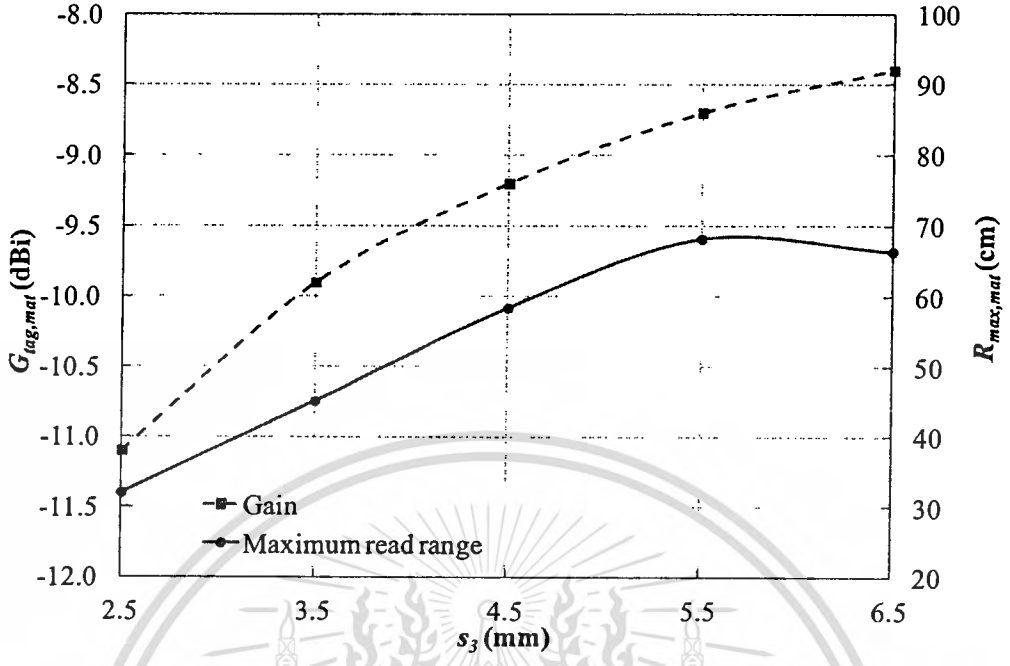

Figure 3.28 The antenna gain and maximum read range as a function of parameter s_3

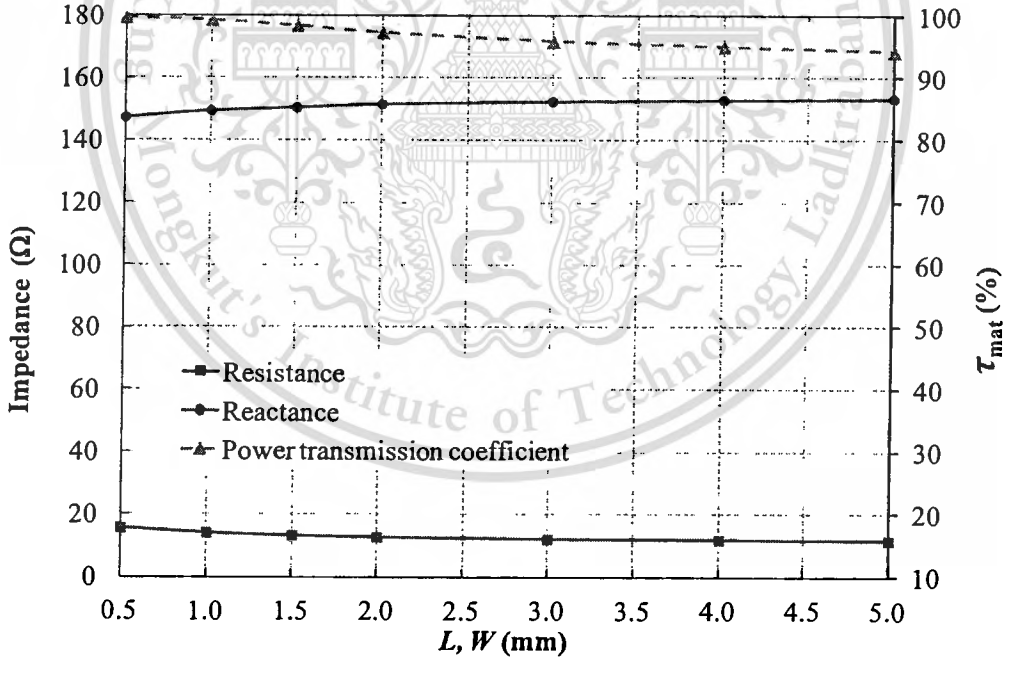

Figure 3.29 The input impedance and the power transmission coefficient as a function of parameter L and W

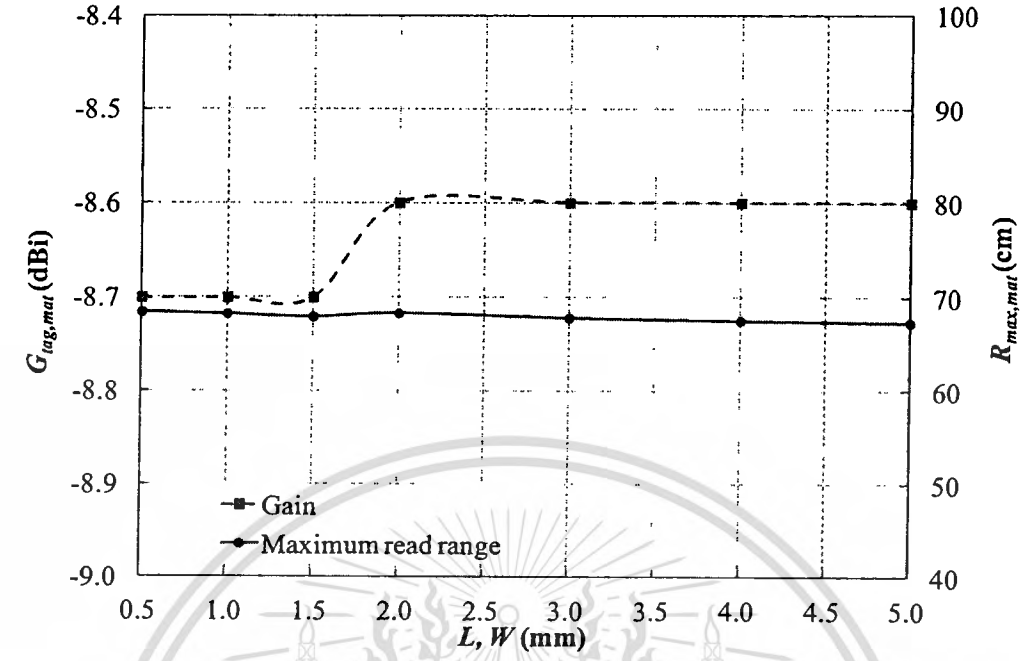

Figure 3.30 The antenna gain and maximum read range as a function of parameter *L* and *W*

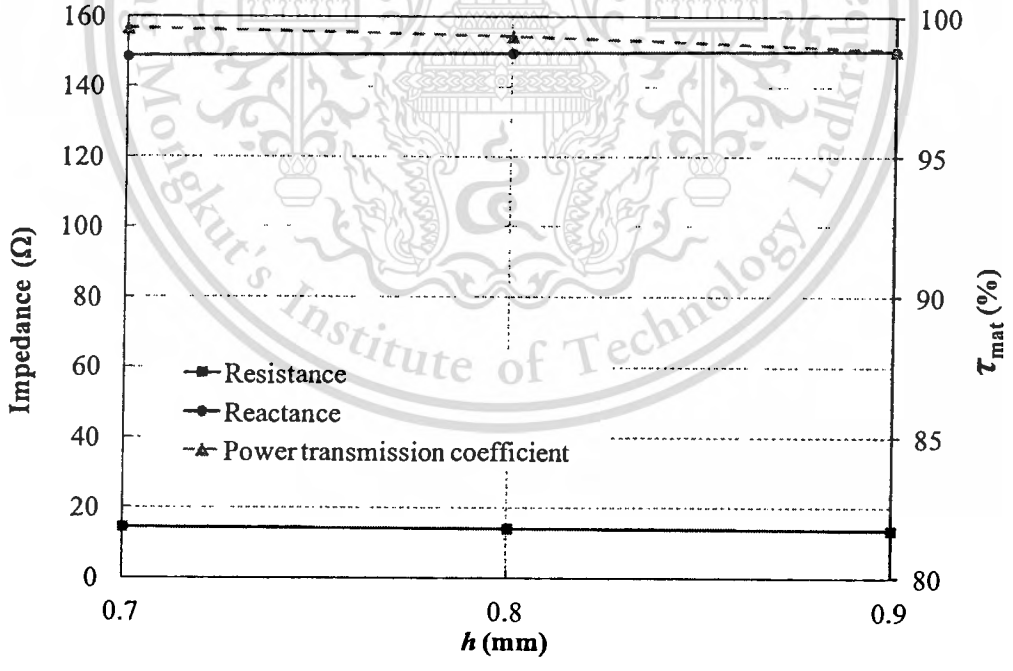

Figure 3.31 The input impedance and the power transmission coefficient as a function of parameter *h*

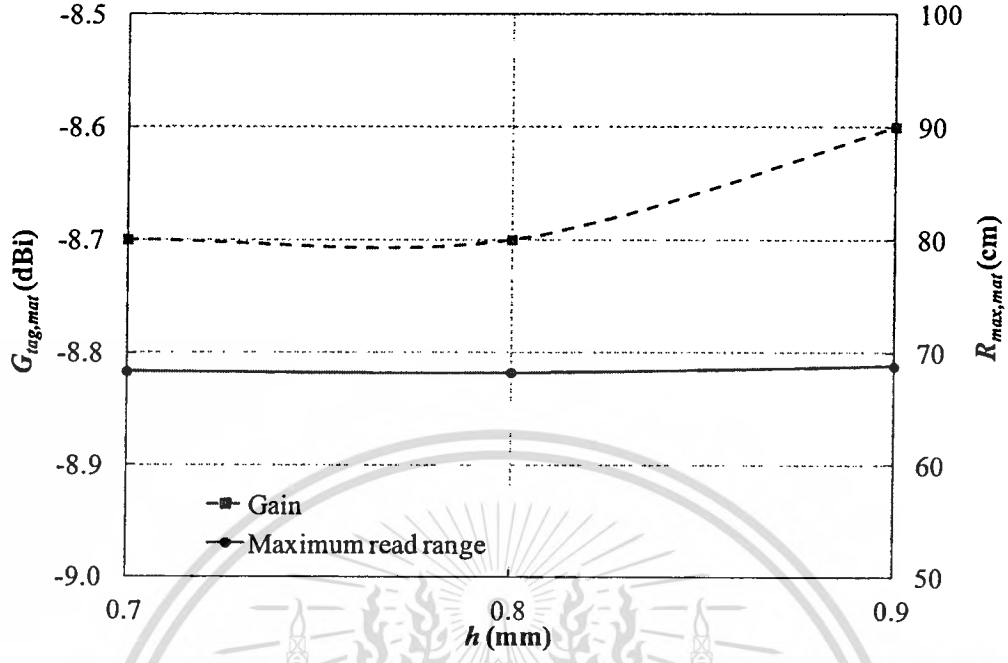

Figure 3.32 The antenna gain and maximum read range as a function of parameter *h*

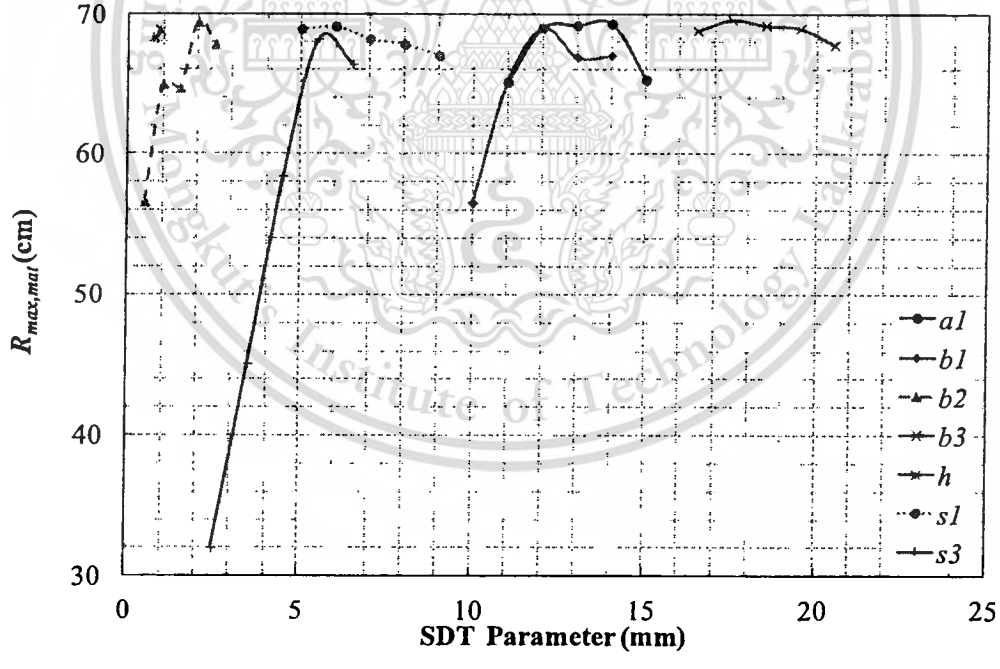

Figure 3.33 The maximum read range as a function of SDT parameters

3.6 Summary

A novel RFID sensor technique operating in the UHF band is designed and analyzed to employ as a remotely read dielectric-property sensors to determine quality of certain CMs through their estimated dielectric properties. It is an NDT technique that does not require additional specific sensors to determine dielectric properties of the materials under test, thereby more convenient in fabrication and usually of lower cost. In addition, the relation between dielectric constant and maximum read range (R_{max}) is illustrated, which it is used to determine material quality in manufacturing and/ or material testing and inspection process. The location error and the tolerance of a novel RFID sensor are analyzed. It is obvious that the characteristics of the SDT antenna depend on tag location on the LWC, especially near the corners and edges of the LWC. However, the SDT characteristics at near center area of the LWC under test (L_5, L_8 and L_{11}) can be obtained the same results. In practice, the location of SDT is flexible for mounted at LWC in RFID sensor applications. Furthermore, the tolerance analysis is implied that the some SDT parameters are important affected to the maximum read range, especially parameter s_3.

CHAPTER 4

ANTENNA MEASUREMENT

4.1 Introduction

From the simulation and analysis of the proposed annular plate antenna with curved and rectangular slots on vertical ground plane is investigated in Chapter 2. This chapter discusses the antenna fabrication and the antenna characteristic measurements to verify the proposed antenna design. The prototype of the annular plate antenna with curved and rectangular slots on vertical ground plane that the optimum parameters are mentioned in previous chapter were fabricated. The antenna measurements were set up to test the antenna characteristics including the radiation patterns in both xz-plane and yz-plane and the antenna gains are also tested. The magnitude of S_{11} is tested by using the Network Analyzer.

4.2 Antenna Fabrication

To verify the antenna characteristics such as the radiation pattern and gain, the experiment was set up at the frequencies of 922.5 MHz and 2.45 GHz for UHF and microwave band of the RFID system. The dimensions of the prototype of the annular plate antenna with curved and rectangular slots on vertical ground plane are tabulated in Table. 4.1.

The fabricated antenna consists of two parts of conductors; first one is the annular plate with curved and rectangular slots as shown in Fig. 4.1 and the other one is the vertical ground plane as shown in Fig. 4.2. The proposed annular plate antenna with curved and rectangular slots on vertical ground plane was fabricated as illustrated in Fig. 4.3. This antenna is fed by using the single probe that made of the metallic conductor is

connected via N-type connector to feed the annular plate with curved and rectangular slots radiating part.

Table 4.1 Antenna dimension used for fabrication

Parameter	Dimension (mm)
Radius of annular plate (a)	83.5
Spacing between annular plate and ground plane (h_1)	7.5
Height of vertical ground plane in x-axis (h_2)	40
Height of vertical ground plane in y-axis (h_3)	50
Width of ground plane (g_x)	187.5
Length of ground plane (g_y)	225.5
Length of rectangular slot (L_s)	49.5
Radius of curved slot (r)	72.5
Radius of circular slot (S_1)	18
Width of curved slot (s_s)	11.5
Width of rectangular slot (W_s)	2
Spacing between rectangular slot and y-axis (x_1)	25
Spacing between the center of rectangular slot and x-axis (y_1)	14.5
Location of feeding in y-axis (y_p)	26
Length of curved slot (ϕ_1)	100°
Angle between the center of curved slot and y-axis (ϕ_2)	90°

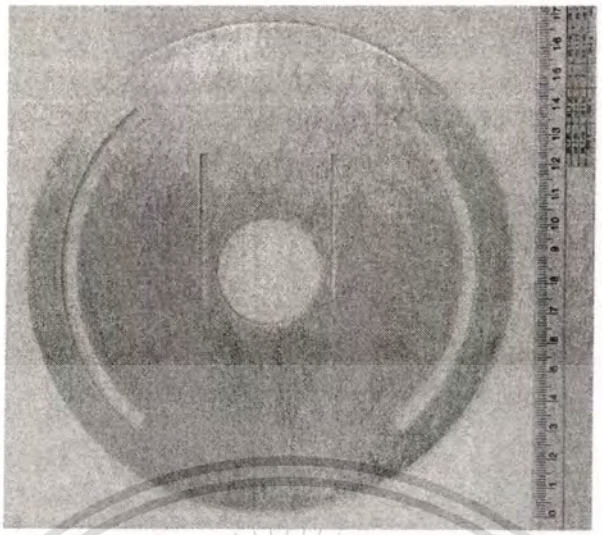

Figure 4.1 The radiating part of the annular plate antenna with curved and rectangular slots on vertical ground plane

Figure 4.2 The part of vertical ground plane

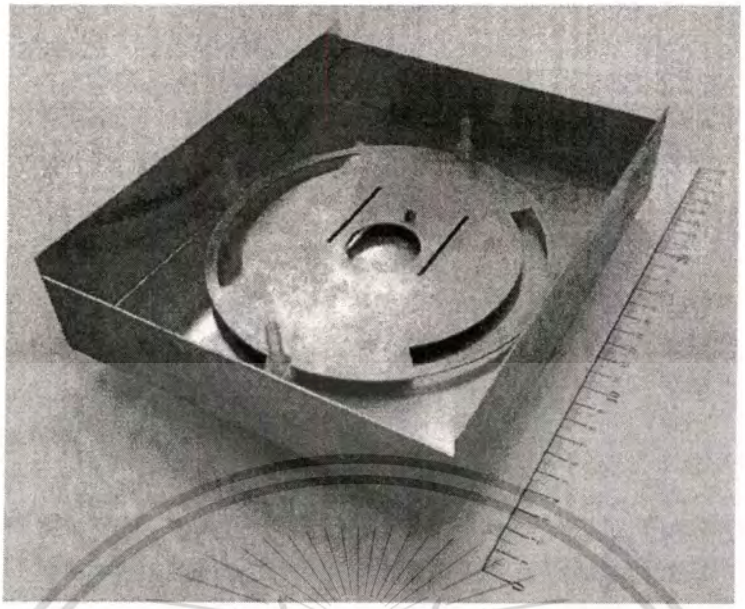

Figure 4.3 Photograph of the annular plate antenna with curved and rectangular slots on vertical ground plane

4.3 Magnitude of S_{11} ($|S_{11}|$)

To measure the magnitude of S_{11} of the proposed antenna, the experiment is set up as shown in Fig. 4.4. Figure 4.5 illustrates the comparison between the simulated and measured results of frequency characteristics of magnitude of S_{11}. It is obvious that the simulated results have the same trend with the experimental ones. However, the experimental and simulated results are different in that bandwidth. The experimental result in microwave band is wider than the simulated one. The magnitude of S_{11} is better than -10 dB from 912 MHz to 925 MHz (13 MHz) and from 2.32 GHz to 2.69 GHz (360 MHz) as shown in Fig. 4.5. Therefore, it can be operated across the UHF and microwave bands in the RFID system.

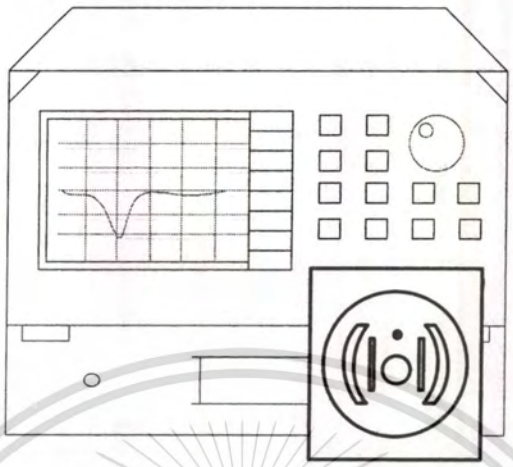

Figure 4.4 Measurement setup of the magnitude of S_{11}

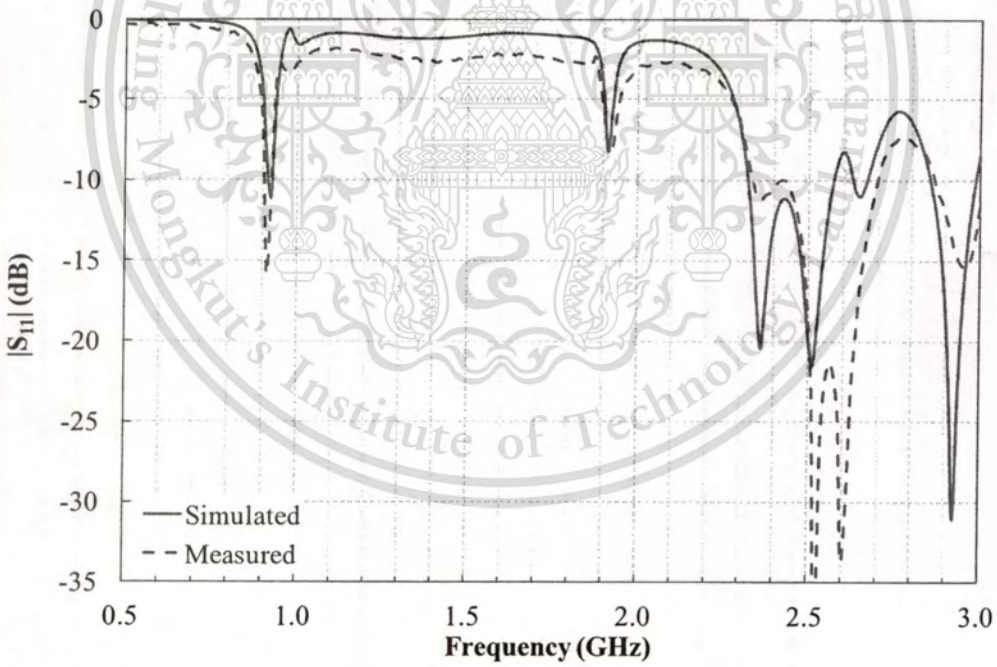

Figure 4.5 Frequency characteristics of magnitude of S_{11}

4.4 Radiation Pattern

The experiments of the radiation pattern need the equipment as follow:

1. The annular plate antenna with curved and rectangular slots on vertical ground plane is shown in Fig. 4.3.

2. The dipole antenna operates in UHF and microwave bands.

3. Network Analyzer (Model: hp 8720C) can operate from 50 MHz to 20 GHz.

For the experiment of radiation pattern, the dipole antenna was employed as transmitting antenna, and the annular plate antenna with curved and rectangular slots on vertical ground plane was rotated to receive the transmitted wave at 10° per step from 0° to 360°. Note that the distance between the transmitting and receiving antennas can be expressed as follow:

$$R = \frac{2D^2}{\lambda}, \tag{4.1}$$

where R is Far-field region

D is a maximum overall dimension of 28.4 cm

λ is wavelength of 2.45 GHz.

When substituted into (4.1), the far-field range in free space is yielded as 132 cm. In this section, the far-field region of 200 cm is used.

To measure the radiation pattern of the annular plate antenna with curved and rectangular slots on vertical ground plane, the measurement set up to test the co-polarized pattern and cross-polarized pattern in xz-plane are depicted in Fig. 4.6 and Fig. 4.7, respectively. After that the measurement also set up to test the co-polarized pattern and cross-polarized pattern in yz-plane are depicted in Fig. 4.8 and Fig. 4.9, respectively.

1. The measurement set up of the co-polarized pattern in xz-plane is illustrated in Fig. 4.6.

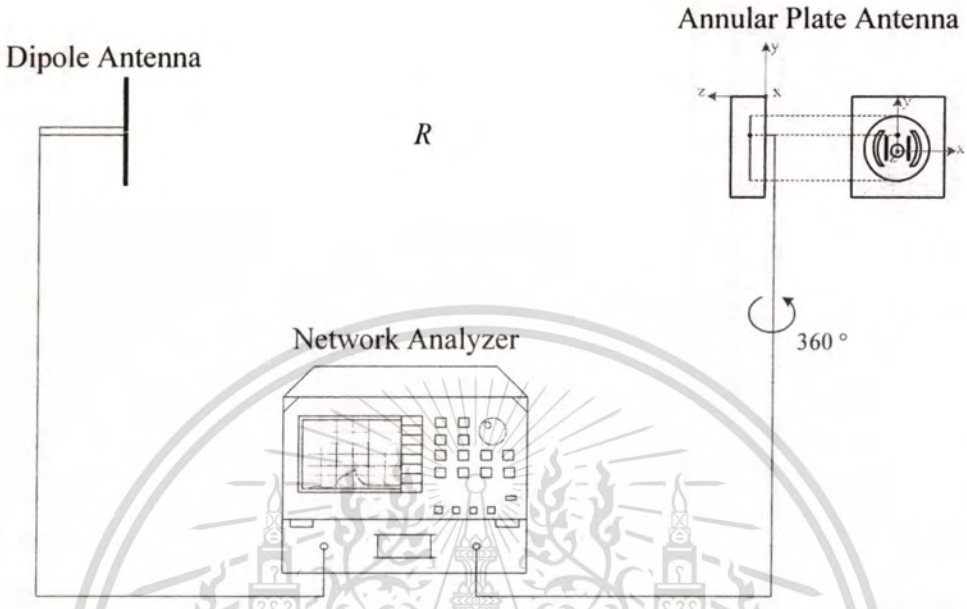

Figure 4.6 Measurement setup of the co-polarized pattern in xz-plane

2. The measurement set up of the cross-polarized pattern in xz-plane is illustrated in Fig. 4.7.

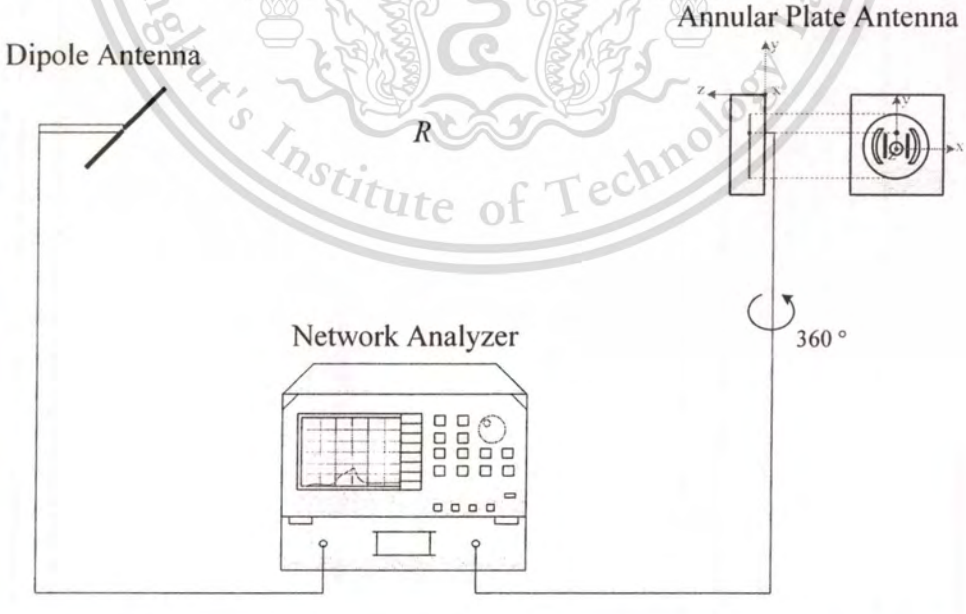

Figure 4.7 Measurement setup of the cross-polarized pattern in xz-plane

3. The measurement set up of the co-polarized pattern in yz-plane is illustrated in Fig. 4.8.

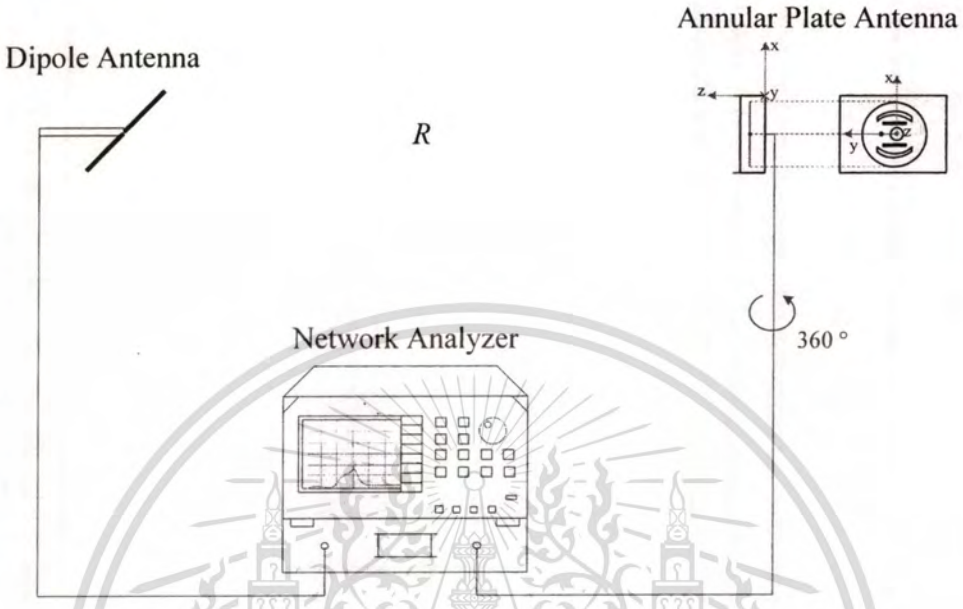

Figure 4.8 Measurement setup of the co-polarized pattern in yz-plane

4. The measurement set up of the cross-polarized pattern in yz-plane is illustrated in Fig. 4.9.

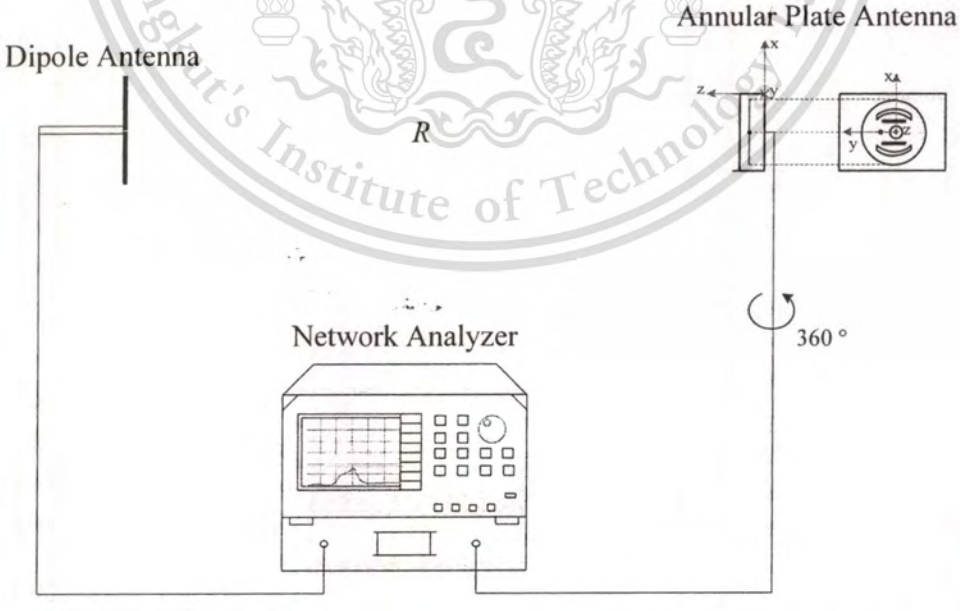

Figure 4.9 Measurement setup of the cross-polarized pattern in yz-plane

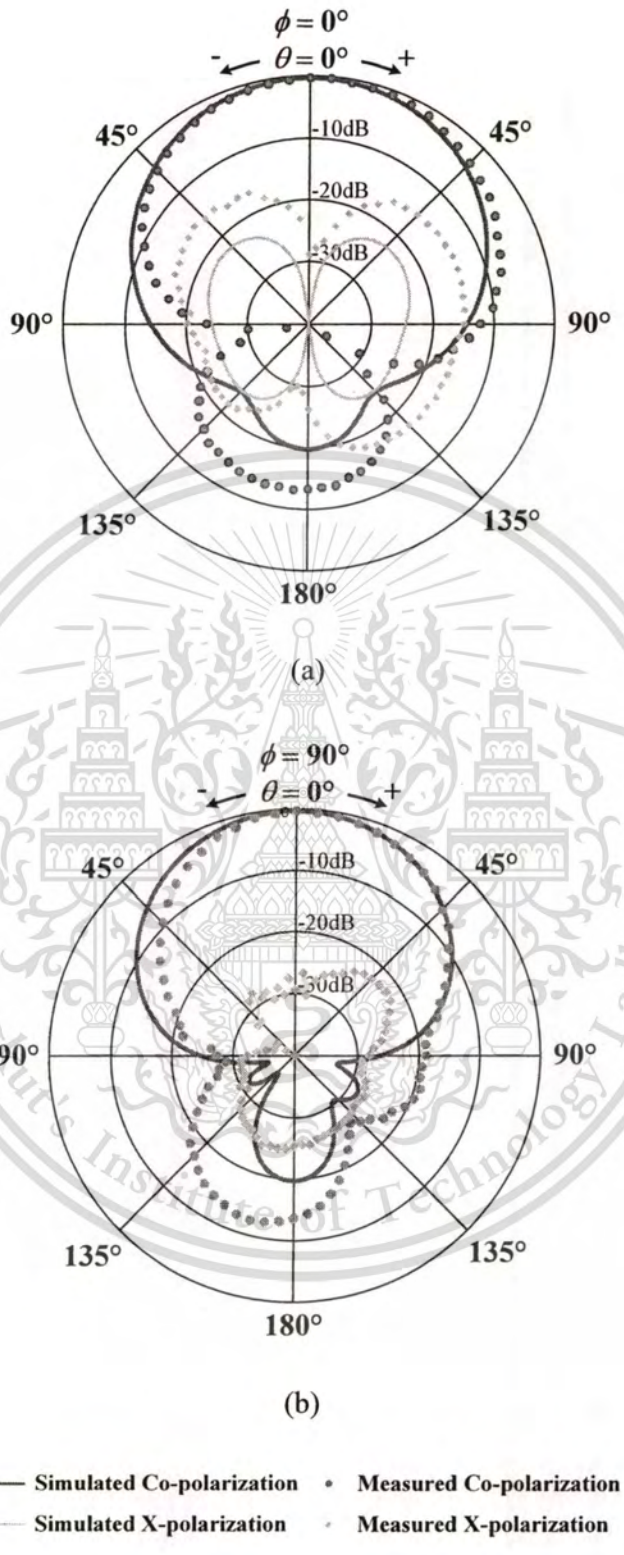

Figure 4.10 Radiation patterns at the frequency of 922.5 MHz (a) xz-plane and (b) yz-plane

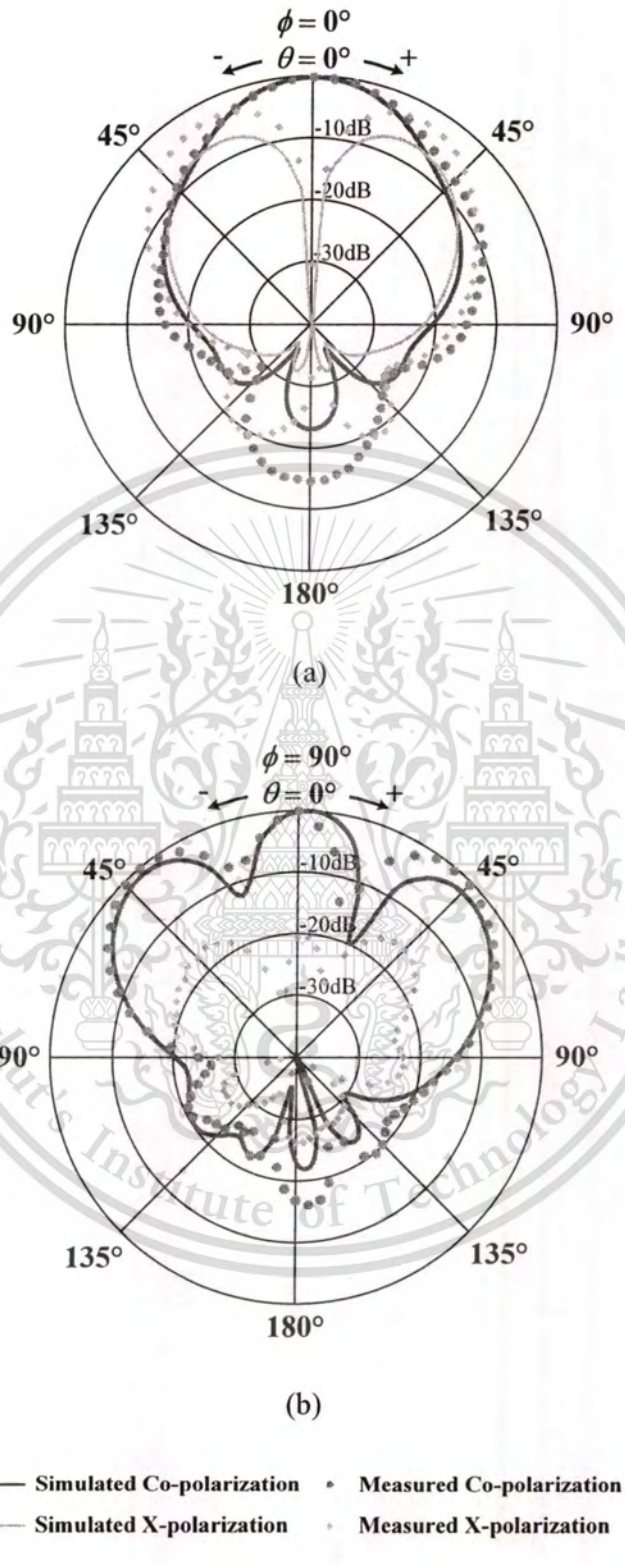

Figure 4.11 Radiation patterns at the frequency of 2.45 GHz (a) xz-plane and (b) yz-plane

Experimental results of the radiation pattern in xz-plane and yz-plane at 922.5 MHz and 2.45 GHz are plotted and compared with the simulation results as shown in Fig. 4.10 and Fig. 4.11, respectively. From the results, it is found that these results are in good agreement. The radiation patterns for both of 922.5 MHz and 2.45 GHz are unidirectional beam with a half-power beamwidth in xz-plane and yz-plane of 80° and 50° at the frequency of 922.5 MHz. At the frequency of 2.45 GHz, the half-power beamwidths in xz-plane and yz-plane are 35° and 10°, respectively.

4.5 Antenna Gain

The measured gains of proposed annular plate antenna with curved and rectangular slots on vertical ground plane in the UHF band from 920 MHz to 925 MHz and the microwave band from 2.4 GH to 2.5 GHz are illustrated and compared with the simulation results in Fig. 27. It is found that the simulated and measured gains have similar trend. Moreover, the measured gains at the beam peak direction (0° in xz-plane and yz-plane) at the center frequency of 922.5 MHz and 2.45 GHz in UHF and microwave band are 8.3 dBi and 9 dBi, respectively.

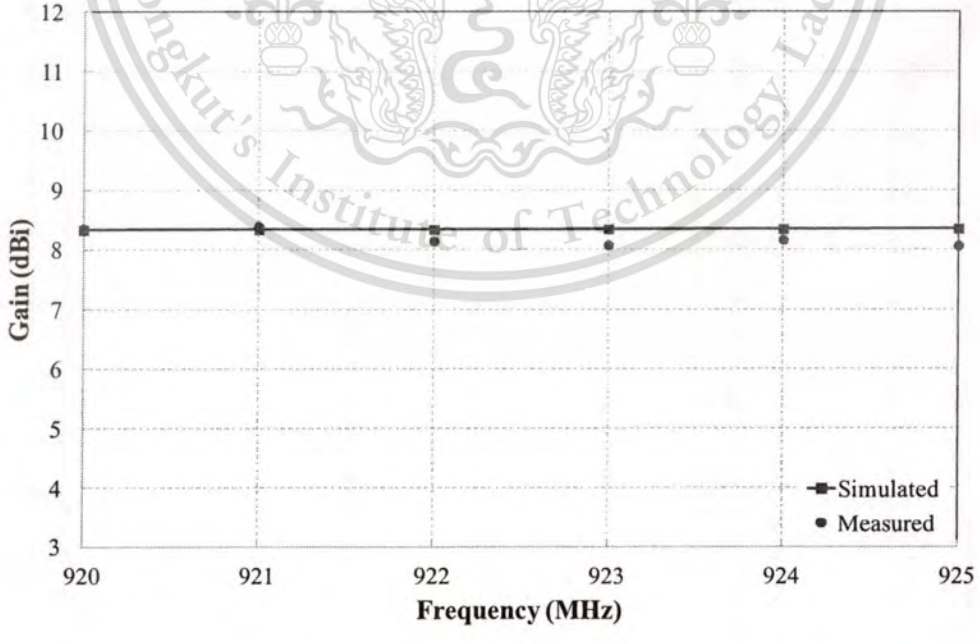

(a)

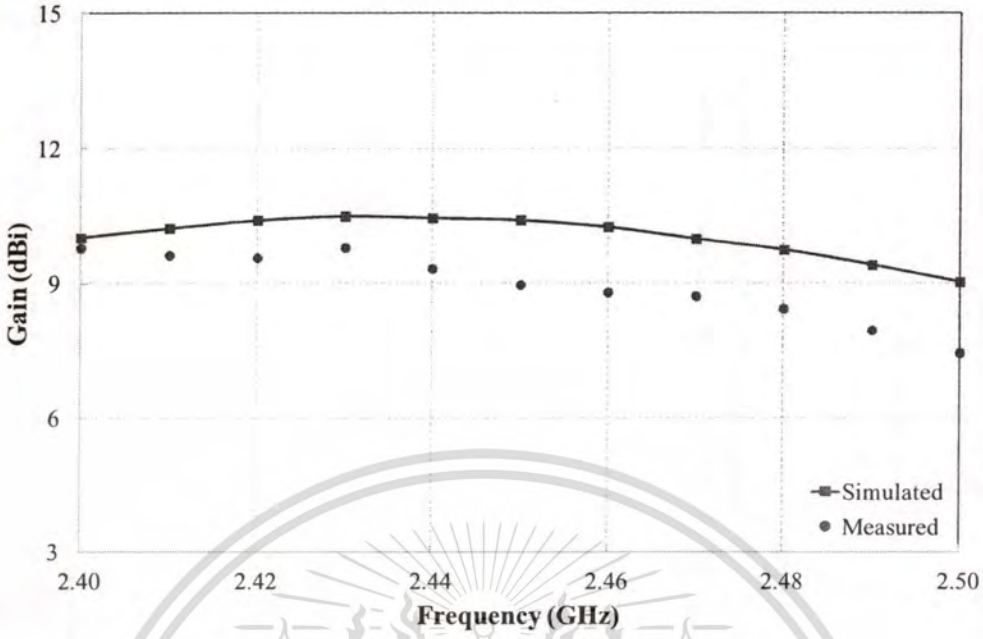

(b)

Figure 4.13 Antenna gain (a) UHF band and (b) Microwave band

4.6 Summary

The experiments of magnitude of S_{11}, the radiation pattern and antenna gain were setup to verify the antenna characteristics that are simulated by using the electromagnetic simulation program. It is found that the simulation and measurement results are agreed very well. The prototype of the annular plate antenna with curved and rectangular slots on vertical ground plane can be operated across both frequencies of UHF and microwave band in RFID applications. The bandwidths cover from 912 MHz to 925 MHz which is 1.4 % and from 2.32 GHz to 2.69 GHz which is 14.7 %. The proposed antenna radiates the unidirectional pattern in both bands. The half-power beamwidths in xz- and yz-plane are 80 degree and 50 degree of 922.5 MHz, respectively. At 2.45 GHz, the half-power beamwidths in xz- and yz-plane are 35 degree and 10 degree, respectively. In addition, the antenna gains are 8.3 dBi in the UHF band and from 7.5 dBi to 10 dBi in microwave band. These results exhibit that the proposed antenna can work well in the practical situation and can be used for RFID reader.

CHAPTER 5

APPLICATION FOR DETERMINATION OF MATERIAL PROPERTY

5.1 Introduction

In this chapter, a series of measurements is performed to measure read ranges of the passive RFID sensor system for an LWC as an example of CMPs, and these measured read ranges will be processed appropriately to inversely determine the dielectric constant of the LWC under test, which in turn provides information on its qualities. A dielectric-constant determination procedure of material under test is investigated using the dependency of the read range of the passive RF identification (RFID) sensor system on the electromagnetic properties of CMPs near or in contact with RFID tags, the qualities of CMPs can be determined through their estimated dielectric properties.

5.2 Read Range Measurement

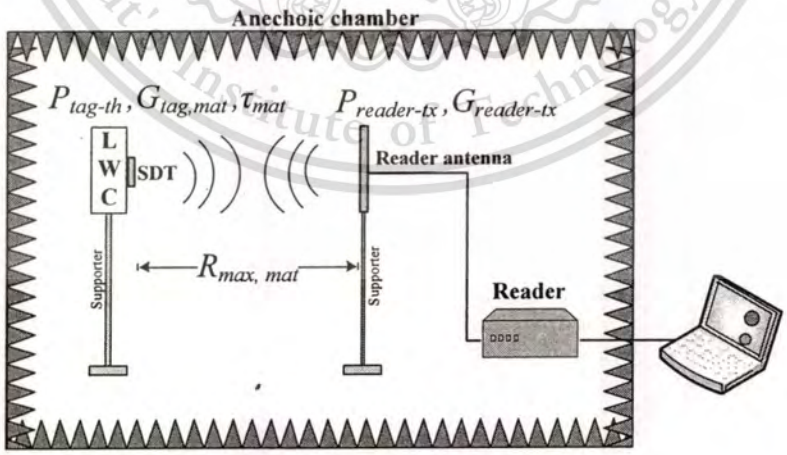

Figure 5.1 The novel RFID sensor setup

The read range between the RFID reader and the SDTs attached to the LWC of interest are measured in an anechoic chamber as illustrated in Fig. 5.1. The prototypes of the SDT_1 and the SDT_2 are a printed meander line with a coupling loop on the FR4 substrate as shown in Fig. 5.2. To measure the maximum read range, the SDT is attached to the LWC under test as shown in Fig. 5.3.

Since the maximum distance ($R_{max,\ mat}$) is calculated by using the modified Friis transmission equation, under assumption that the reader antenna has perfect impedance matching and perfect polarization matching to the tag antenna and the preliminary parameters as determined in chapter 3. Thus, to verify the methodology of determination of dielectric property of material of interest, the dipole antenna is first employed as the transmitting antenna. Note that the linear polarization is acquired.

Subsequently, replace the dipole antenna with the annular plate antenna with curved and rectangular slots on vertical ground plane to transmit wave.

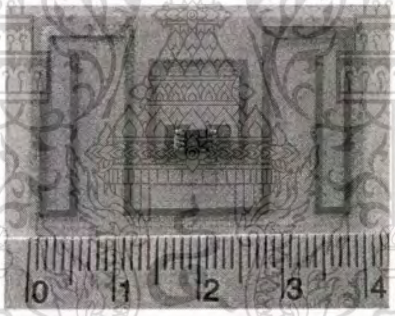

(a)

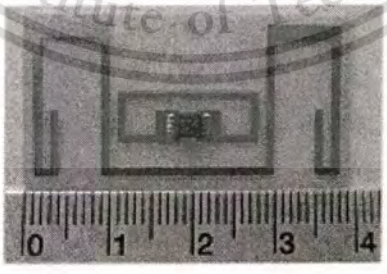

(b)

Figure 5.2 The SDT prototypes. (a) SDT_1 for the dry LWC. (b) SDT_2 for the saturated LWC

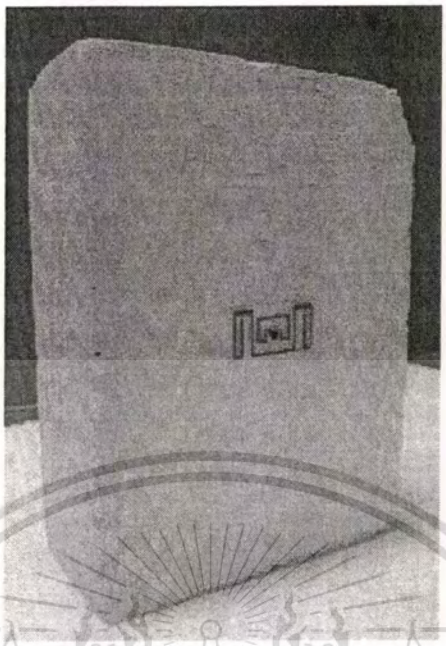

Figure 5.3 The photograph of an SDT attached to the LWC of interest

The experiment of read range, to determine the dielectric property of material of interest, is required the equipment as follow:

1. The SDTs are shown in Fig. 5.2.

2. The dipole antenna is employed as transmitting antenna as illustrated in Fig. 5.4.

3. The annular plate antenna with curved and rectangular slots on vertical ground plane is employed as transmitting antenna as shown in Fig. 5.5.

4. UHF RFID Reader Model: Motorola XR450 is shown in Fig. 5.6.

5. Computer

6. Coaxial Cable

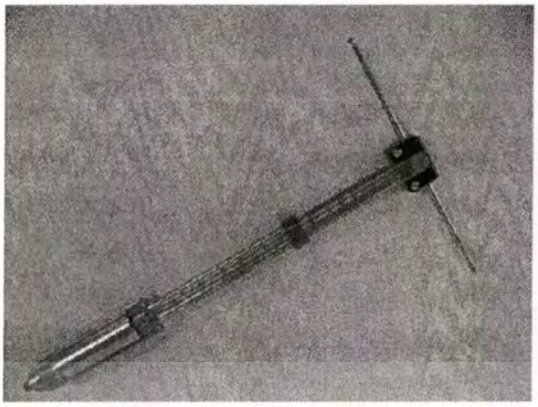

Figure 5.4 The dipole antenna

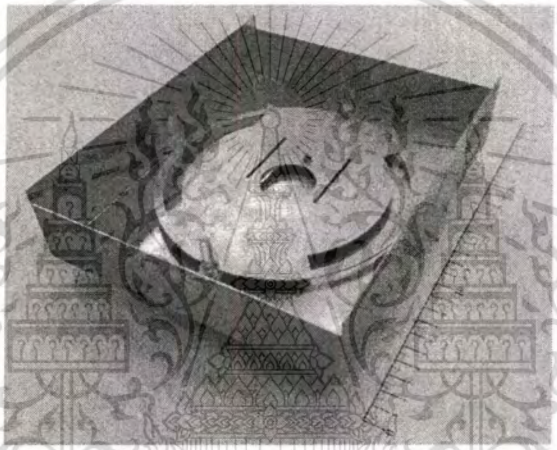

Figure 5.5 The annular plate antenna with curved and rectangular slots on vertical ground plane

Figure 5.6 UHF RFID Reader Model: Motorola XR450

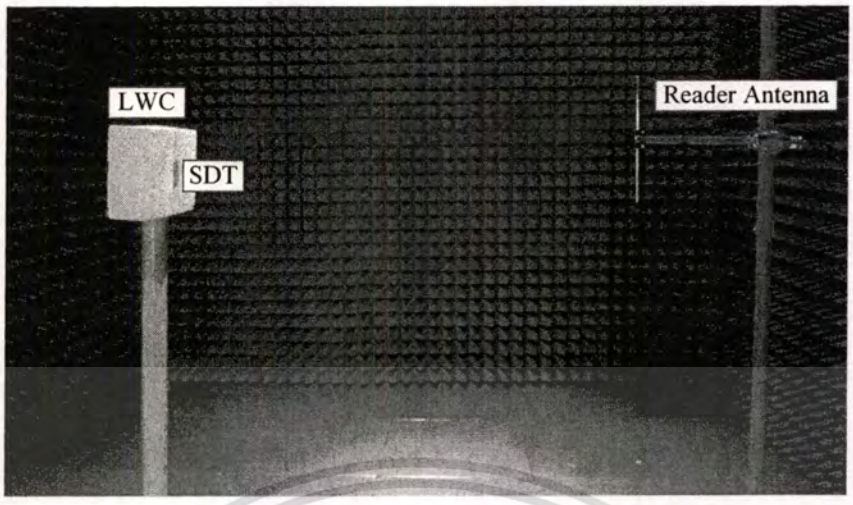

Figure 5.7 The RFID sensor measurement setup in an anechoic chamber, when the dipole antenna is employed as transmitting antenna

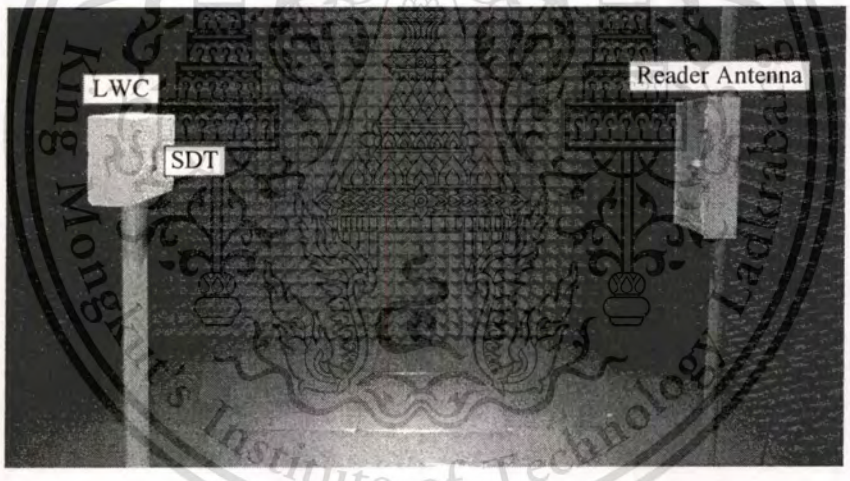

Figure 5.8 The RFID sensor measurement setup in an anechoic chamber, when the annular plate antenna with curved and rectangular slots on vertical ground plane is employed as transmitting antenna

From measurements, the read ranges of SDTs attached to lossy LWCs under test can be calculated are shown in Table 5.1. The read ranges from the simulations and measurements agree reasonably well. The discrepancies between the simulated and

measured results may derive from the measurement error and the SDT fabrication error. Therefore, the measured read range can be used to inversely determine the dielectric constant of LWCs under test with reasonable accuracy.

Table 5.1 Read range of SDTs attached to lossy LWCs under test, when the dipole antenna is transmitting antenna.

LWC State	Simulation (cm)	Measurement (cm)
Dry	68.3	69
Saturated	54.7	50

5.3 Dielectric-Constant Determination Procedure

Once the read ranges of all SDTs attached to the LWC under test are known via measurements, including the corresponding read ranges of the SDTs in the free space, the dielectric constant of the LWC under test can be determined from the following procedure.

For the lossy LWC case, both ε_r' and ε_r'' of the lossy LWC under test are required. It will be shown that two SDTs are required to uniquely determine both ε_r' and ε_r'' from the measurements of associated read ranges. In this study, the SDT_1 and the SDT_2, specifically designed for the dry and saturated LWC states respectively, are attached to the lossy LWC under test. Using the simulations, the plot of ε_r' versus $R_{\max,mat}/R_{\max,fs}$ for each SDT is illustrated in Fig. 5.9 for ε_r'' =0.20, 0.64 and 1.08. It is clearly seen from Fig. 5.9 that either SDT_1 or SDT_2 alone cannot be employed to uniquely determine ε_r' and ε_r'' from a measurement of $R_{\max,mat}/R_{\max,fs}$ since several combinations of ε_r' and ε_r'' yield the same $R_{\max,mat}/R_{\max,fs}$. However, using both SDT_1 and SDT_2 with a measurement of $R_{\max,mat}/R_{\max,fs}$ for each SDT, ε_r' and ε_r'' can be determined uniquely as shown in the following three examples.

Consider a sample of lossy LWCs (sample#1) as shown in Fig. 5.9(a), where its dielectric constant ε_r is equal to 7.5-j1.08 obtained from the dielectric probe measurement, which requires a network analyzer. From the read range measurements, it

is found that $R_{max,mat}/R_{max,fs}$ for the SDT_1 and the SDT_2 are equal to 0.5 and 2.10 respectively, as shown in Fig. 5.9(a) as the two vertical lines. It should be pointed out that the maximum distances $R_{max,fs}$ of each SDT are generally different. In Fig. 5.9(a), each vertical line of $R_{max,mat}/R_{max,fs}$ intersects the family of the relation between ε_r' - $R_{max,mat}/R_{max,fs}$ curves for each SDT at P_1 and P_2 for the SDT_1 and P_3, P_4, P_5 and P_6 for the SDT_2. At each intersection point, a pair of ε_r' and ε_r'' is obtained. Due to the fact that the sample of lossy LWCs is identical for both SDT_1 and SDT_2, only the intersection points, providing the identical pair of ε_r' and ε_r'', are valid. It can be seen from Fig. 5.9(a) that the intersection points P_1 and P_3 correspond to (ε_r', ε_r'') = (7.40, 1.08), which is the estimated dielectric constant of the LWC sample#1.

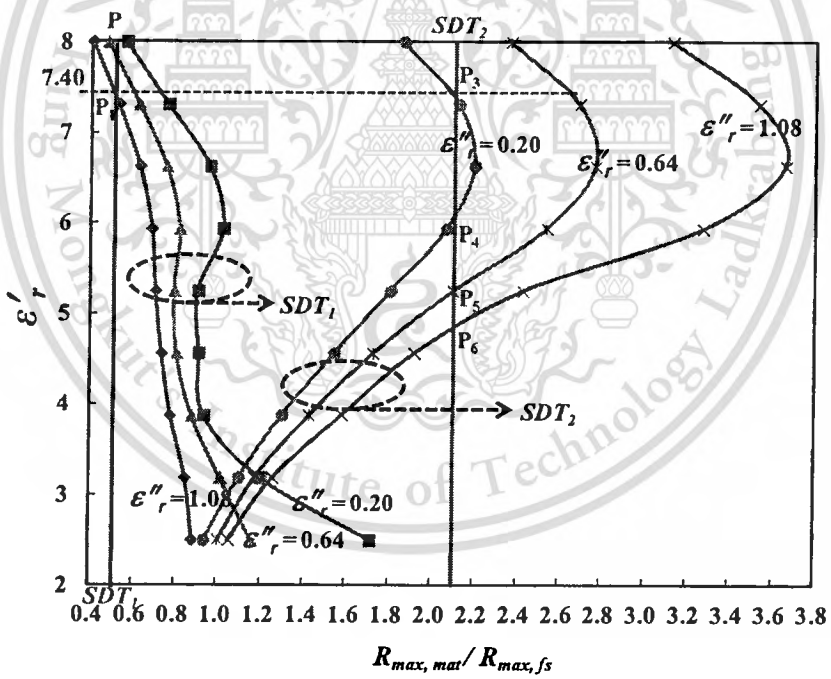

(a) The LWC sample#1

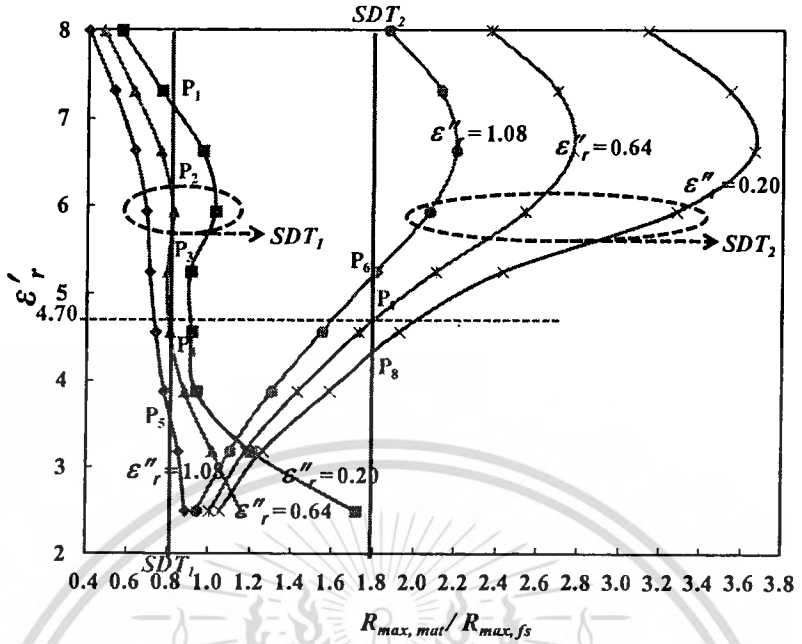

(b) The LWC sample#2

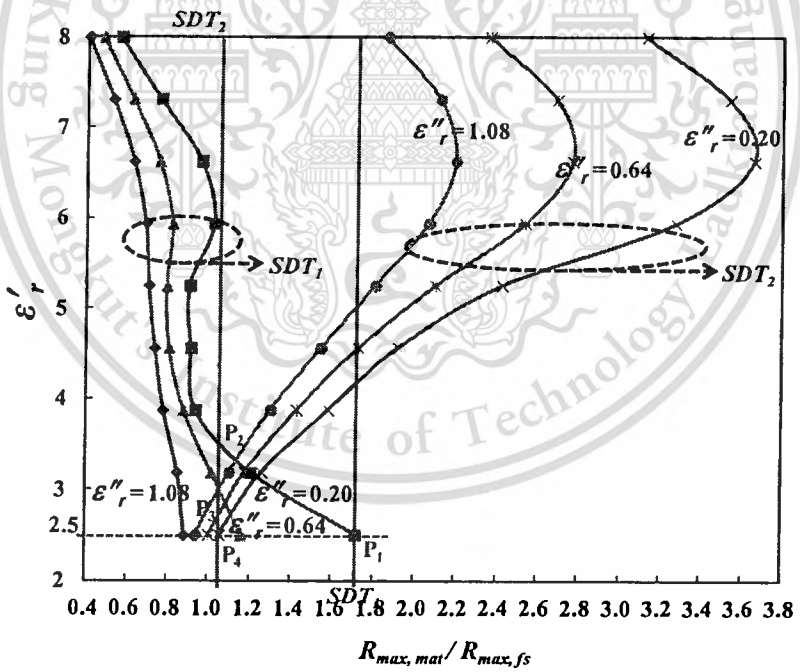

(c) The LWC sample#3

Figure 5.9 The relation between ε_r' and $R_{\max,mat}/R_{\max,fs}$ for the SDT_1 and the SDT_2 with ε_r'' =0.20, 0.64 and 1.08 obtained from the simulations

Consider another sample of lossy LWCs (sample#2), where its dielectric constant ε_r is equal to 4.8-*j*0.4 obtained from the dielectric probe measurement. Using the same determination procedure as in the case of the LWC sample#1, $R_{max,mat}/R_{max,fs}$ for the SDT_1 and the SDT_2 are found to be 0.77 and 1.77 respectively, as shown in Fig. 5.9(b) as the two vertical lines. It can be seen from this figure that the intersection points P_4 and P_7 correspond to $(\varepsilon_r', \varepsilon_r'') = (4.70, 0.64)$, which is the estimated dielectric constant of the LWC sample#2.

For the last example, let us consider the sample of lossy LWCs (sample#3), where its dielectric constant ε_r is equal to 2.5-*j*0.2 also obtained from the dielectric probe measurement. Using the same determination procedure as in the case of the LWC sample#1, $R_{max,mat}/R_{max,fs}$ for the SDT_1 and the SDT_2 are found to be 1.71 and 1.05 respectively, as shown in Fig. 5.9(c) as the two vertical lines. It can be seen from this figure that the intersection points P_1 and P_4 correspond to $(\varepsilon_r', \varepsilon_r'') = (2.5, 0.2)$, which is the estimated dielectric constant of the LWC sample#3.

Thus, two SDTs can be employed to uniquely determine the dielectric constant of the lossy LWC under test. For these examples, the relative error of 1.3%, 5.4 % and 0 % for sample#1, sample#2 and sample#3, respectively, can be obtained using the novel RFID sensor, which is reasonably accurate. It should be pointed out that the relative error can be decreased by reducing the measurement error of associated read ranges and the SDT fabrication error. It is important to note that the dielectric constant of sample#3 is also obtained with 0 % by using the dipole antenna. For this reason, the annular plate antenna with curved and rectangular slots on vertical ground plane can be used as an RFID reader antenna in a novel RFID sensor to determine the dielectric property of material under test. Once the dielectric constant of the LWC sample is estimated, the quality of the LWC sample can be determined by using the relation between the dielectric constant and the LWC quality, predetermined by measurements and testings or other approaches [53]-[55].

5.4 Summary

The promising approach based on a novel RFID sensor is successfully employed to determine the dielectric property of LWC samples through associated read-range measurements. The dielectric-constant determination procedure for lossy LWCs is discussed in detail in this chapter. It is found that the novel RFID sensor provides reasonably accurate results. Note that to use this RFID sensor, it is necessary to know size and shape of material under test, and then perform simulation for desired size and shape first. Furthermore, the annular plate antenna with curved and rectangular slots on vertical ground plane is designed in the previous chapter that can be employed as a reader antenna in a novel RFID sensor.

CHAPTER 6

CONCLUSION

6.1 Summary of Preceding Chapters

As mentioned in the first chapter, this thesis proposes a determination of dielectric property of material of interest using a novel RFID sensor. This procedure is categorized into NDT technique. The benefits is based on using this technique that the novel RFID sensor does not require additional specific sensors to determine dielectric properties of the materials under test, thereby more convenient in fabrication and usually of lower cost. In addition, the novel RFID sensor does not require a network analyzer and other expensive accessories.

Chapter 2 presents a principle of the antenna design procedure and the simulation to determine the optimum parameters of the annular plate antenna with curved and rectangular slots on vertical ground plane. The proposed antenna can be operated in a dual-band of UHF and microwave bands in RFID applications. The radiation pattern of the antenna appears to be a unidirectional beam in the broadside direction both of frequency bands. In addition, the antenna gain is high because that air substrate is used. Therefore, the proposed antenna can be employed as an RFID reader antenna in a novel RFID sensor system.

In Chapter 3, a novel RFID sensor technique operating in the UHF band is designed and analyzed to employ as a remotely read dielectric-property sensors to determine quality of certain CMs through their estimated dielectric properties. The relation between dielectric constant and maximum read range (R_{max}) is illustrated, which it is used to determine material. Moreover, the sensitivity of the novel RFID sensor on the location error and the tolerance are discussed and analyzed in this chapter.

Chapter 4 verifies the principle and theory presented in the chapter 2. The antenna prototype is fabricated with the optimum parameters to test its characteristics. The experiments of magnitude of S_{11}, the radiation pattern and antenna gain were setup. It is found that the simulation and measurement results are agreed very well. These results corroborate that the proposed antenna can be used as an RFID reader.

Chapter 5 corroborates a determination of dielectric property of material under test using a novel RFID sensor. The dielectric-constant determination procedure for lossy LWCs is performed and discussed. It is found that the novel RFID sensor provides reasonably accurate results. Furthermore, the annular plate antenna with curved and rectangular slots on vertical ground plane is designed in the previous chapter that can be employed as a reader antenna in a novel RFID sensor.

Finally, the summary of this thesis and the remark for the future studies are included in chapter 6.

6.2 Remark for Future Studies

In this thesis, the determination of dielectric property of LWC using a novel RFID sensor is investigated and analyzed. However, this technique is based on the modified Friis transmission equation under the assumption that the reader antenna has perfect impedance matching and perfect polarization matching to the tag antenna. To be more accurate, hence, these hypotheses should be taken into account when calculating the maximum read range.

In addition, this thesis is mentioned on the development of a reliable sensor technique to determine material quality in manufacturing and/ or material testing and inspection process. The LWC is employed as an example of CMPs that is assumed to be a homogeneous. This is left for further works.

Further works include reducing associated errors of estimating the dielectric constant of CMPs and other interest materials. In addition, effects of sizes and shapes of materials under test will also be studied based on the same sensor principle, including the practical approaches to mount SDTs on these materials.

REFERENCES

[1] Finkenzeller, K, *RFID Handbook: Fundamentals and Applications in Contactless Smart Cards and Identification*, John Wiley and Sons, Ltd., 2003.

[2] D. M. Dobkin, *The RF in RFID: Passive UHF RFID in Practice*, Elsevier Inc., 2008.

[3] NBTC, [Online] Available: http://www.nbtc.go.th/wps/portal/NTC/eng.

[4] D. Shin, P. Park, J. Kim, W. Seong and J. Choi, "A novel dual-band circularly polarized antenna," *2007 Electromagnetics in Advanced Applications International Conference (ICEAA 2007)*, pp. 511 – 514, Sep. 2007.

[5] M. Yi, S. Li, H. Liu and W. Hong, "Optimization of dual-L antenna designs for portable RFID reader," *2008 Wireless Communications, Networking and Mobile Computing (WiCOM '08)*, pp. 1 - 4, Oct. 2008.

[6] V. Deepu, S. Mridula, R Sujith and P. Mohanan, "Compact uniplanar antenna for multiband applications," *Proceedings of International Conference on Microwave 08*, pp. 502-503, Nov. 2008.

[7] Z. Xu and X. Li, "Aperture coupling two-layered dual-band RFID reader antenna design," *2008 Microwave and Millimeter Wave Technology (ICMMT 2008)*, pp. 1218 – 1221, April 2008.

[8] H. Yang, S. Yan, L. Chen and H. Shi, "Investigation and design of a modified aperture-couple fractal antenna for RFID applications," *2008 ISECS International Colloquium on Computing, Communication, Control, and Management*, pp. 505-509, Aug. 2008.

[9] F.-Y. Kuo, P.-H. Pan, C.-Y. Chiang, H.-T. Hsu, and H.-T. Chou, "Dual-band Aperture-Coupled Patch Antenna for RFID Mobile Terminal Applications," *Proceedings of Asia-Pacific Microwave Conference 2010*, pp. 2201-2204, Dec. 2010.

[10] M.-T. Zhang, Y.-C. Jiao and F.-S. Zhang, "Dual-band CPW-fed folded-slot monopole antenna for RFID application," *Electronics Letters*, vol. 42, no. 21, Oct. 2006.

[11] J. R. Panda and R. S. Kshetrimayum, "A printed F-shaped dual-band monopole antenna for RFID and WLAN applications," *2010 Computer and Communication Technology (ICCCT)*, pp. 789-791, Sept. 2010.

[12] W.-J. Lul, R. Liul, Z.-Y. Zhangl, C. Panl and H.-B. Zhul, "Dual-band balanced antipodal dipole-slot antenna," *2010 Communication Technology (ICCT)*, pp. 203-206, Nov. 2010.

[13] J. R. Panda and R. S. Kshetrimayum, "A printed 2.4 GHz/5.8 GHz dual-band monopole antenna for WLAN and RFID applications with a protruding stub in the ground plane," *2011 Communications (NCC)*, pp. 1-5, Jan. 2011.

[14] S. Laurens, J. P. Balayssac, J. Rhazi, G. Klysz, and G. Arliguie, "Non-destructive evaluation of concrete moisture by GPR: Experimental study and direct modeling," *RILEM Materials and Structures*, vol. 38, pp. 827-832, Jan. 2005.

[15] O. Buyukozturk, "Electromagnetic properties of concrete and their significance in nondestructive testing," *Transport. Research Board*, Paper No. 970872, 1997.

[16] U. C. Hasar, "Thickness-independent complex permittivity determination of partially filled thin dielectric materials into Determination of property of construction material pro ducts 15 rectangular waveguides," *Progress In Electromagnetics Research*, vol. 93, pp. 189-203, 2009.

[17] U. C. Hasar, "Thickness-independent automated constitutive parameters extraction of thin solid and liquid materials from waveguide measurements," *Progress In Electromagnetics Research*, vol. 92, pp. 17-32, 2009.

[18] H. Zhang, S. Y. Tan, and H. S. Tan, "An improved method for microwave nondestructive dielectric measurement of layered media," *Progress In Electromagnetics Research B*, Vol. 10, pp. 145-161, 2008.

[19] L. Capineri, D. J. Daniels, P. Falorni, O. L. Lopera, and C. G. Windsor, "Estimation of relative permittivity of shallow soils by using the ground penetrating radar response from different buried targets," *Progress In Electromagnetics Research Letters*, vol. 2, pp. 63-71, 2008.

[20] G. Marrocco, "RFID antennas for the UHF remote monitoring of human sub jects," *IEEE Trans. Antennas Propag.*, vol. 55, no. 6, pp. 1862-1870, Jun. 2007.

[21] T. Deleruyelle, P. Pannier, M. Egels, and E. Bergeret, "An RFID tag antenna tolerant to mounting on materials," *IEEE Antennas Propag. Mag.* , vol. 52, no. 4, pp. 14-19, Aug. 2010.

[22] J. Siden, X. Zeng, T. Unander, A. Koptyug, and H. E. Nilsson, "Remote moisture sensing utilizing ordinary RFID tags," *2007 IEEE Sensors Conference*, pp. 308-311, Oct. 2007.

[23] D. Pena, R. Feick, H. D. Hristov, and W. Grote, "Measurement and modeling of propagation losses in brick and concrete walls for the 900-MHz band," *IEEE Trans. Antennas Propag.* , vol. 51, no. 1, pp. 31-39, 2003.

[24] G. Marrocco, L. Mattioni, and C. Calabrese, "Multip ort sensor RFIDs for wireless passive sensing of ob jects | Basic theory and early results," *IEEE Trans. Antennas Propag.* , vol. 56, no. 8, pp. 2691-2702, Aug. 2008.

[25] C. Occhiuzzi, S. Cippitelli, and G. Marro cco, "Modeling, design and exp erimentation of wearable RFID sensor tag," *IEEE Trans. Antennas Propag.*, vol. 58, no. 8, pp. 2490-2498, Aug. 2010.

[26] P. F. Baude and S. D. Theiss, "RFID sensor," US 2007/0215709 A1, Sep. 2007.

[27] V. R. Marinov, Y. A. Atanasov, A. Khan, D. Vaselaar, A. Halvorsen, D. L. Schulz, and D. B. Chrisey, "Direct-write vap or sensors on FR4 plastic substrates," *IEEE Sensors Journal*, vol. 7, no. 6, pp. 937-944, Jun. 2007.

[28] C. A. Balanis, *Antenna Theory, Analysis and Design*, John Wiley& Sons, 2005.

[29] Y.-X. Guo, L. Bian, and X. Q. Shi, "Broadband Circularly Polarized Annular-Ring Microstrip Antenna," *IEEE Trans. on Antennas and Propag.*, vol. 57, no. 8, pp. 2474 – 2477, Aug. 2009.

[30] X. L. Bao and M.J. Ammann, "Microstrip-fed dual-frequency annular-slot antenna loaded by split-ring-slot," *IET Microw. Antennas Propag.*, vol. 3, pp. 757 – 764 pp. 757 – 764, 2009.

[31] H.-L. Zhang, X. Y. Zhang, B.-J. Hu, "Compact Broad-Band Annular Ring Antenna for Global Navigation Satellite Systems," *2010 Antennas Propagation and EM Theory (ISAPE)*, pp. 189 – 192, 2010.

[32] Finkenzeller, K., *RFID Handbook: Radio-Frequency Identification Fundamentals and Applications*, Wiley, New York, 1999.

[33] P. V. Nikitin, K. V. S. Rao, S. F. Lam, V. Pillai, R. Martinez, and H. Heinrich, "Power reflection co efficient analysis for complex impedances in RFID tag design," *IEEE Trans. Microw. Theory Tech.*, vol. 53, no. 9, pp. 2721-2725, Sep. 2005.

[34] Symbol XR450, [Online] Available: http://www.motorola.com/Business/US-EN/Business+Product+and+Services/RFID/RFID+Readers/XR450+Fixed+RFID+ Reader US-En.

[35] C. A. Balanis, *Antenna Theory, Analysis and Design*, John Wiley& Sons, 2005.

[36] C.-H. Loo, K. Elmahgoub, F. Yang, A. Elsherbeni, D. Kajfez, A. Kishk, and T. Elsherbeni, "Chip imp edance matching for UHF RFID tag antenna design," *Progress In Electromagnetics Research*, vol. 81, pp. 359-370, 2008.

[37] K. V. S. Rao, P. V. Nikitin, and S. P. Lam, "Impedance matching concepts in RFID transponder design," *Fourth IEEE Workshop on Automatic Identification Advanced Technologies (AutoID'5)*, pp. 39-42, 2005.

[38] J. D. Grifin, G. D. Durgin, A. Haldi, and B. Kipp elen, "RF tag antenna performance on various materials using radio link budgets," *IEEE Antennas and Wireless Propagation Letters*, vol. 5, pp. 247-250, 2006.

[39] J. D. Grifin, "A radio assay for the study of radio frequency tag antenna performance," *Master's Thesis, Georgia Institute of Technology*, Atlanta, 2005.

[40] A. Lazaro, D. Girbau, and D. Salinas, "Radio link budgets for UHF RFID on multipath environments," *IEEE Trans. Antennas Propag.*, vol. 57, no. 4, pp. 1241-1251, Apr. 2009.

[41] Standard dipole, [Online] Available: http://www.testmart.com/ sp.cfm/ANT/ANRI/MP651B.html.

[42] CST-Microwave Studio, User's Manual, 2006.

[43] NXP UCODE G2XL, Ultrahigh frequency smart lab el ICs [On-line] Available: http://www.nxp.com/acrobat download/literatu-re/9397/75016225.p df.

[44] Light weight concrete, [Online] Available:http://www.ebrindia.c-om/cellular-light-weight-concrete-blo cks.htm.

[45] Smart block [Online] Available: http://www.smartblock.in.th/view product.php?pro duct=A001&mcat=&cat id=137&lang=th &page=1.

[46] S. Stavrou and S. R. Saunders, "Review of constitutive parameters of building materials," *2003 Antennas and Propagation (ICAP 2003)*, pp. 211-215, Apr. 2003.

[47] T. Takizawa, "Reduction of ghost signal by use of magnetic absorbing material on walls," *IEEE Trans. on Broadcasting*, vol. 25, no. 4, pp. 143-146, Dec. 1979.

[48] X. Jin, and M. Ali, "Embedded antennas in dry and saturated concrete for application in wireless sensors," *Progress In Electromagnetics Research*, pp. 197-211, 2010.

[49] X. Jin and M. Ali, "Reflection and transmission properties of embedded dipoles and PIFAs inside concrete at 915 MHz," *2009 IEEE Antennas and Propagation Society International Symposium, APSURSI' 09*, pp. 1-4, Jun. 2009.

[50] U. C. Hasar, "Permittivity determination of fresh cement-based materials by an op en-ended waveguide probe using amplitude-only measurements," *Progress In Electromagnetics Research*, vol. 97, pp. 27-43, 2009.

[51] Dielectric probe, [Online] Available: http://www.home.agilent.co-m/agilent/product. jspx?pn=85070E&lc=eng&cc=US.

[52] J. W. Lee and B. Lee, "Design of high-Q UHF radio-frequency identi¯cation tag antennas for an increased read range," *IET Microw. Antennas Propag.*, vol. 2, no. 7, pp. 711-717, Apr. 2008.

[53] N. Nakhla, , A. A. El-deen, K. Maurice, L. Youssef, N. Mahfouz, T. Youakim, M. N. A. Zeid, K. Nassar and A. Darwish, "Electrostatics utilization for concrete performance measurements," *2010 IEEE Middle East Conference on Antennas and Propagation (MECAP 2010)*, 1-2, Oct. 2010.

[54] S.J. Ford, J.-H. Hwang, I.D. Shane, R.A. Olson, G.M. Moss, H.M. Jennings, and T.O. Mason, "Dielectric amplification in cement pastes," *Advanced Cement Based Materials*, vol. 5, no. 2, 41–48, Mar. 1997.

[55] S. Wen and D.D.L. Chung, "Cement-based materials for stress sensing by dielectric measurement," *Cement and Concrete Research*, vol. 32, no. 9, 1429-1433, Sep. 2002.

VITA

Rattapong Suwalak was born in Songkhla, Thailand, on 23 August 1982. He received the B. Eng. degrees in Electrical Engineering from the Department of Electrical Engineering, Faculty of Engineering, Prince of Songkla University (PSU), Songkhla, Thailand, in 2005. After one year, he entered the department of Telecommunications Engineering, Faculty of Engineering, King Mongkut's Institute of Technology Ladkrabang (KMITL), Bangkok, Thailand, and received the M. Eng. degree in Telecommunication Engineering in 2008. During his study for Ph.D. in Electrical Engineering at KMITL, he received a Thailand Graduate Institute of Science and Technology (TGIST), NSTDA. He was an assist. researcher at National Electronics and Computer Technology Center (NECTEC), Bangkok, Thailand. His research interests include the antenna design for portable and wireless communication, especially, in the RFID technology.

PUBLICATIONS

[1] R. Suwalak, C. Phongcharoenpanich, D. Torrungrueng and M. Krairiksh, "Determination of Dielectric Property of Construction Material Products Using a Novel RFID Sensor," *Progress in Electromagnetics Research*, vol.130, pp.601-617, Aug. 2012.

[2] K. Lertsakwimarn, R. Suwalak and C. Phongcharoenpanich, "A Compact Loop Antenna with Parasitic Split Ring for UHF RFID Application," *Progress in Electromagnetics Research Symposium (PIERS2013)*, March 2013.

[3] R.Suwalak, K.Lertsakwimarn, C.Phongcharoenpanich, M.Krairiksh and D.Torrungrueng, "Effects of Tag Location on Light Weight Concrete for an RFID Sensor Application," *Proceedings of the 2012 Electrical Engineering/Electronics, Computer, Telecommunications, and Information Technology International Conference (ECTI-CON2012)*, Hua Hin, 4 pages, May 2012.

[4] R.Suwalak, K.Lertsakwimarn and C.Phongcharoenpanich, "A Circularly Polarized Patch Antenna with Rectangular Slot on Defected Ground Plane for RFID Reader," *Proceedings of The 1st International Symposium on Technology for Sustainability (ISTS 2011)*, Bangkok, pp.293-296, Jan.2012.

[5] C.Phongcharoenpanich and R.Suwalak, "Dual Band Antenna for RFID Applications," *Proceedings of the 12th International Conference on Electromagnetics in Advanced Applications (ICEAA'10)*, Sydney, pp.633-636, Sept.2010.

[6] R.Suwalak, P.Pongpaiboon, C.Phongcharoenpanich and M.Krairiksh, "An Annular Microstrip Antenna with Sectoral Slots for RFID Reader," *Proceedings of the 2009 Asia-Pacific Microwave Conference (APMC2009)*, pp. 1040 - 1043, Singapore, Dec.2009.

[7] R.Suwalak, P.Pongpaiboon and C.Phongcharoenpanich, "Characteristics of Dual-Band Antenna for RFID Reader," *NECTEC Technical Journal Special Issue on*

NECTEC Annual Conference & Exhibition 2009 (NECTEC-ACE 2009), pp.196-199, Bangkok, Sep. 2009.

[8] R.Suwalak, C.Phongcharoenpanich, D.Torrungrueng, N.Surittikul and W. Villarroel, "A Probe-Fed Eight-Branch Folded Strip with Notched-Annular-Ring Parasitic Patch Antenna on Circular Ground Plane," *Proceedings of the 2009 International Symposium on Antennas and Propagation (ISAP2009)*, pp.955-958, Bangkok, October 2009.

[9] R.Suwalak, P.Pongpaiboon and C.Phongcharoenpanich, "Dual-Band Flat Antenna for RFID Reader," *Proceedings of the Thailand-Japan MicroWave 2009 (TJMW2009)*, Bangkok, pp.123-126.

[10] K.Phaebua, R.Suwalak, C.Phongcharoenpanich and M.Krairiksh, "Statistical Characteristic Measurements of Propagation in Durian Orchard for Sensor Network at 5.8 GHz," *Proceedings of the 2008 International Symposium on Communications and Information Technologies (ISCIT2008)*," Vientiane, pp.520-523, October 2008.

[11] R.Suwalak, K.Phaebua, C.Phongcharoenpanich and M.Krairiksh, "Path Loss Model and Measurements of 5.8 GHz Wireless Network in Durian Garden," *Proceedings of the 2008 International Symposium on Communications and Information Technologies (ISCIT2008)*," Vientiane, pp.698-701, October 2008.

[12] R.Suwalak and C.Phongcharoenpanich, "A Two-Square-Aperture Antenna Excited by a Probe on Rectangular Ground Plane with Elliptical Parasitic Patch for UHF-RFID Reader," *Proceedings of the 2008 Electrical Engineering/Electronics, Computer, Telecommunications, and Information Technology International Conference (ECTI-CON2008)*, Krabi, vol.1, pp.I-309 to I-312, May 2008.